Failure Prediction in Multiphase Deep-Water Buoyancy Systems

Eirik Hoel

THE NORWEGIAN UNIVERSITY
OF SCIENCE AND TECHNOLOGY
DEPARTMENT OF ENGINEERING DESIGN
AND MATERIALS

MASTER THESIS SPRING 2013
FOR
STUD.TECHN. EIRIK HOEL

Failure prediction in multiphase deep-water buoyancy systems
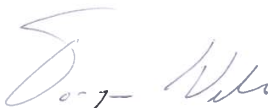Bruddprediksjon i flerfase dypt vann oppdriftssystemer

Cost efficient buoyancy is needed for many subsea applications such as risers, ROVs, anchor handling and pipelines. With oil and gas exploration moving into ever deeper waters suitable buoyancy materials able to withstand these high pressures need to be developed.

NTNU has developed a new type of buoyancy solution based on polypropylene with mineral fillers. This project shall explore how these materials will fail under the combination of buoyancy loads and hydrostatic pressure. Representative buoyancy elements shall be selected and their failure mechanisms and strength shall be analyzed.

The thesis should include the signed problem text, and be written as a research report with summary both in English and Norwegian, conclusion, literature references, table of contents, etc. During preparation of the text, the candidate should make efforts to create a well arranged and well written report. To ease the evaluation of the thesis, it is important to cross-reference text, tables and figures. For evaluation of the work a thorough discussion of results is appreciated. Safety evaluations for experimental work shall be added to the Appendix.

Three weeks after start of the thesis work, an A3 sheet illustrating the work is to be handed in. A template for this presentation is available on the IPM's web site under the menu "Masteroppgave" (http://www.ntnu.no/ipm/masteroppgave). This sheet should be updated one week before the Master's thesis is submitted.

The thesis shall be submitted electronically via DAIM, NTNU's system for Digital Archiving and Submission of Master's thesis.

Torgeir Welo
Head of Division
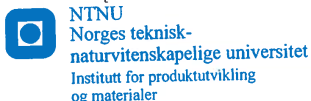
Andreas Echtermeyer
Professor/Supervisor

Sammendrag

Målet med denne oppgaven er å undersøke hvordan en ny type oppdriftsmateriale for offshore applikasjoner vil opptre under driftsforhold. Dette inkluderer oppdriftskrefter og et ekstremt hydrostatisk trykk. Det nye materialsystemet, Compbuoy, består av porøse, lavkostnads pellets i en polymer matriks. Konvensjonelle oppdriftselementer i dag er fylt med syntaktisk skum, et mye mer kostbart materiale. Ettersom det lovende materiale Compbuoy nå har blitt utviklet, må kritiske sviktmekanismer undersøkes for å sikre bærekraften i løsningen.

Skjærspenning ble identifisert som den mest kritiske spenningskomponenten og testing av skjærstyrke ble utført både eksperimentelt og numerisk. En ny testmetode ble utviklet for å måle belastningen som kreves for å brekke prøven i skjær og beregne skjærstyrke ved å analysere resultatene. En testrigg ble konstruert og testprøver ble produsert og testet. Elementmetoden ble brukt for verifisere gyldigheten av ulike parametre. De numeriske resultatene viste seg å stemme godt overens med den generelle mekaniske oppførselen materialet viste under den eksperimentelle skjærtesten. Elementmetoden ble også brukt til å estimere skjærstyrke og bruddtøyning av prøven, men noen store avvik ble oppdaget. Videre testing av materialegenskaper ble utført for å forklare årsaken til disse avvikene.

Skjærtestresultatene ble sammenlignet med designkriteriene for operasjoner på 2500 meters dyp. Tiltak er foreslått for å bedre kompresjons- og skjærstyrke.

Abstract

The objective of this thesis is to explore how a new type of buoyancy material for offshore applications will perform under operating conditions. This includes buoyancy loads and extreme hydrostatic pressure. The new material system, Compbuoy, consists of porous, low cost pellets in a polymer matrix. Conventional buoyancy elements today are filled with syntactic foam, a much more expensive material. As the promising material Compbuoy has been developed, critical failure mechanisms must be investigated to ensure the sustainability of the solution.

Shear stress was identified as the most critical stress component and shear strength testing was performed both experimental and numerical. A new punch tool test method was developed to measure the load required to break the sample in shear, and calculate the shear strength by analyzing the results. A test rig was constructed and test samples were produced and tested. Finite element analysis was performed to verify the validity of different test parameters. The numerical results were found to coincide well with the general mechanical behavior of the experimental shear test. FEA was also used to estimate the shear strength and failure strain of the sample, but some large deviations were discovered. Further testing of material properties was performed to explain the reason for these deviations.

The shear test results were compared with the design requirements for service at 2500 m water depth. Improvements are suggested to improve the compressive and shear strength.
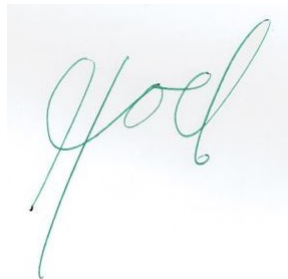
Preface

This report has been submitted as the master thesis in the spring of 2013 at the Norwegian University of Science and Technology, Faculty of Engineering Science and Technology, Department of Engineering Design and Materials.

This master thesis shall explore how a new buoyancy solution developed at NTNU will fail under the combination of buoyancy loads and hydrostatic pressure. The work presented is a continuation of a project thesis presented last semester, "New Deepwater Buoyancy Solution" by Eirik Hoel.

I thank my supervisor Professor Andreas Echtermeyer for inspirational guidance throughout the project. I would also like to thank Professor Nils Petter Vedvik for Abaqus support, and the students sharing my office for a great work environment.

I hereby declare that this thesis represents my own work.

Eirik Hoel

June 10, 2013

Trondheim

Contents

List of Figures

Chapter 1

Introduction

Subsea is the newest and most exciting part of the offshore oil and gas industry. Exploitation is continuously moving towards deeper waters in harsh environments. The discovery of new oil fields in ultra-deep or arctic waters presents new challenges and the industry must continuously develop new solutions for products and procedures in order to keep up with the changing scenery. Increased water depth results in increased riser weight. This substantiates the need for advanced buoyancy solutions. Reduced weight supported by the platform may reduce operating costs dramatically by enabling reduction of the required platform size. Deeper water also means that the components used in this environment needs to be able to handle the extreme hydrostatic pressure applied to the submerged structures.

Considering the sky-high operating costs of a platform and the substantial losses of income during a shutdown or workover, the demands for design life time are justified. Not only are the offshore conditions harsh, buoyancy components have to endure this environment for extensive lengths of time, usually 25 years. This makes the material selection crucial with regards to corrosion, wear and fatigue.

This report investigates the material properties of a newly developed material system for buoyancy applications, Compbuoy. The work is based on a project thesis about the design and analyses of buoyancy modules utilizing the Compbuoy material. Numerical analyses on the Compbuoy material used in buoyancy modules results in a list of design criteria and requirements from for the buoyancy material under operating conditions. Here, shear stress is identified as the critical stress parameter and the failure prediction performed in this thesis is based on this notion. Compbuoy buoyancy elements have been produced and tested both numerically and mechanically. The results are not considered to be final, as more development, testing, prototyping and the development of an industrial production method needs to be done before the project is ready.

Chapter 2

Background

2.1 Buoyancy modules

Buoyancy elements[1] are used for many different applications offshore, and a cheaper solution is of course desirable in all cases. Compbuoy is a NTNU based company who have developed a new material system for buoyancy applications, like riser pipe buoyancy modules.

A riser is essentially a simple pipe transferring fluids from the wellhead at seabed, to a skip or platform topside as shown in Figure 2.1.
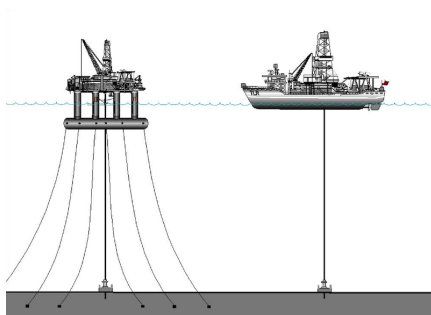
Figure 2.1: Riser from platform/ship to seabed

Buoyancy modules[2] are clamped on to a riser pipe with the main purpose to reduce the total weight of the riser assembly. The environment varies from warm, shallow waters, to arctic deep water operations, in order to reduce the amount of

---

[1] Also referred to as BEs
[2] Also referred to as BMs

customization needed for each project, the buoyancy elements should be able to operate in ultra deep waters. The design environment is 2500 meters below the surface, in cold water, with current forces in addition to the hydrostatic pressure acting on the construction. In this environment, the buoyancy system should be designed for an expected lifetime of 25 years. The buoyancy system consists of an external skin for protection, a clamping mechanism to attach the BMs to the riser pipe, and finally the element focused in this thesis, a light and robust buoyancy core material providing the buoyancy.

Buoyancy material

Buoyancy modules are used to reduce the total weight of the riser. The filling material in the buoys has to be as light as possible. Normally, syntactic foam is used. It has a density[28] between 380-720 kg/m^3. A material developed at NTNU, named Compbuoy, shown in Figure 2.2, has an expected density of 620 kg/m^3.
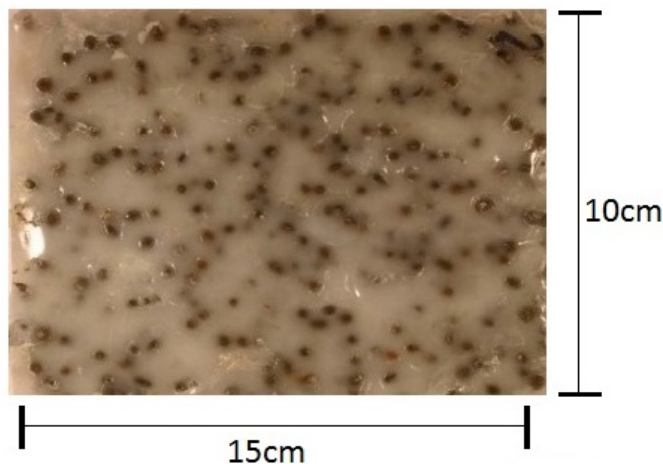
Figure 2.2: Compbuoy specimen. Adapted from[23]

The multiphase Compbuoy material consists of Leca pellets in a polypropylene[3] matrix. The most important difference between syntactic foam and Compbuoy is the price. The glass microspheres that make up the basis for syntactic foam are expensive and the cheapest grades start at 13 000 NOK/m^3, the Compbuoy material system uses a filler material with a cost of 500 NOK/m3[23, p.28]. This reduces the total price of the system significantly while still achieving the necessary material qualities.

---

[3]Also referred to as PP

2.2 Previous work

Eirik Hoel has in his Project Thesis created a design for the Compbuoy material in buoyancy elements, as shown in Figure 2.3.

<table>
<tr><td>(a)</td><td>(b)</td></tr>
</table>
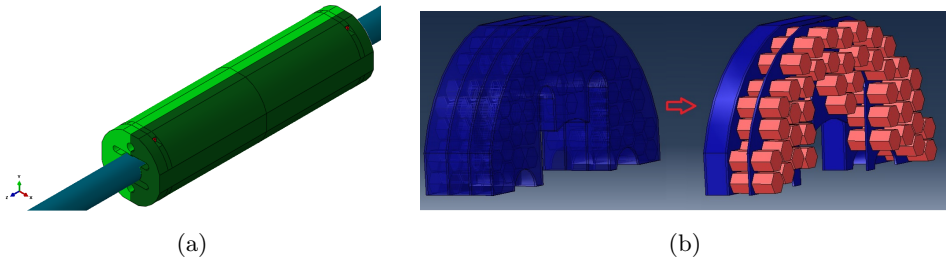
Figure 2.3: Buoyancy element design **(a)** Protective skin on riser pipe **(b)** Compbuoy elements in syntactic foam

Numerical testing of this system has been performed, and analyses show that during operating conditions, a critical factor is the shear stress in the Compbuoy elements. During simulations, the maximum shear stress was found in the path shown in Figure 2.4.
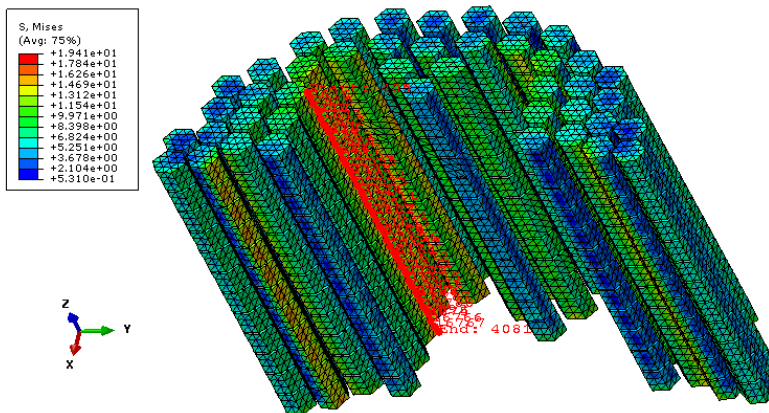
Figure 2.4: Path through the height of the Compbuoy element stack

The shear stress values found in this path are plotted in Figure 2.5.
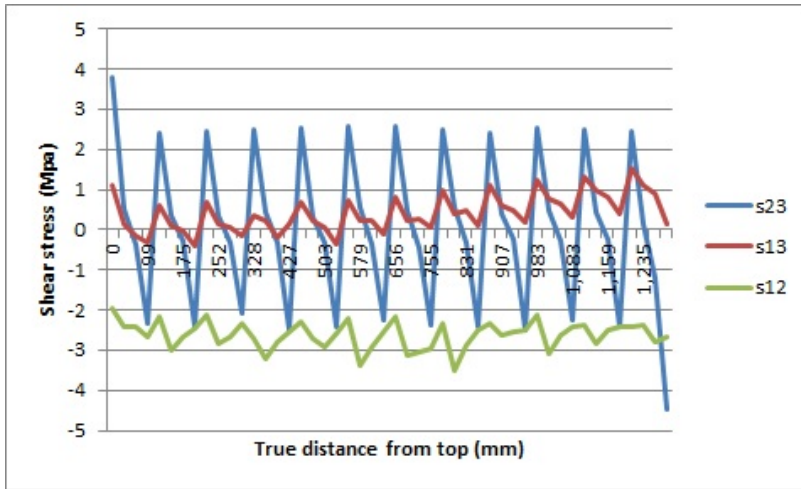
Figure 2.5: Plotted shear stress in Compbuoy element stack

The most critical factor is found to be shear stress, during operations, maximum shear stress the Compbuoy material will be exposed to is found to be 4 MPa. This is not including any safety factors. API Specication for Marine Drilling Riser Equipment uses a safety factor of 1.25 for the buoyancy material[3]. Consequently, the Compbuoy material is required to withstand shear stress of 5 MPa in order to reach the objective; "to develop and deliver cost leading insulation and buoyancy material for deep water applications"[4].

Chapter 3

Theory

Shear strength can be defined as a material's ability to resist forces that attempt to cause the internal structure of the material to slide against itself [32]. In buoyancy applications, the buoyancy material will be exposed to both a massive hydrostatic pressure and buoyancy forces. The proposed solution from previous work, Eirik Hoels project thesis "New Deepwater Buoyancy Solution" contains compbuoy elements in a syntactic foam matrix. Sufficient adhesion between the two materials is important to maintain the structure of the buoyancy material[1]. Shear stresses exceeding critical value will compromise the structural integrity.

3.1   Shear Strength

A failure in a polymer material can be viewed as any change of properties that makes the material structurally, functionally or aesthetically unacceptable. This can occur through different mechanical modes of failure of the polymers such as fracture, wear, creep or fatigue [30]

For ductile materials, the most common type of yield failure is caused by slipping. Slipping occur along the contact surface of molecule crystals in the material. These slipping planes are oriented with approximately $45\,°$ angle relative to the principal stress or tension direction. This phenomenon is caused by shear stress.

---

[1]In this thesis, sometimes referred to as BM

Where metals have the Von Mises yield criterion, composites have several failure criteria as shown in Figure 3.1[33].
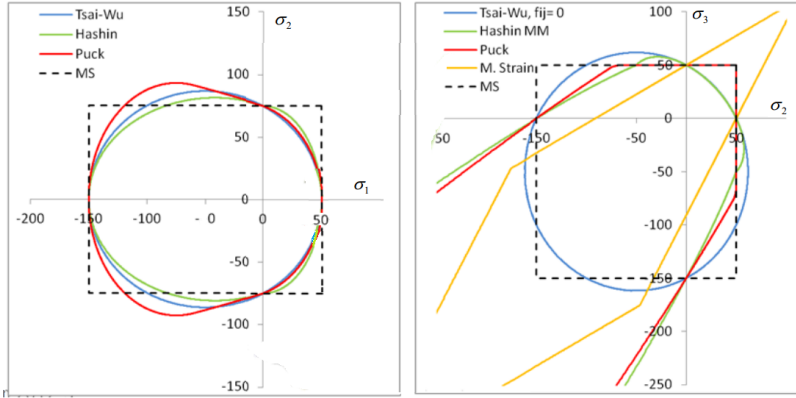
Figure 3.1: Graphic display of different composite failure criteria, adapted from[33]

One of the criteria in Figure 3.1, the Tresca yield criterion, also known as the maximum-shear-stress theory, is considered to be a conservative estimation of failure. Tresca states that for an isotropic material maximum shear stress is calculated by the following formula.

$$\tau_{max} = \sigma_{yield} * cos(\Theta) * cos(\Theta) \tag{3.1}$$

According to the theory of Tresca, yielding begins in the material when the absolute maximum shear stress exceeds the shear stress required to cause the same material to yield if subjected to pure axial tension. Because $cos(45)^2 = 0.5$, the shear stress has to be less than or equal to $\frac{\sigma_{yield}}{2}$ to avoid failure. σ_{yield} can be determined from a simple tensile test[13].

Shear Field

When a test sample breaks or suffers failure, the deformations are the result of a stress field induced by the loads applied to the sample. In case of a pure shear break, this stress field is called a shear field. The extent and the geometry of this stress field are important to control to be sure the failure is caused by shear alone, and not by bending moments, torque or other stress components in the sample. The stress field from the tests will be visualized in simulations presented in chapter 6. Two important variables that can cause changes to the stress field are the size of the nominal shearing zone and the thickness of the sample.

A stress field in a shear test is shown in figure 3.2, in this figure, red color indicates zero stress.
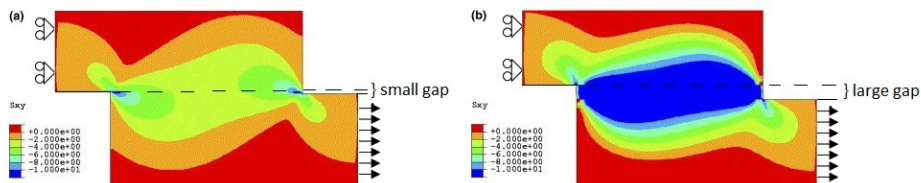
Figure 3.2: Difference in shear field due to difference in nominal shear zone. Adapted from[31]

Figure 3.2 is from a test where a solder joint on two copper bars was shear tested. The materials are not comparable to Leca pellets and PP, but the development of the stress field is nevertheless informative. One thing is clear from the visualization of the stress field, the increase from 0.06mm to 0.5mm solder thickness, while maintaining the same nominal strain, results in much larger span of stress in the sample. The reason for this given by the equation for nominal strain, shown in Equation 3.2, with a decreased thickness, the overall deformations are decreased and the shear load is transferred through the thin layer of solder which is heavily constrained to the copper[31].

$$\epsilon = \frac{\Delta L}{t} \tag{3.2}$$

In the case of shear testing the Compbuoy material, the correlation between sharing zone and stress field implies that aspiring to minimize the distance between the constrained parts, will decrease the interference of stress components other than shear, as the stress is concentrated in a small area, as shown to the left in Figure 3.2.

3.2 Material Properties

Some material properties other than shear strength needs to be defined before commencing shear strength testing. First it is important to understand the stress-strain curve, one example from a tensile test is shown in figure 3.3.
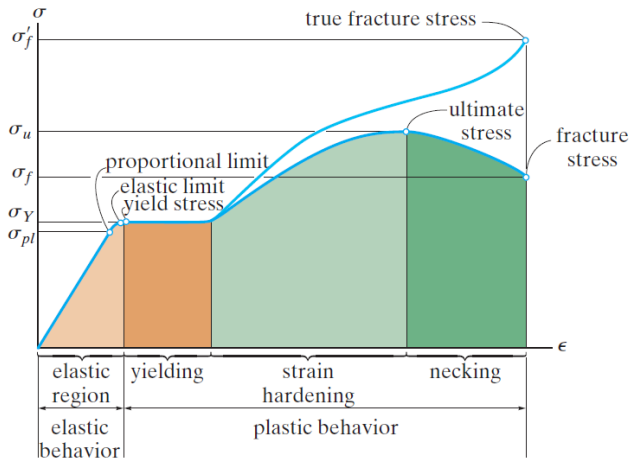
Figure 3.3: Example of a stress-strain diagram. Adapted from [13]

In a stress-strain diagram, two different curves can be plotted. True stress-strain curve or engineering stress-strain curve. The difference between true stress and engineering stress is the cross-section area used to calculate the stress. Engineering stress uses the same cross-section area during the entire test, the area measured before the test is started. True stress, however, is the current load divided by the actual cross-section area of the sample at the time the load was measured.

$$\sigma_{engineering} = \frac{F}{A_0} \qquad \sigma_{true} = \frac{F}{A} \qquad (3.3)$$

In this diagram (3.3) the material exhibits a linear elastic behavior up to the point of yield stress, σ_y. The yield point is the transition point where the behavior of the material shifts from elastic to plastic. In some materials, the stress at which the material changes from elastic to plastic behavior is not easily detected as the exact point where transition from linear to non-linear stress-strain curve may be hard to identify. A yield offset is used in these cases. For most metals, 0.2% is used. This is a line, constructed parallel to the linear section of the stress-strain curve, with an 0.002mm/mm (0.2%) offset from origin. The value of the yield offset varies with different materials, ranging from 0.01% to 1%. The standard value is considered 0.2% and is used in the analysis performed. [18][29][8].

The relationship between the hardness of a material and the yield stress can be

described as Equation 3.4.

$$H_v = \sigma_{yield} * c = \sigma_{yield} * 3 \tag{3.4}$$

The relationship is described by a widely used empirical equation where H_v is the hardness of the material and c is a material constant with a standard value of 3 for metals. This value can be obtained through the Vickers hardness test [35].

Strain beyond the elastic region will cause the material to suffer plastic deformations. After yielding, a load increase can be supported by the material, and the curve rises with a declining slope until it flattens out at a maximum stress on the engineering stress curve, referred to as the ultimate stress, σ_u. The strain hardening region is shown in figure 3.3 as the light green region. The specimen's cross-sectional area decreases fairly uniform over the length of the sample from yielding up to the ultimate stress, and this is the reason for the gap between true stress and engineering stress in this area. After the ultimate stress, the cross-section will decrease locally, this phenomenon is called necking. The cross-section area in this section of the specimen is reduced heavily and the gap between the two curves increases accordingly. The area of necking is highlighted in figure 3.3 with a dark green color. The specimen suffers total failure at the true fracture stress, σ_f'[13, p.84].

$$\sigma = E * \epsilon \tag{3.5}$$

In the elastic region of the stress-strain curve from a tensile test, the linear relationship between stress and strain can be expressed mathematically by Hooke's law, shown in Equation 3.5. E is a proportionality constant called Young's modulus or the modulus of elasticity.
In a shear test, as in a tensile test, the material subjected to shear will have a linear-elastic behavior that can be described by Hooke's law for shear.

$$\tau = G * \gamma \tag{3.6}$$

τ is the shear stress, γ is the shear strain and G is the shear modulus of elasticity given by the equation relating the shear modulus to the tensile modulus, Equation 3.7[20, p.25].

$$G = \frac{E}{2(1+\nu)} \tag{3.7}$$

In equation 3.7, ν is the Poisson's ratio, a material property relating the lateral and longitudinal strain of a sample, calculated by $\nu = \dfrac{-\epsilon_{lat}}{\epsilon_{long}}$.

The strain hardening exponent, noted as n, is a measure for the increase in hardness and strength caused by plastic deformation[19]. The value of the strain hardening exponent lies between 0 and 1. A value of 0 means that a material is a perfectly

plastic solid, while a value of 1 represents a 100% elastic solid. The flow curves of many homogeneous materials in the region of uniform plastic deformation can be expressed by the simple power law:

$$\sigma_{\mathrm{p}} = K\epsilon_{\mathrm{p}}^{\mathrm{n}} \qquad (3.8)$$

where σ_p is the true plastic stress, ϵ_p is the true plastic strain, n is the strain hardening exponent and K is the strength coefficient. The strength coefficient, K equals the stress at $\epsilon_p = 1.0$[9].

An important difference in terminology is that when talking about polymers as opposed to metals, σ_{yield} is considered the same as $\sigma_{ultimatestress}$, thus the maximum value of the engineering stress curve[24].

3.3   Abaqus terminology

Abaqus, the CAE[2]-software used for the numerical analyses, defines shear with a 1,2,3 coordinate system instead of z,y,z. Normally, shear stress is defined as shown in figure 3.4.
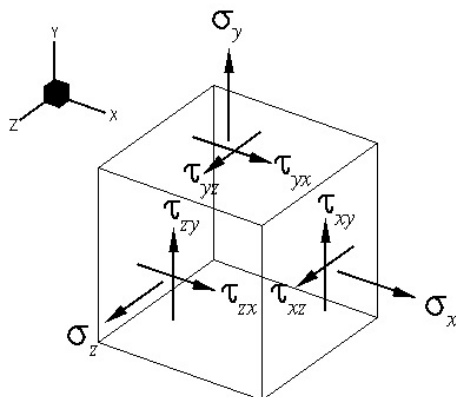
Figure 3.4: Shear stress on cube in Abaqus

Shear stress in Abaqus is named s13, s31, s23, s32, s12 and s21. The first number defines which plane the shear is in, and the second number defines the direction. s13 means shear in the 3-direction, on a plane perpendicular to the 1-axis, the 2-3-plane.

The same transformation from stress in x,y,z to 1,2,3 also applies to deformations and forces.

---

[2]CAE means computer aided engineering

3.4 Polypropylene

The BEs are made from a mixture of LECA pellets and polypropylene. Two types of polypropylene[3] was investigated in this report, BH345MO and BJ356MO. Complete data sheets for the two plastic materials and LECA pellets are given in Appendix B, Table 3.1 shows some important properties.

	BH345MO	BJ356MO
Melt Flow Rate (ISO 1133) (230 °C /2,16 kg)	45 g/10min	100 g/10min
Density (ISO 1183)	904 kg/m^3	906 kg/m^3
Tensile Modulus (1 mm/min) (ISO 527-2)	1.400 MPa	1.650 MPa
Tensile Stress at Yield (50 mm/min) (ISO 527-2)	26 MPa	29 MPa
Charpy Impact Strength, notched (23 °C) (ISO 179)	6,5 kJ/m^2	4,5 kJ/m^2
Hardness, Rockwell (R-scale) (ISO 2039-2)	89	93

Table 3.1: Characteristics of polymers

The newest BEs use BJ356MO and the BEs produced some time ago are made from the BH345MO polymer. BJ356MO was chosen over BH345MO because of the increased melt flow rate[4], and consequently a better distribution of polymer in between the LECA pellets during production. Higher melt flow rate means that the molecular chains the material consists of are shorter. There are, of course, several parameters affecting the properties of a polymer, and two different polymers with the same MFR can have significant differences in properties. However, changes to the MFR have implications for both the conversion and for end-use performance. Increased MFR is associated with enhanced mold packing and reduced levels of shrinkage in the production of the BEs. Related to physical performance, rigidity and resistance to creep is increased, while abuse resistance and impact strength declines[14]. Therefore, it is not unexpected that when BJ356MO has 122% increased MFR compared to BH345MO, the tensile modulus and yield stress are increased with respectively 17.8% and 11.5% as the impact strength of BJ356MO is 30% lower than BH345MO.

The relation between shear module and Young's modulus described in Equation 3.7 is an argument to expect a higher shear strength in the test specimens made from BH345MO. However, higher melt flow rate may prove to increase the shear strength found in the tests as well. Testing of shear strength in polymers is based on the principle that a small area is exposed to pure shear. This small area however, will in a plate of pure polypropylene consist of a semi-homogeneous material with thousands of molecules. In the Compbuoy BEs, this is not the case. The LECA pellets have a diameter between 2-4 mm. Most polymer shear tests recommend test samples with less than 12 mm thickness (ASTM D7078, ASTM D5379, ASTM D732)[6][5][7].

---

[3]In this thesis, sometimes referred to as PP

[4]Melt flow rate is sometimes referred to as MFR in this report

In an "unlucky" situation the sample may only have two 4 mm LECA pellets in the cross-section of the shear zone[5]. This can not be considered anywhere near homogeneous, and therefore, the results may be considered invalid. Also, the randomness in the distribution of LECA pellets combined with a low MFR can result in three LECA pellets situated in contact with each other without an absorbing layer of PP between the pellets. This may cause a crack initiation through the PP matrix, as the pellets are very brittle, and result in a much lower measured shear strength.

3.5   LECA pellets

Leca is the brand name for light weight expanded clay aggregate. Leca pellets are produced from natural clay which is expanded in a rotary kiln at approximately 1200 °C to produce sphere shaped granulates. This makes grains that are porous with a ceramic surface[11].
Leca pellets are commonly used as geotechnical fillings and in lightweight concrete, or they can be casted in square blocks and used in construction. It is a versatile material with advantages of light weight, high durability and excellent sound and thermal insulating properties due to the porosity and air pockets within the pellets.[26]

Leca pellets are produced in different sizes, the Norwegian company Weber-Norge produce Leca pellets with a diameter ranging from 2-32 mm. The pellets used in the production of Compbuoy's BEs are called "Leca lettklinker" and have a diameter between 2-4 mm. Collecting accurate data on these pellets proved to be a challenge. The only information Weber-Norge could supply, was a comprehensive SINTEF report on 8 different Leca products from 7 different manufacturers. The problem is that none of these products have the same size as the pellets used by Compbuoy. In the report, two products from Weber-Norge are tested, fraction 10-20 mm and 4-32 mm. A representative from the company recommended to use data from the 10-20 mm fraction as a substitute for the missing data for the 2-4 mm fraction. Data given by the manufacturers of Leca states that the Leca pellets used in the Compbuoy material has a dry loose bulk density of 275 kg/m^3 and a bulk crushing resistance of 1.39 MPa on a vibration compacted sample[15].

---

[5]In this report, shear zone is defined as the unconstrained area between the punch tool and the die surface.

Chapter 4

Production of Compbuoy Buoyancy Elements

Before testing the Compbuoy material it is important to know how the samples are produced. Therefore, a short description of the production method follows.

The Compbuoy samples being produced consists of a core and a coating. The core is made up of Leca pellets and PP pellets structured as shown in figure 4.1b. The PP and Leca pellets are alternately distributed evenly in a mold, as shown in Figure 4.1a. The Leca and PP mix are placed in a mold and heat treated in

(a)	(b)
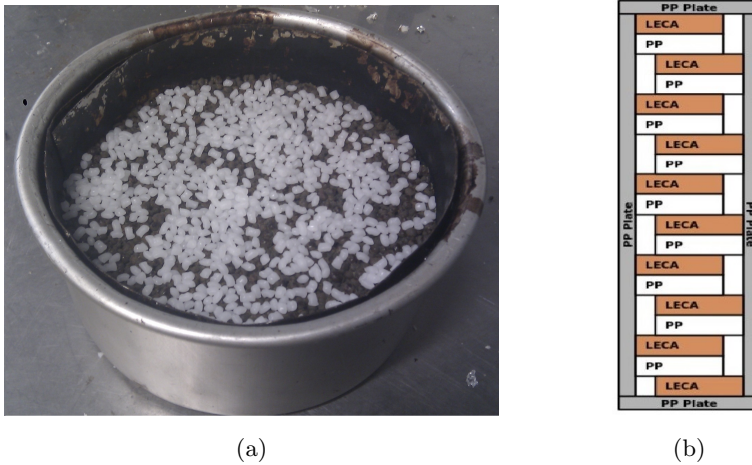
Figure 4.1: Compbuoy core **(a)**Sample in production, top view **(b)** PP and Leca structure

an oven for several hours following a specific heat treatment program as shown in Figure 4.2. The details of the heat program is confidential information and for this reason the axis in the heat diagram is without values. In some cases the Compbuoy
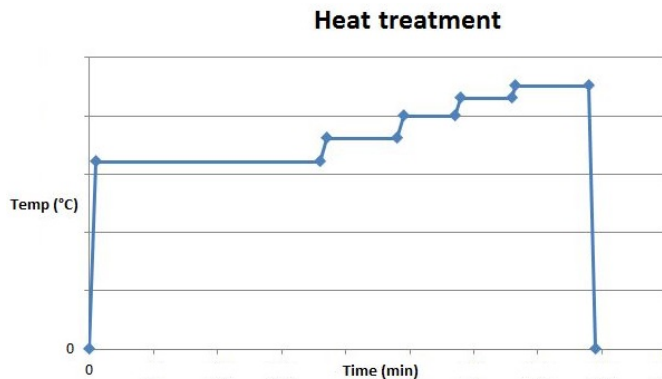
Figure 4.2: Temperature program for Compbouy

samples are produced with a polyethylene[1] coating around the core, this layer of PE makes the sample more water resistant. In the shear tests performed however, this layer is removed, and PE is not a part of the analyses performed in this thesis. The produced sample, after having cooled in room temperature, is shown in Figure 4.3. The melted PP has sinked a bit so that the top of the sample consists mostly of Leca, and the bottom of the sample consists mostly of PP. When producing test specimens from this sample, both the top and the bottom is cut away, and the test specimens are created from the center of this sample.

(a)   (b)
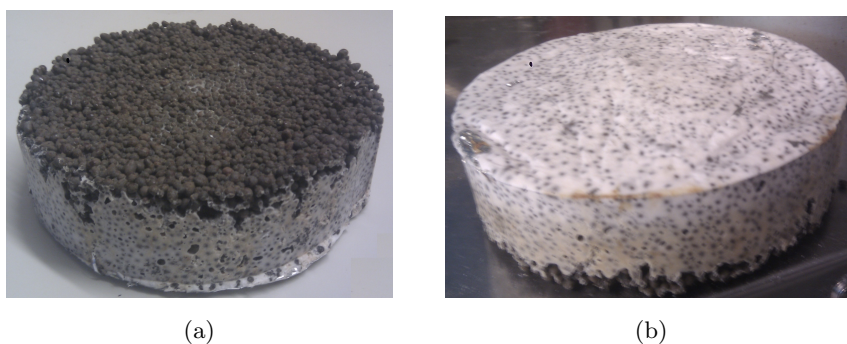
Figure 4.3: Compbuoy core **(a)**Produced sample, top view **(b)**Produced sample, bottom view

---

[1]In this thesis, sometimes referred to as PE

Chapter 5

Objective

As NTNU has developed a new type of buoyancy solution, this project shall explore how the Compbuoy material will fail under the combination of buoyancy loads and pressure. Earlier works has shown that the shear strength of Compbuoy is a critical parameter. To investigate the shear strength of Compbuoy, representative buoyancy elements shall be selected and their failure mechanisms and strength when exposed to shear forces shall be analyzed.

To analyze the shear failure and shear strength of Compbuoy, both analytical simulations and physical testing in the lab will be performed. A shear strength test procedure from ASTM, D-732, is used as guide for the testing. This test uses a punch tool to penetrate a polymer sample and measures the strength of the material. The ASTM D-732 test setup is shown in figure 5.1. This design will be replicated and modified in both CAE-software and in the mechanical lab at NTNU.
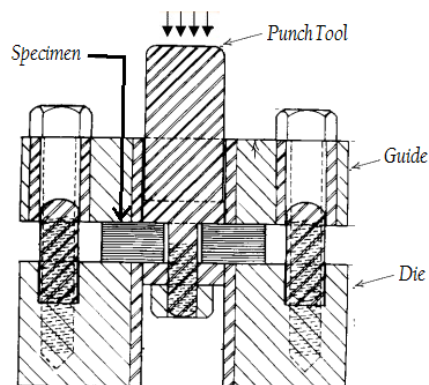
Figure 5.1: Cross-sectional view of ASTM test rig. Adapted from[7]

Chapter 6

Computer Aided Engineering

When testing the Compbuoy material shear strength, important issues are the sample thickness and the stress field induced by the test, as discussed in chapter 3. In order to further investigate these elements, a 3D-model is created and the shear test is simulated. The reason for doing this is to ensure that the stress component breaking the sample, is in fact shear stress. Also, it is interesting to see how the stress field develop through the thickness of the sample. The results may indicate a need for a thickness reduction if the stress field spreads far outside the shear zone after a given thickness. It may also indicate a need for an increase of thickness if the stress field shows large inconsistencies around the Leca pellets.

Two models are created. One where the Leca pellets have remained completely intact, and one where the Leca pellets have been completely crushed by the hydrostatic pressure. The reason for the two models is the investigation of the Compbuoy samples after pressure testing. This revealed that several of the pellets were completely crushed. The hollow sphere in the PP however, was remained intact, but containing nothing but Leca dust. To emulate this, a "worst case scenario"-model is created where all Leca pellets have been crushed, leaving only PP with hollow spheres in the model.

6.1 Modeling

Two models of the shear test specimens were created in Abaqus. One with Leca-pellets, and one with hollow spheres in the polypropylene specimens. The modeling

18

procedure was as follows. First, a circular solid with 50 mm outer diameter was extruded to a thickness of 2.5 mm. One quarter of the circle was partitioned out, and the rest was deleted. On the surface, 18 circles with diameters between 1.5 and 2 mm was drawn as shown in Figure 6.1.
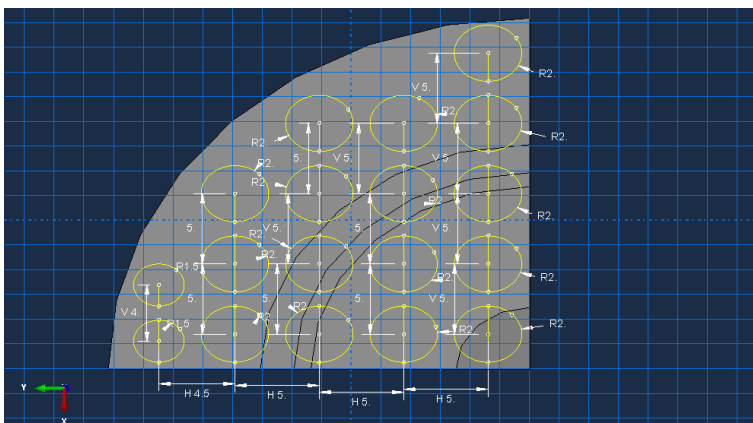
Figure 6.1: Sketch of the circles

Different approaches were used to create the Leca pellets and the air bubbles in the PP. When creating an empty void, the circles from figure 6.1 was revolved with the function "cut revolve" 180 °C around the center line of the circle. This removes the content within the revolved circle, leaving hollow spheres as shown in Figure 6.2.
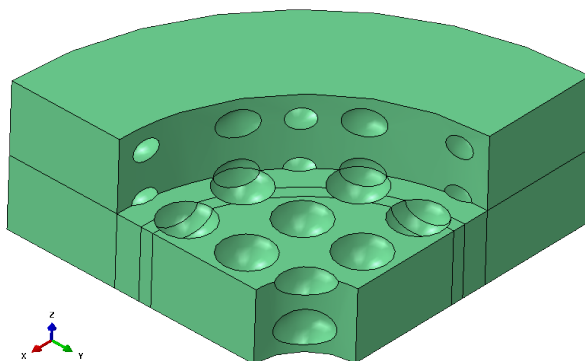
Figure 6.2: Hollow spheres in the PP block

In order to create Leca-pellets in the PP, it was necessary to partition out a sphere from the solid part. To do this, the command "Partition Cell: Extrude/Sweep Edges" was used. The circles sketched in 6.1 was modified to open semicircles to form the profile of the sweep in the xy-plane. On a plane perpendicular to xy-plane,

the path of the sweep is sketched, as shown in Figure 6.3.
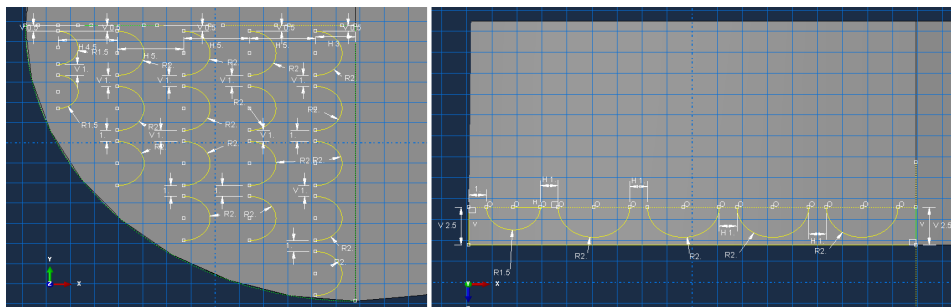
Figure 6.3: Pellet partitioning. Left: Sweep Profile. Right: Sweep Path

One by one the profiles was swept along the corresponding curved line of the path-sketch. This formed a hemisphere. The section of the solid part above the cross-section of the hemisphere was deleted, and the section below the cross-section was mirrored about the xy-plane on which the cross-section was located. This creates a solid cylindrical part with solid spheres partitioned inside, as shown in Figure 6.4 where one section of PP has been removed to show the Leca pellets.
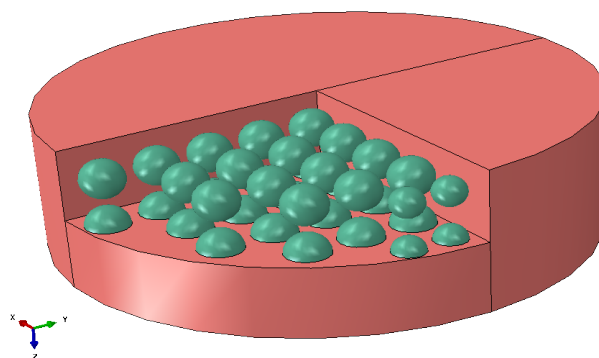
Figure 6.4: Partitions. Red: PP-partition. Green: Leca-partition

An alternative way to model the Leca pellets is to create the PP cylinder with empty spheres, and separately create the Leca pellets as a different part. The pellets can be placed inside the hollow spheres and constrained to the PP surfaces. This is, however, a lot of work, and the material properties of the interaction between PP and Leca is not easily obtained. By creating everything as one solid partitioned into two materials, Abaqus "understands" they are bonded together, and no further adhesive behavior constraints are needed.

6.2 Material properties and interactions

In the shear testing, three material were used: Polypropylene and Leca in the Compbuoy elements, and steel in the test rig. Steel is so strong compared to the two other materials in the test, that the steel parts are modeled as discrete rigid parts in Abaqus for convenience. Polypropylene and Leca are defined in Abaqus to best emulate the real behavior.

Polypropylene

The manufacturers of the polypropylene used in Compbuoy, a company named Borealis, was not able to supply documentation of the stress-strain curves. This could have been acquired with a tensile test, but this was not performed due to the time limitation. Instead, a comparable polypropylene, commercially named APPRYL 3020 BN1 was used to plot the plasticity in Abaqus. The stress-strain-curve is shown in Figure 6.5. The Appryl polypropylene was considered comparable as it has a density of 902 g/cc, and a tensile yield stress of 26.5 MPa, both values relatively similar to the BJ365MO and the BH345MO[25][21].
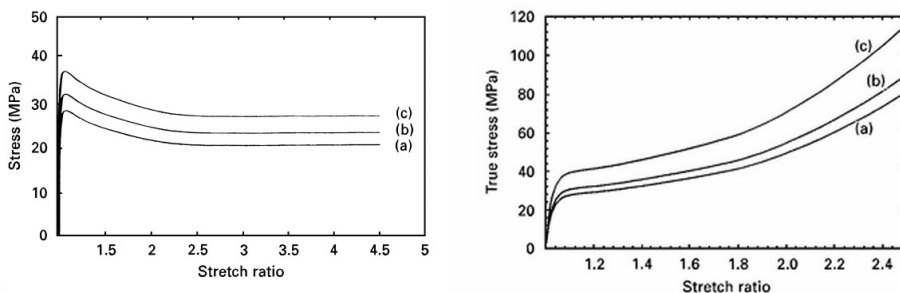
Figure 6.5: Stress-strain curve at cross-head speeds of (a) 0.1 mm/min, (b) 1.0 mm/min and (c) 10 mm/min

There are different approaches to model the plastic behavior of PP in Abaqus. One way is to plot the elastic behavior and the plastic behavior separately, extracting values from the stress-strain diagram as shown in Figure 6.5. Another way is to create a deformation plasticity damage model. For this, Abaqus requires data from the following mechanical properties: Young's Modulus, Poisson's Ratio, yield stress, strain hardening exponent and the yield offset[2, 23.2.13]. Both of these ways to model the PP were performed, but the deformation plasticity model is only presented in Appendix D because some of the input data had to be estimated and the results were not considered to be realistic.

Young's Modulus and the tensile yield stress are given in the BJ356MO material data sheets as 1650 MPa and 29 MPa, presented in Appendix B.

The Poisson's Ratio for polypropylene is found to be 0.45[16].

To supply Abaqus with data for the plastic behavior, Figure 6.6 was created to extract the true plastic strain from the stress-strain curve. The red lines indicate the elastic strain, and the plastic strain is the total strain minus the elastic strain. The values are plotted in Table 6.1.
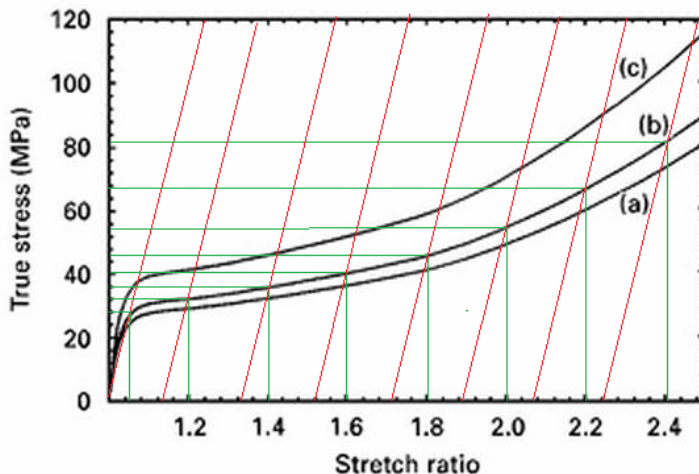
Figure 6.6: True plastic strain plot for PP

True Stress	Plastic Engineering Strain	Plastic True Strain
29 MPa	0	0
32 MPa	0.13	0.122
36 MPa	0.33	0.285
40 MPa	0.52	0.418
46 MPa	0.71	0.536
56 MPa	0.89	0.636
67 MPa	1.07	0.727
82 MPa	1.24	0.806

Table 6.1: Plastic strain plot

Leca

Two ways to model Leca in Abaqus were considered. One way was to model the pellets as tiny balls of regular concrete due to the lack of material properties data for Leca. This was done using the "concrete damaged plasticity model" featured in Abaqus. The other way to do it was to consider the Leca as an isotropic homogeneous material and defining the material using the stress-strain curve to define elastic and plastic properties.

The concrete damaged plasticity model requires input of the following data: Dilation Angle, ψ, in degrees. Eccentricity, ϵ, defines the rate at which the hyperbolic flow potential approaches its asymptote. $\dfrac{\sigma_{b0}}{\sigma_{c0}}$, the ratio of initial equibiaxial compressive yield stress to initial uniaxial compressive yield stress. K_c, the ratio of the second stress invariant on the tensile meridian, to that on the compressive meridian. And finally μ, a viscosity parameter.

Modeling Leca as a brittle, rather than a plastic material is more accurate as the Leca pellets are very brittle, as shown by the ceramic voided structure in Figure 6.7. However, due to the lack of material properties for Leca, concrete properties was used. This might be a good approximation, but because of the uncertainty in the validity of these properties, the simulations performed using this material definition are only presented in Appendix D.
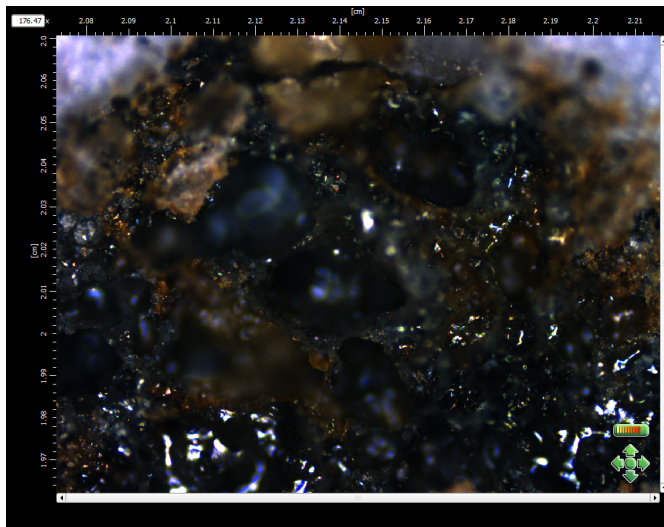
Figure 6.7: Leca pellet investigated in a confocal microscope

When considering Leca as an isotropic material, stress-strain curves provided by the manufacturer of the pellets are analyzed. The curves are shown in Figure 6.8.

(a)

(b)
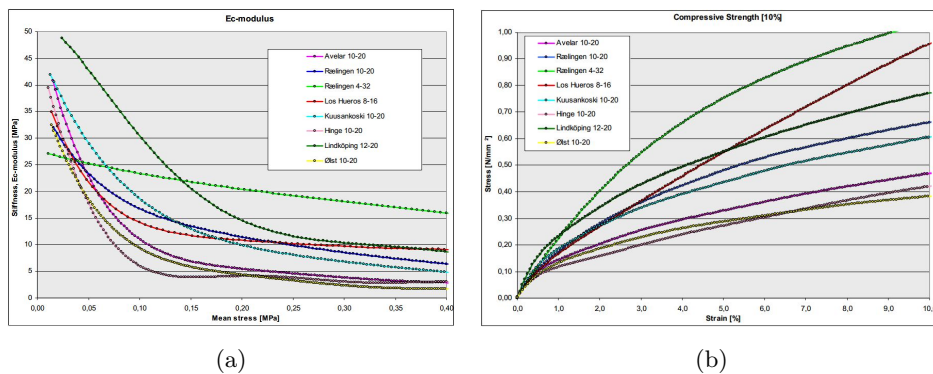
Figure 6.8: **(a)**E_c-modulus plots of the combined linear fit of all modulus. **(b)**Average plots of the compressive strength at maximum strain (10 %). Adapted from [15].

The E-module for Leca is extracted from figure 6.8a to be between 17 and 28 MPa depending of the mean stress in the sample. The starting value is set to be 28 MPa. The yield stress however is not easy to extract from figure 6.8b. The plotted line has more or less the same curvature over the given interval and determining an exact point of yield is difficult. However, drawing a linear line from the origin gives an approximation to the yield point at 2.6% strain, 0.5 MPa. The plastic behavior of Leca is extracted from Figure 6.8b and plotted, as shown in Table 6.2.

Yield Stress	Plastic Strain
0.5 MPa	0
0.7 MPa	0.8%
0.9 MPa	2.4%
1.0 MPa	3.9%

Table 6.2: Plastic strain plot

It is important to emphasize that Leca is not a homogeneous isotropic material. Neither will Leca pellets display the plastic behavior described in this section. The stress-strain curves are from compression bulk tests, not one Leca pellet tested. As Leca is a ceramic material, plastic strain of 10% will not be possible, it will break. The curves in Figure 6.8b show how the pellets crush in contact with each other, which increases the contact area thus reducing the stress, and the slope of the curve flattens. Even though the material properties does not describe the behavior of a singular pellet, it is considered a good approximation when simulating the test up till failure.

Loads and Boundary Conditions

The shear test in the lab was performed with a punch tool displacement of 1.24 mm/min, or 0.020666 mm/sec. This displacement is sustained from before the punch tool touches the sample, and till it has penetrated through the entire thickness of the sample. To simulate this, a velocity boundary condition was applied to a rigid surface acting as the punch tool, the punch is placed onto the center surfaces, as shown in Figure 6.9. The cross-head speed of the punch was controlled by defining the time of the step in the simulation. The setup for a 1 mm penetration test is shown in Table 6.3. To simulate a penetration of 2 mm, the only value needed to be changed is the time period of the step.
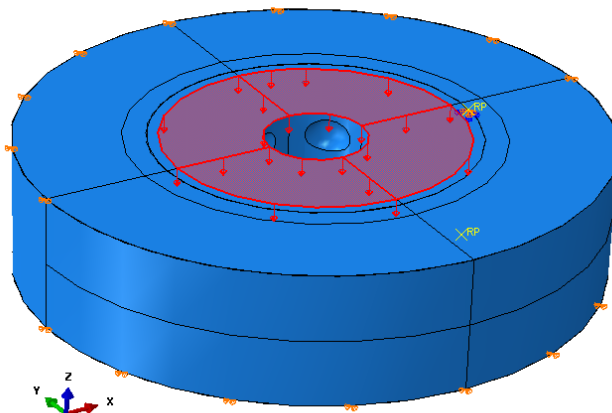
Figure 6.9: Displacement control applied to the punched surfaces

Time period of the step	$\dfrac{1\,\text{mm}}{1.24\,\text{mm/min}} = 48.38\,\text{s}$
Initial time increment	$1\,\text{s}$
Minimum time increment	$0.05\,\text{s}$
Maximum time increment	$5\,\text{s}$
Velocity displacement	$0.020666\,\text{mm/s}$

Table 6.3: Specified amplitude of the punch displacement

To investigate the effect of the cross-head speed during the test, a static simulation with no velocity defined was performed. Instead, only the displacement length was

defined. In this case, Abaqus considers the displacement rate to be infinite low, and large discrepancy in the results from these two analyses would indicate that the displacement rate in the test is too high. No deviations were found, meaning that the cross-head speed is valid for a static analysis.

There are no applied loads in the x- or y-direction. Nevertheless, if the model is not constrained in these directions, it will float around in the x-y-plane. This is avoided by constraining nodes on the outer diameter of the sample in both x and y-direction. Because the sample is not exposed to loads in these directions, and will not experience expansion or shrinkage of the outer diameter (observed during testing), this boundary condition will not compromise the validity of the results. To make sure this assumption is correct, a simulation with only one node constrained in x and y-direction was performed and the results compared without finding noticeable deviations. This would allow for expansion/shrinkage of the sample.

The main boundary condition issue in the simulations was how to constrain the top and bottom surface. The most realistic way to constrain the sample, is to create two plates acting like the guide plate and die plate in the test rig. In the test, these plates are made in steel, in Abaqus, the plates are modeled as rigid shells. The deformation of the plates are insignificant and this approximation is therefore considered valid. The rigid plates are shown in Figure 6.10, the green part is the Compbuoy sample and the red parts are the rigid plates.
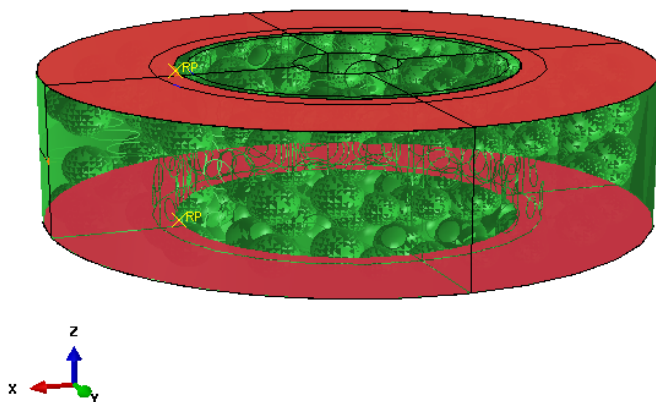
Figure 6.10: Rigid shell plates to constrain the sample

The rigid plates are given reference points and constrained with no movement in any directions. Contact properties between the sample and the plates are defined. A tangential behavior with friction coefficient of 0.5 and a normal direction behavior defined as "hard contact" to simplify the analyses and prevent any unwanted deformations of the sample.

6.3   Mesh

After the modeling was complete, all parts had to be meshed. Meshing a perfect square is no problem, but the more complex the geometry of the part is, the more challenging the meshing becomes. The two models to be meshed are very similar, and the same meshing strategy is used on both.

Due to the complex geometry containing spheres inside the body, Abaqus considers the part unmeshable using hexahedral elements such as C3D8R, or wedge elements like C3D6. To mesh the part tetrahedral elements are used. The simulations performed will deform the materials until failure, thus into the plastic region of the stress-strain curve. Unlike deformations where the stress is below the yield stress, large plastic deformations requires a non-linear approach. The selected element type is a 3D stress element with a quadratic (as opposed to linear) geometric order, 4 integration points and 10 nodes called C3D10. For the model with Leca pellets intact, a variation of this element, called C3D10I was used on the exterior surface of the Leca Pellets. This was done because the C3D10I has an improved surface stress formulation which calculates the stress directly on the surface and is recommended for simulations with surface to surface contact. The C3D10I was not used on the PP section of the model as it has a slight performance degradation relative to the C3D10[2][1]

To reduce the number of elements in the model and at the same time achieve a fine mesh in the critical areas, the command "Seed Edges" was used. The critical area is the nominal shear zone and the surrounding areas. Figure 6.11 shows the edges seeded manually highlighted in pink.
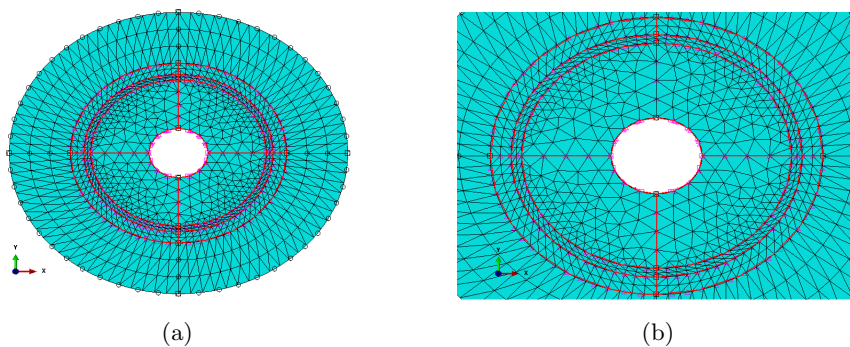
Figure 6.11: Part Mesh **(a)**Top view **(b)** Enhanced view

The part is seeded with a global element size of 2 mm. The area inside the shear zone has an element size of 1.5 mm, the unconstrained shear zone is given a 1 mm element size and the transition areas around the shear zone is given an element

---

[1]For this entire section the Abaqus Manual and Abaqus has been used as source of information.

size between $1\,\text{mm}$ and $1.5\,\text{mm}$.

A common problem is that the angle on tetrahedral elements can be too small, resulting in invalid results from the analysis. To counter this, the Abaqus feature, "verify mesh" was used. This tool checks the mesh to confirm that all angles are within the critical limits. Elements outside critical limits will be highlighted. Once identified, two main procedures were used to fix the problems. Local seeding, and partitioning of faces. To achieve a fine enough mesh, a generalized course of action for the meshing of all parts were: Mesh roughly, identify critical areas, seed edges, mesh, verify mesh, seed edges, mesh... repeat the last three steps until no error and an acceptable number and placement of warnings is achieved. Another way to check if the mesh is acceptable is to run the analysis, refine the mesh and then run the same analysis again. When the variation in results is negligible, a fine enough mesh is created. Mesh check is shown in Figure 6.12.

(a) (b)
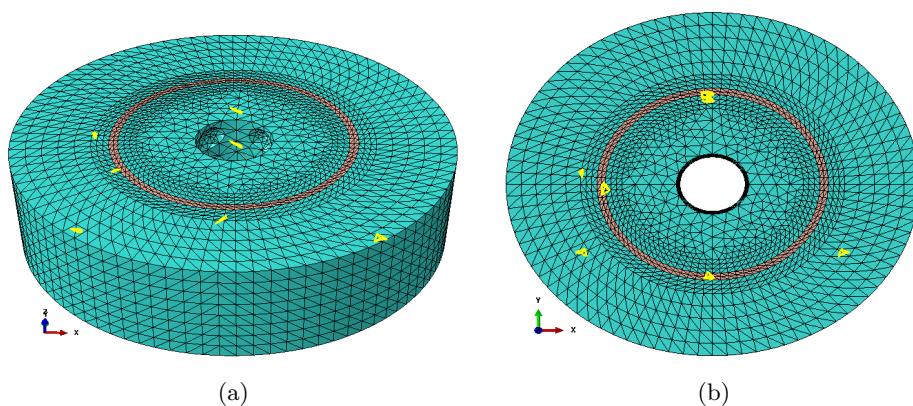
Figure 6.12: Verify mesh **(a)**Isometric view **(b)**Top view

The mesh check revealed no errors and 8 warnings, highlighted yellow in figure 6.12. The model consists of 170 000 elements which means only 0.0047% of the elements have warnings. It is important that the warnings are few and mostly placed outside critical areas, in this case the unconstrained shear zone. This mesh is considered acceptable.

The shell faces representing the test rig in the analyses also have to be meshed. Since the part is made as rigid shell, it will not be exposed to any deformations and thus the mesh do not have such significants. The shell is meshed with 4-node 3-D bilinear rigid quadrilateral R3D4-elements. When using quad elements, two types of mesh control algorithms are selectable, "Medial axis" or "Advancing front". The difference between the two alternatives is shown in Figure 6.13

Both algorithms create a mesh with no warnings or errors detected by the "verify mesh" feature in Abaqus. The circular cross section will require a mesh transition from large elements on the outer diameter, to smaller elements on the inner diame-
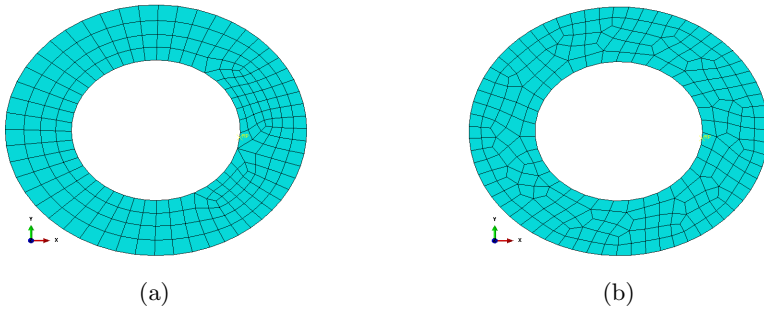
Figure 6.13: Part Mesh **(a)**Medial axis **(b)**Advancing front

ter. The algorithm "medial axis" creates smoother transitions because it does not follow the seeding to the same extent as advancing front. In this case, it is not critical, nevertheless, medial axis was selected because it creates a more homogeneous mesh.

When meshing the model with Leca pellets, the same seeding as in the model with hollow spheres was used. The automatic mesh generator was not able to create mesh on all of the pellets, as shown in Figure 6.14.
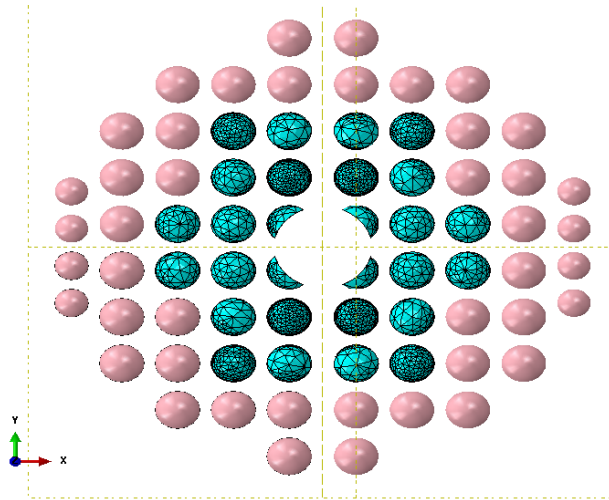
Figure 6.14: Meshing of leca pellets

To generate mesh on the spherical surfaces, they had to be partitioned. Datum planes was created to intercept all the pellets, and then meshed. The "verify mesh" feature detected no errors and 500 warnings in the mesh containing 330000 elements. Warnings on 0.15% of the elements, mostly outside the shear zone, is considered non-critical.

6.4 Simulations

Several simulations was performed to emulate the shear test in Abaqus. All simulations were attempts to replicate the same situation, and differ only slightly as experimental changes was made to the simulations to improve the results. The penetration stroke length is one of these changeable parameters. In the shear test, the punch tool was pushed all the way through the sample, even though the shear beak occurred after only a few millimeters of penetration. This was attempted in the Abaqus simulation as well, but this was not successful. To simulate the breakage of elements a damage model needs to be created to delete elements when they exceeds a max stress/deformation limit. Providing the necessary input for Abaqus to understand how to deform and delete elements is a complex and time consuming project, and this was dismissed. Instead, the shear test up to the point of breakage was simulated. Finding the exact point of failure required an iterative approach where the first estimate was very conservative, and the penetration length was increased for each simulation until the solution did not converge. Different penetration depths was simulated until the results show that the point of failure is included in the simulation.

Another important factor affecting the shear strength result in the simulation is the radius of the punch tool. Changing the radius of the punch tool can increase or decrease the number of pellets/spheres in the shear zone as shown in Figure 6.15.

(a)   (b)
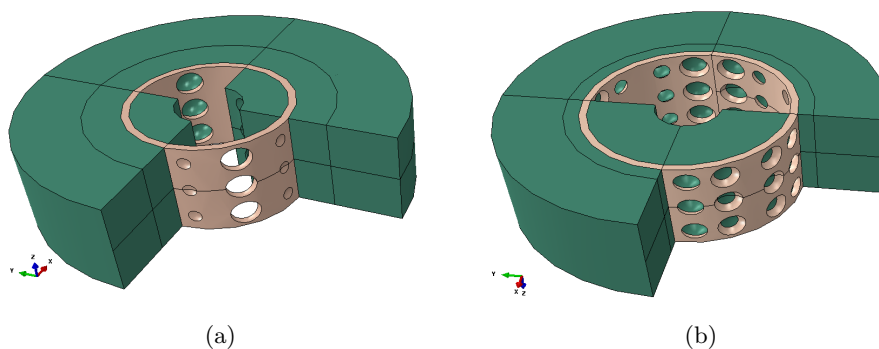
Figure 6.15: Shear zones with different tool radius **(a)**10 mm radius **(b)**13 mm radius

In the shear tests, the punch tool radius was 10 mm. Investigating the tested samples reveals that the shear zone has approximately three Leca pellets through the thickness of the sample. The number of pellets in the shear zone is considered more important than the punch tool radius to achieve comparable results. Therefore, the punch radius in the simulations deviates from the punch radius in the test, so that the number of pellets can be comparable in the simulation and the tests. For the model without Leca pellets, the aim is to create a "worst case" scenario, consequently, the punch tool radius was set to be 13 mm as shown in Figure 6.15b. For the Leca model, 10 mm punch tool radius was selected.

In Chapter 3 the effect of the width of the shear zone is discussed. In order to investigate this, models with 0.5, 1 and 2 mm wide shear zone, shown with brown color for 1 mm in Figure 6.15. The original model was 15 mm thick. In order to investigate the effect of sample thickness, a 10 mm thick model was created and simulated for comparison.

Chapter 7

CAE Results

In this chapter, the results from the simulations presented in the previous chapter. Investigation of the shear zone thickness, sample thickness and the development of shear stress in different areas of the model is performed and discussed. As stated in Section 2.2, the most interesting result is the shear stress in the sample, especially the shear stresses S_{13} and S_{23} which are shear in Z-direction of the samples. However, looking at displacements and Von Mises stress[1] in the model is useful when evaluating if the simulation performed is a realistic recreation of the mechanical tests.
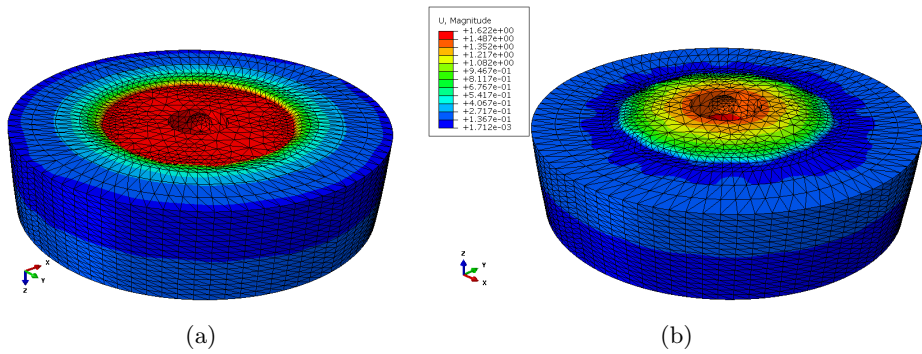
Figure 7.1: 1.5 mm penetration deformations **(a)**Top view **(b)**Bottom view

The deformations occurring during the simulations are similar to each other and to what was expected to happen. Figure 7.1 shows displacement in Z-direction. The center area is pushed down while the rest of the model is held in place. In the area of transition from red to blue color ,the shear zone, is where the material is

---

[1]Also referred to as mises stress

allowed to deform freely.

This deformation behavior is as shown in Figure 7.1 for all the simulations performed both with or without Leca pellets and also with different boundary conditions. Therefore, these illustrations are considered informative, not only for the simulations they are taken from, but for all simulations performed on the Compbuoy elements.

(a)   (b)
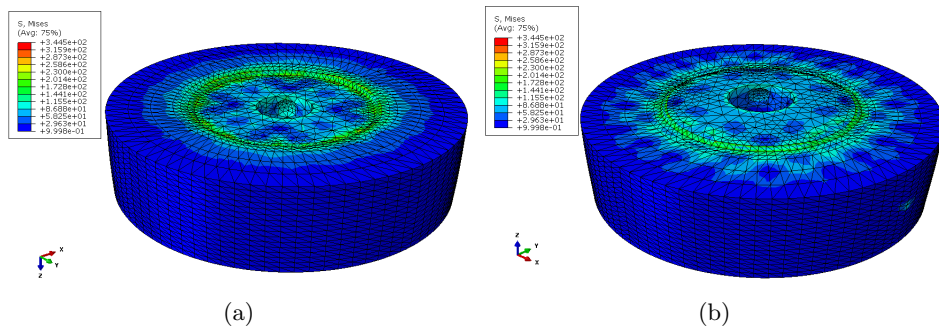
Figure 7.2: 1.5 mm penetration mises stress **(a)**Top view **(b)**Bottom view

Mises stress is good way to show the general stress situation in a sample, as it incorporates different stresses like shear, tensile and compressive stress into one value[20, p.21]. Figure 7.2 shows the mises stress in a simulation performed on a model without Leca pellets. The mises stress situation on the exterior surfaces is quite similar for all simulations performed both with or without Leca and for different thicknesses of the sample. From the figure it is clear that the most critical area is around the shear zone. This is expected as the transition area between the constrained area and the displaced area is where the mesh elements are most deformed. Another characteristic shown in Figure 7.2 is that the top of the sample has a much sharper transition from low to high stress and also higher concentrations of high stress areas than the bottom. This is related to the sharper geometrical transition on the top surface of the sample.

One of the fixed nodes constraining the model from movement in x-y-direction is shown in Figure 7.2b, the node is colored light blue which represents a stress between 18-40 MPa at 1 mm penetration of the punch tool. This value is considered low and not disruptive for the rest of the analysis as the mises stress in the critical parts of the model, at the same time, is more than 400% higher.

7.1 Test specimen thickness

Because both the model and the loads and boundary conditions are symmetrical, s23 in the y-z-plane equals s13 in the x-z-plane. Therefore, graphs and figures presented in this section will only picture one of the shear stresses, but the values will be valid for both stresses in the z-direction.

A concern with shear testing the Compbuoy material was the sample thickness. As discussed in Chapter 3, the issue is the trade-off between a homogeneous sample, and a pure shear break. Therefore a numerical approach was performed to investigate the effect of the sample thickness and estimate a critical value for this parameter.

Figure 7.3 shows the shear stress in the cross-section of samples with 10 and 15 mm thickness.

(a)

(b)
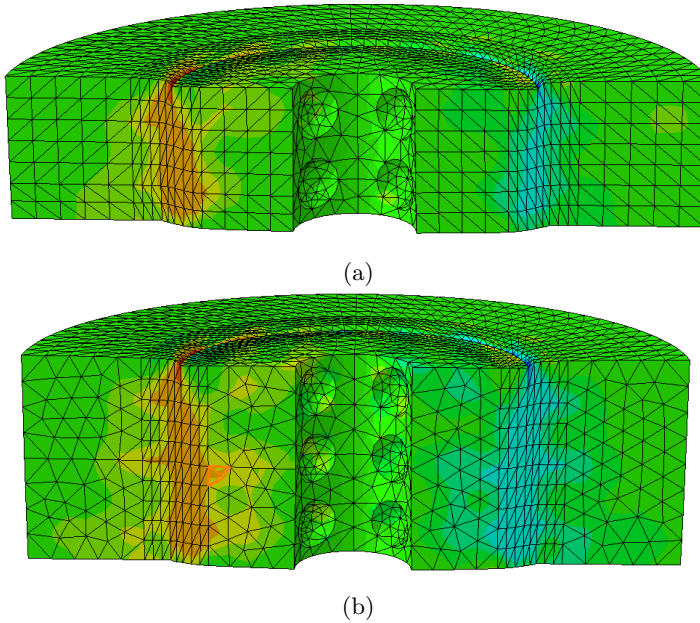
Figure 7.3: 1.5 mm penetration s23 stress **(a)**Top view **(b)**Bottom view

From the figures it is shown that the maximum stress is not very affected by the thickness as the orange areas are similar in both models. What significantly deviate in the models are the stresses surrounding the shear zone. In the thick model, almost the entire bottom surface is affected by shear stress as opposed to the thinner model where large areas in the bottom is colored dark green, indicating shear stress below 2 MPa.

In Figure 7.4, the mises stress in the same cross-sections as in Figure 7.3 is shown. Here we see the same tendency as in the the shear stress cross-section, in the cen-

(a)

(b)
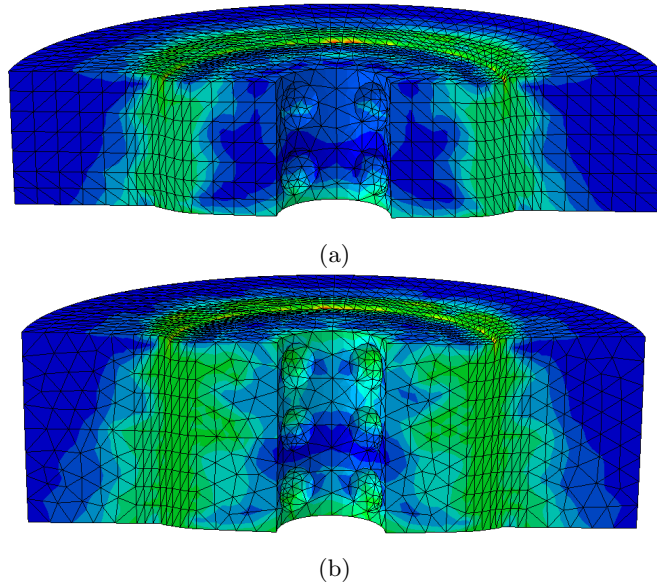
Figure 7.4: 1.5 mm penetration mises stress **(a)**Top view **(b)**Bottom view

ter of the shear zone, both models have mises stress just above 30 MPa. In the surrounding areas however, there are dissimilarities. To better show these dissimilarities, the stress values in a path created in the outermost part of the shear zone are plotted, as shown in Figure 7.5.
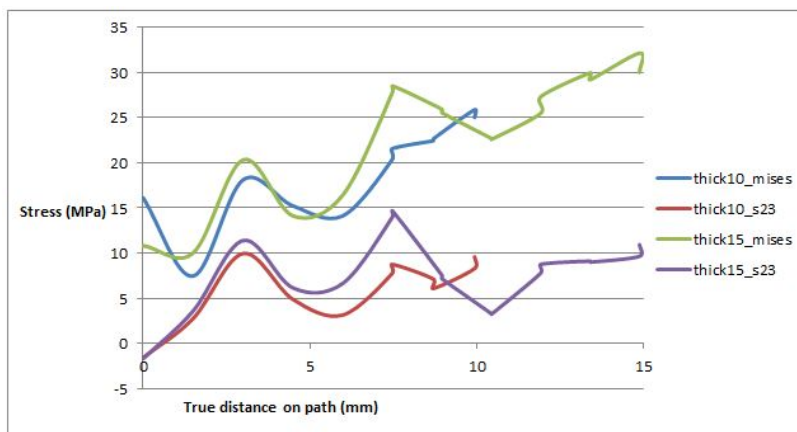
Figure 7.5: Mises and shear stress plotted through thickness of the cross-section for two models with different thicknesses

What is most interesting from the stress plot is the deviation between mises and shear as a function of thickness. The deviation is increasing, and this is further shown in Figure 7.6 where the y-axis shows the absolute value of mises stress minus shear stress. The shear stress fluctuates mostly between 5 and 10 MPa while the mises stress increase. The linear trend line is placed to emphasize the stress development through the thickness.
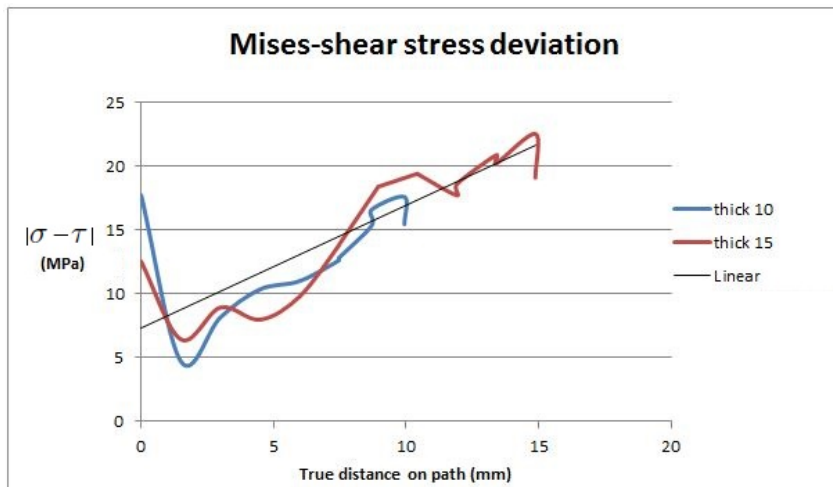
Figure 7.6: Deviation between mises and shear stress through thickness

The perfect scenario of the shear test is when the sample breaks in pure shear. The deviation between mises and shear stress is an indication of stress components other than shear. For a sample thickness of 10mm, the deviation is 15 MPa, for a sample thickness of 15 mm, the deviation is 20 MPa. Tables with the values from these graphs are shown in Appendix C.1.

7.2 Shear zone thickness

(a)   (b)
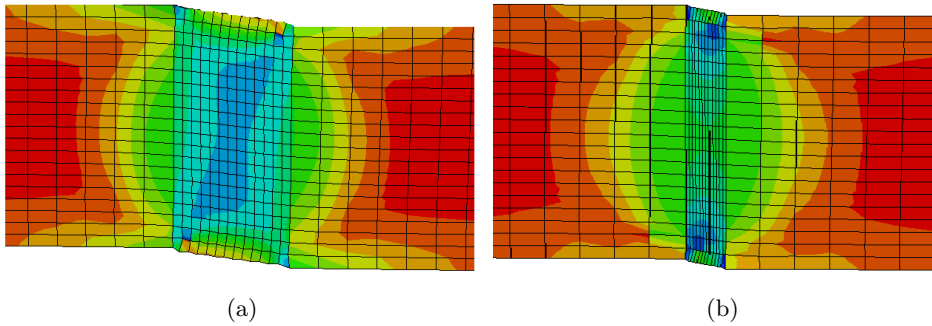
Figure 7.7: Shear stress with different shear zone thickness **(a)** 20 mm gap **(b)** 6 mm gap

Figure 7.7 shows a model created to illustrate the effect of shear zone thickness more clear than in the Compbuoy model. In this model the left side is fixed and the right side is given a downward displacement, while the center part is unconstrained. The two models in 7.7a and 7.7b both have maximum LE strain (logarithmic strain componenets at integration points) of 0.2. The shear stress plots show that the model with a large shear zone has much higher stress concentrations in the center than the model with a thin shear zone, as shown by the large blue area in 7.7a. The exact values are plotted in Figure 7.8. Values are extracted from a vertical path through the center of the shear zone in both models.
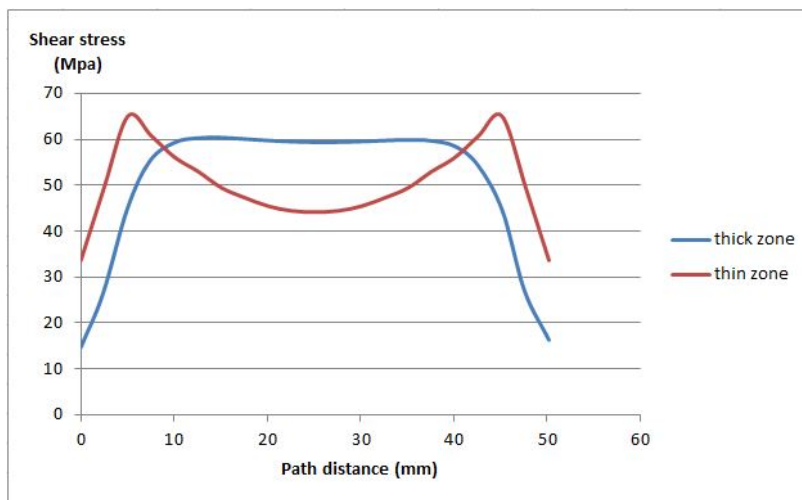
Figure 7.8: Shear stress plotted through thickness of two different shear zones

<div align="center">(a)   (b)</div>
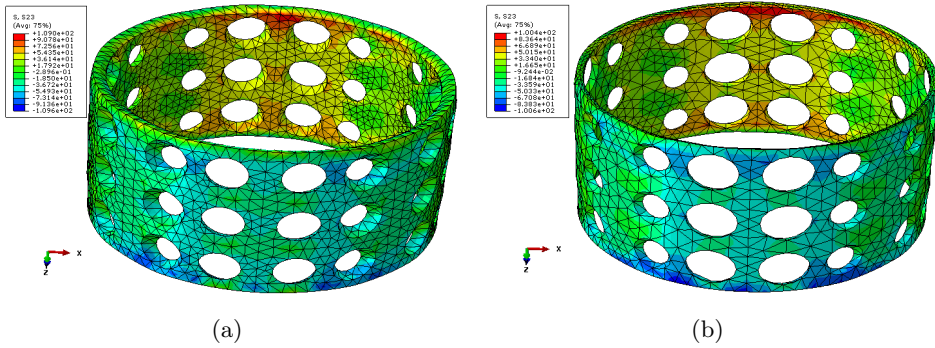
Figure 7.9: Shear stress s23 in shear zone **(a)** 1 mm gap **(b)** 0.5 mm gap

Figure 7.9 shows the shear stress in shear zone with different thicknesses. The critical areas with respect to s23 stress, are the surfaces perpendicular to the y-axis. Correspondingly, these surfaces are the least critical once with respect to s13 stress. In Figure 7.9b most of the critical surfaces are colored yellow with stress between 33 and 50 MPa. Between the hollow spheres, small areas of orange are formed, this implies stress between 50-66 MPa. In Figure 7.9a, the stress situation is quite similar, but the orange areas have developed further, and orange implies in this model stresses between 54-73 MPa.
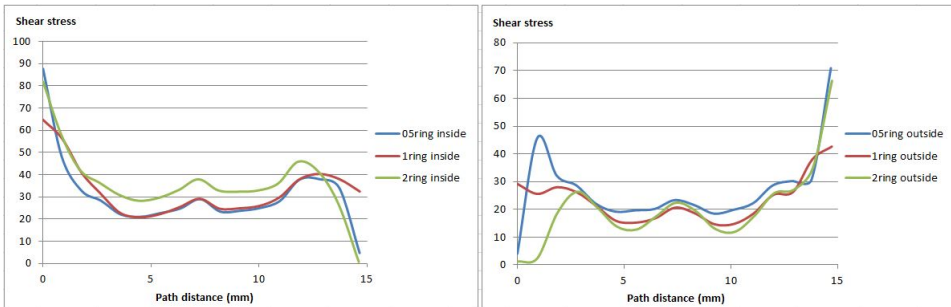
Figure 7.10: Shear stress for three different shear zones

7.3   Failure analysis

An interesting thing to use the numerical test simulation for is to estimate the point of failure. The time in the simulation where the sample fails in compressive yield. To do this, the shear stress in z-direction in the shear zone is considered. Because of the holes in the model, the stress varies a lot in the shear zone, as shown in Figure 7.11. In this model the stress is transformed using a cylindrical coordinate system, s13 is shear in z-direction on a plane perpendicular to the radial direction.
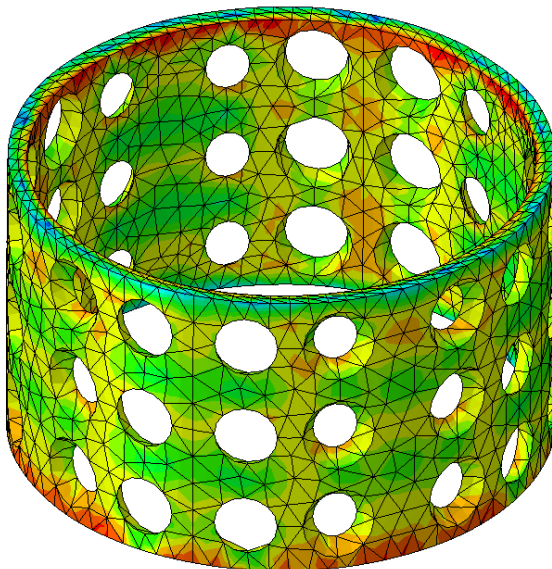
Figure 7.11: Shear zone, s13 varies over the cross-section

Point of failure identification can by done by evaluating the cross-section of the shear zone and find a possible critical area and monitor this area over the length of the simulation.

The holes affect the stress in the sample. Loads will compress the sphere increasing the displacement and stress in the neighboring areas. As shown in Figure 7.11 the stress is low in the areas distanced from holes and high in areas with holes placed close to each other. Similarly the size of the spheres affect the stress situation. Large holes in the shear zone causes large deformations of the upper surface of the sphere due to the lack of support, resulting in high stress in the surrounding areas.

With Leca pellets placed in the empty spheres, the deformation of the PP around the holes is reduced and thereby also the stress. This being said, the Leca pellets do not provide the material system with a large strength distribution as the crush resistance is only 1.39 MPa. After the failure of the pellets, a similar situation as in the model without pellets occur with stress concentrations around the pellets.

(a)   (b)
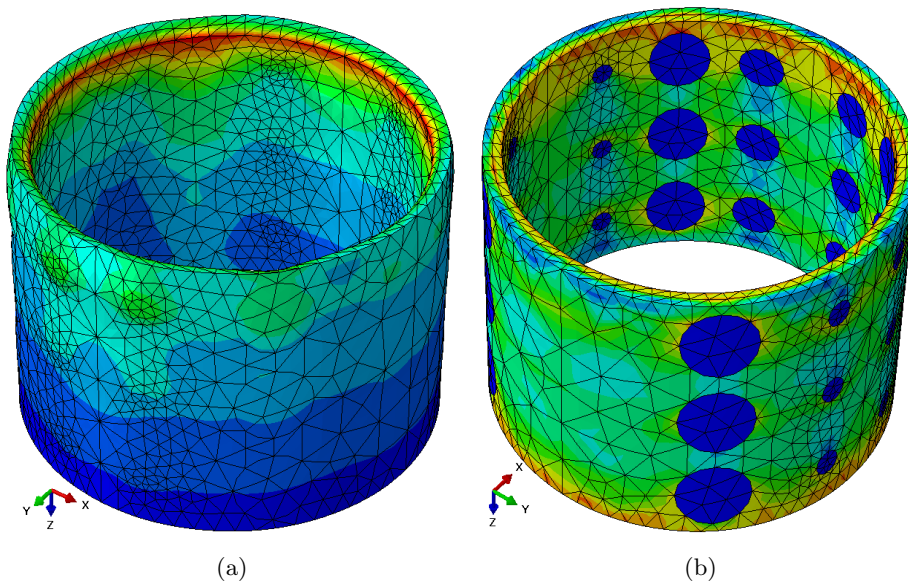
Figure 7.12: Shear zone with Leca pellets.**(a)**Deformations in z-direction **(b)**Mises stress

The deformations plotted in Figure 7.12a show that areas around Leca pellets, in particularly the big once, are more deformed in z-direction than areas with no Leca. This deformation creates an increased curvature on the side of the spheres, and a decreased curvature in the bottom of the sphere, resulting in higher stress (yellow color) on the sides of the pellets and lower stress (blue color) below the pellets, as shown in Figure 7.12b.

(a)

(b)

(c)

(d)
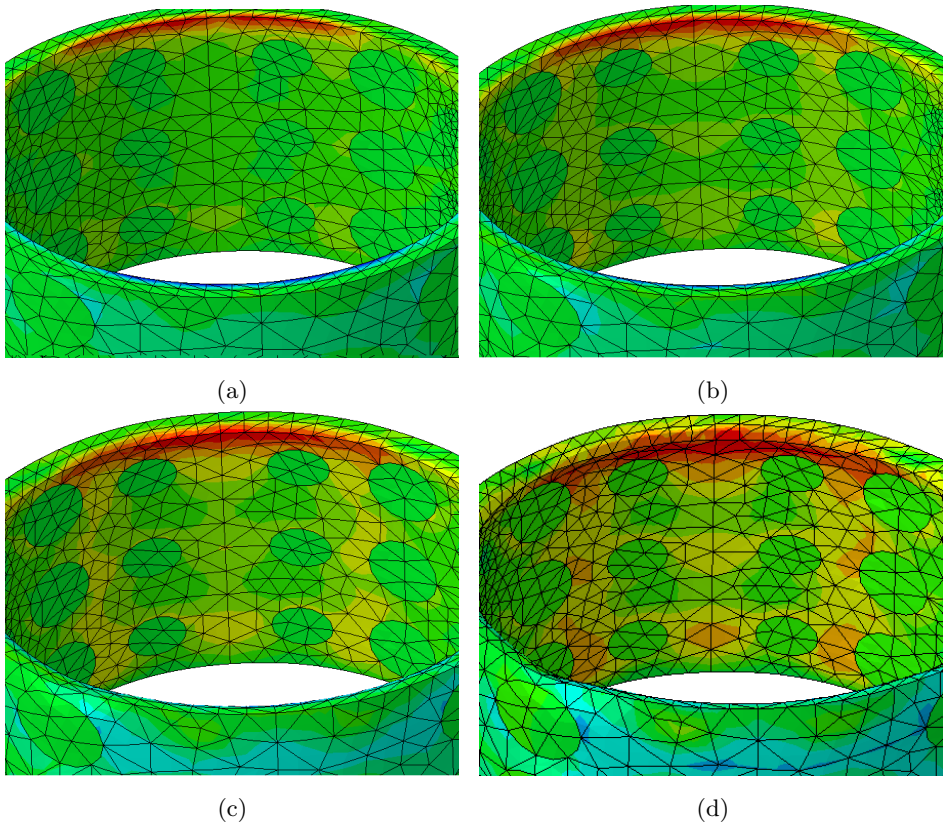
Figure 7.13: Shear stress delevopment at **(a)** 0.3 mm **(b)** 0.6 mm **(c)** 0.98 mm **(d)** 1.4 mm

In Figure 7.13 the development of shear stress is shown. The punch tool penetration of the sample is given in the caption. In 7.13a most of the shear zone is green which indicates a shear stress between 2 and 14 MPa. In 7.13b a light green area is developing between the Leca pellets, this color represents shear stress between 18 and 34 MPa. In 7.13c most of the area is light green and between the Leca pellets the area is colored yellow. These areas has shear stress between 38 and 50 MPa. Figure 7.13d shows the end state of the simulation where most of the area have shear stress between 18 MPa (light green) and 74 MPa (orange)[2].

---

[2]The color codes for stress in Abaqus are dynamic and the values for green, yellow etc. are not the same during the length of the simulation, but changes for each frame

Because of the stress variation as a function of both geometry and time, it is hard to identify in which area the break will initiate and how large area above the critical shear stress is necessary to initiate the break. So instead, average and extreme values for the whole shear zone can be used. Figure 7.14 shows the shear stress of every element in the shear zone without Leca plotted versus time.
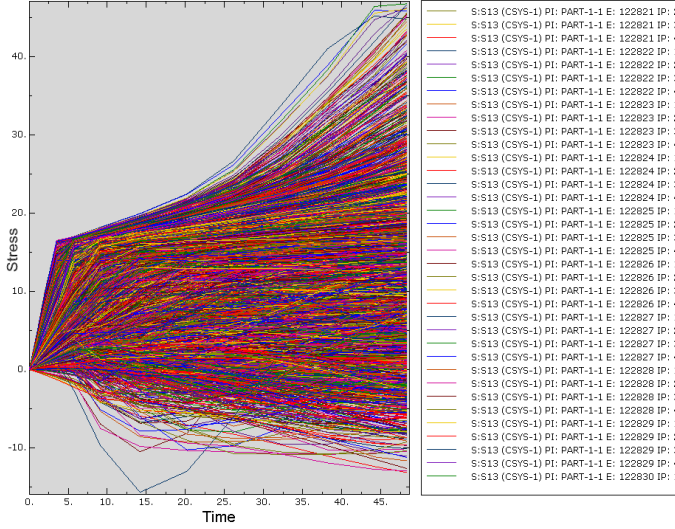
Figure 7.14: Elemental shear stress for all elements in the shear zone

The 5500 elements in the shear zone have shear stress between -15 and 45 MPa. The time is between 0 and 48 s as this is the duration of the simulation of 1 mm punch tool penetration. Strain is easily calculated from time as the displacement rate is constant, as shown in Equation 7.1. In this calculation the strain after 22.5 s is calculated as an example.

$$\epsilon = \frac{\Delta L}{L_0} = \frac{15\,\text{mm} - (15\,\text{mm} - 22.5\,\text{s} * \dfrac{1.24\,\text{mm/min}}{60\,\text{sec/min}})}{15\,\text{mm}} \equiv 0.031 \qquad (7.1)$$

This calculation is used to create a stress-strain diagram for shear in the shear zone, as shown in Figure 7.15. The curves show $\mathcal{T}_{\text{absolute max}}$, $\mathcal{T}_{\text{center max}}$, $\mathcal{T}_{\text{average}}$ and $\mathcal{T}_{\text{min}}$. Absolute max is the node with the highest shear stress in the entire shear zone, center max is the highest shear stress in the model excluding the top and bottom part as these areas have higher stress than the rest of the model. The average value is calculated from the entire model and the minimum likewise. Absolute values are used, so the the plot does not show if the value is calculated from tensile or compressive stress, the most critical is the tensile stress as it is much higher, shown in Figure 7.14

$\mathcal{E}_{\text{absolute max}}$, $\mathcal{E}_{\text{center max}}$, $\mathcal{E}_{\text{average}}$ and $\mathcal{E}_{\text{min}}$ are extracted from Figure 7.15. The crit-
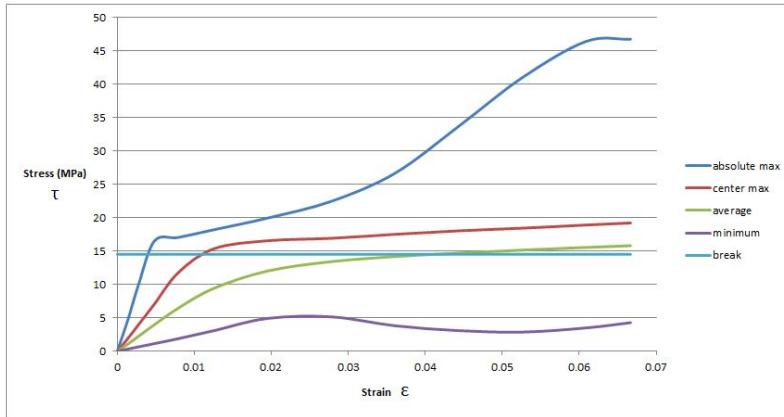
Figure 7.15: Stress-strain diagram for shear zone without Leca pellets

ical value where the PP yield from shear is $14.5\,\mathrm{MPa}$ according to Equation 3.1. It is shown that the average shear stress in the shear zone exceeds the critical value at 0.04 strain. Abs.Max stress reaches critical shear after 0.004 strain, center max at 0.012 strain and the minimum shear stress in the model never exceeds the critical value.

Next the load causing these shear stresses is plotted. The force applied is extracted by selecting the nodal contact force on the center surfaces where the displacement is applied, as shown with the contact pressure (legend values in MPa) in Figure 7.16. These values are summed and the total force is plotted versus $\mathcal{E}$, as shown in Figure 7.17.
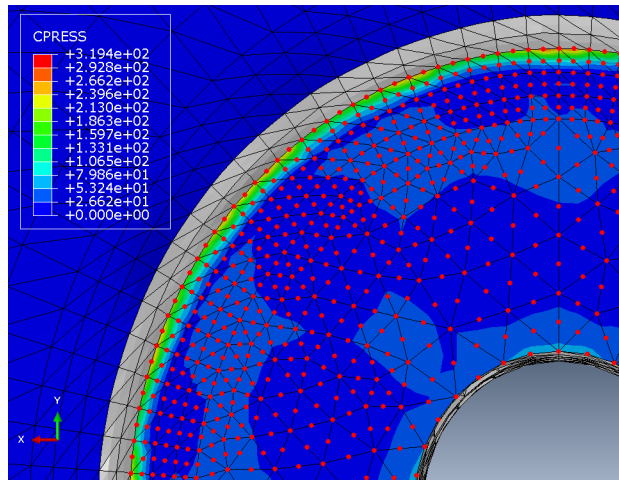
Figure 7.16: Nodes in direct contact with the punch tool
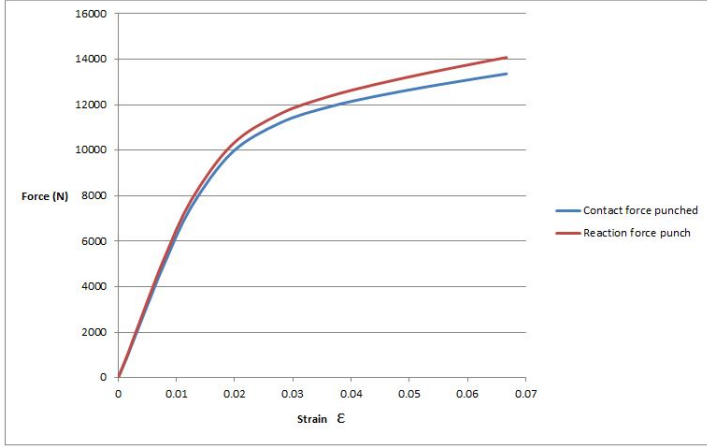
Figure 7.17: Force-strain diagram showing reaction force and contact force for model without Leca

The strain values corresponding to $\mathcal{T}_{\text{absolute max}}$, $\mathcal{T}_{\text{center max}}$, $\mathcal{T}_{\text{average}}$ and $\mathcal{T}_{\text{min}}$ gives us an estimated load required for the sample to fail in the mechanical test. These values are $F_1 = 2.8\text{kN}, F_2 = 7.5\text{kN}$ and $F_3 = 12.5\text{kN}$.

Two curves are plotted in Figure 7.17, "Contact force punched" and "Reaction force punch". "Contact force punched" is the sum of nodal contact forces in z-direction on the specimen surface in contact with the punch tool. "Reaction force punch" is the total force applied to the punch tool (modeled as a rigid surface) to achieve the given displacement. Large deviations between these two curves would indicate that the sample is not exposed to pure shear, for instance if the whole sample is compressed by the punch tool, the compression force will not be absorbed in the contact surface. Deviation between the reaction force and contact force in this model, is $720\,\text{N}$ or around 5%.

This gives four different scenarios:

1. The sample breaks when the shear stress in one element of the shear zone reaches critical value of $14.5\,\text{MPa}$.

2. The sample breaks when the shear stress in one element in the center of the shear zone reaches $14.5\,\text{MPa}$.

3. The sample breaks when the average shear stress in the shear zone reaches $14.5\,\text{MPa}$.

4. The sample breaks when the shear stress in every element of the shear zone reaches $14.5\,\text{MPa}$.

Details for each scenario are given in Table 7.1. Because the punch tool radius

in the Abaqus model is 13 mm, and 10 mm in the mechanical test, the estimated measured load is calculated by multiplying the Abaqus load by a factor of $\frac{10}{13}$. The deduction for this factor is shown in Equation 7.2.

$$\tau = \frac{F_1}{A_1} = \frac{F_2}{A_2} \quad, \quad F_1 = \frac{A_1}{A_2} * F_2 \quad = \frac{2\pi * r_1 * t}{2\pi * r_2 * t} * F_2 \quad = \underline{\frac{r_1}{r_2} * F_2} \tag{7.2}$$

Scenario #	Failure Strain	Abaqus Load	Estimated Load
1	0.004	2.7 kN	2.08 kN
2	0.011	7.4 kN	5.7 kN
3	0.042	12.5 kN	9.6 kN
4	Did not fail	Did not fail	Did not fail

Table 7.1: Scenario table

This section has estimated the necessary load to break the sample in shear based on a maximum shear value calculated from the yield stress given in the material data sheet. This value will be compared to the experimental value in later sections.

The same point of failure identification using average and extreme values is performed on the shear zone with Leca. Figure 7.18 show element shear stress of every element on both Leca and PP in the shear zone, 9300 elements.
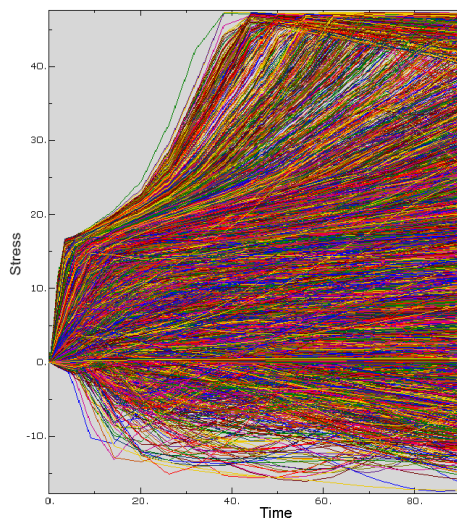
Figure 7.18: Shear stress on elements in shear zone

Stresses are in the same range as the model without Leca. The x-axis show from

0-90 s, as the simulation performed had a duration of 90 s thus a punch tool penetration depth of 1.86 mm. Strain is calculated from Equation 7.1 and the stress-strain diagram is shown in Figure 7.19.
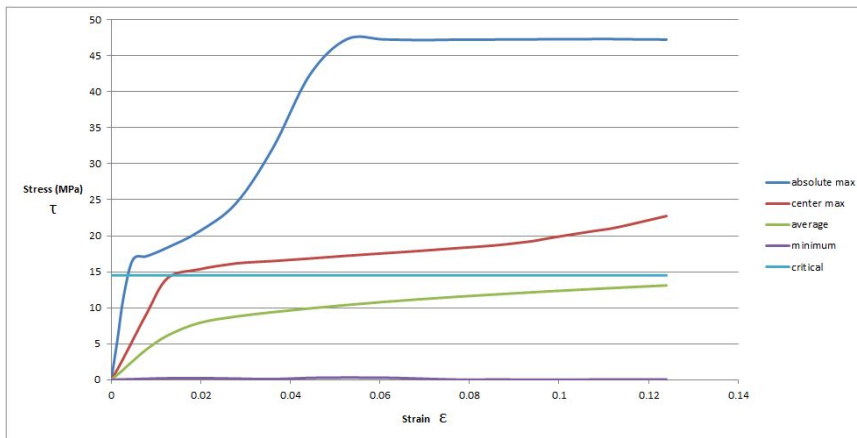
Figure 7.19: Stress-strain diagram for shear zone with Leca pellets

Absolute max shear stress intersects the critical limit curve at 0.005 strain, center max at 0.015 strain, average at 0.04 and in the same manner as without Leca, minimum shear stress never exceeds 14.5 MPa. Selecting, plotting and summing the nodal contact forces on the Compbuoy surface in contact with the punch tool similarly as with the previous model gives the force-strain graph shown in Figure 7.20
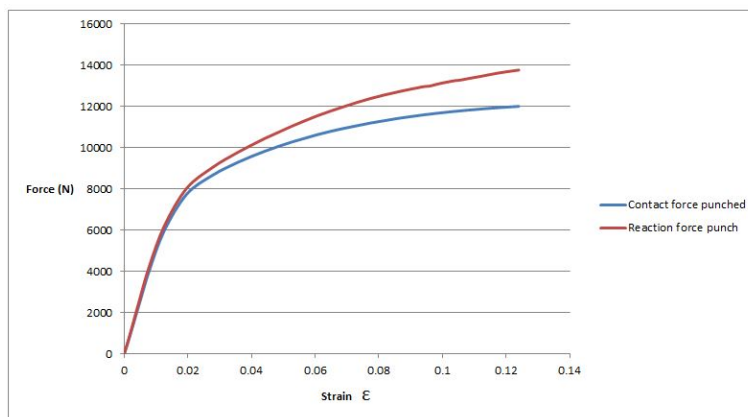
Figure 7.20: Force-strain diagram showing reaction force and contact force for model with Leca

At the end of the simulation, the reaction force and contact force in the Leca model are 13769 N and 12011 N. A deviation of 1758 N or 12.7%. To compare with the model without Leca, the difference at 1 mm punch tool penetration is 1054 N or 8.8%, 3.3% higher than in the model without Leca. Since both the Abaqus model with Leca and the test test rig have a punch tool radius of 10 mm, the adjustment done for the model without Leca is not necessary in this case.

Scenario #	Failure Strain	Estimated Load
1	0.0035	2.2 kN
2	0.0136	6.53 kN
3	Did not fail	Did not fail
4	Did not fail	Did not fail

Table 7.2: Scenario table 2

7.4   Discussion

Without Leca

Simulations for 1 mm, 1.5 mm and 1.7 mm penetration of punch tool were successfully completed. When simulating 1.8mm penetration, the analysis aborted at 95%, when simulating 2mm penetration, the analysis aborted at 57%.
When looking at the results from the 1.5 mm penetration analysis it is shown that the shear stress in the shear zone clearly surpasses maximum shear strength of the material, up to 120 MPa. This implies that the critical point of breakage is included in the analysis.

The hollow spheres in the model were intended to emulate the pressure tested samples where the Leca pellets are completely crushed before the shear test is commenced. The model created shows the same behavior as a model with crushed Leca modeled in the empty spheres would, as neither of the two contributes to the strength or structural integrity of the material system.

Stress variation in samples with different thicknesses has been investigated and as shown in Figure 7.5, the interference from stress components other than shear stress in z-direction is found to be correlated with increased sample thickness. The difference between reaction forces and contact forces shown in Figure 7.17 supports the notion that for a 15 mm thick sample, other stress components than shear stress in z-direction are present. This finding suggest the purest shear break is obtained by using a sample as thin as possible. Because of the Leca pellets and the strive for some degree of homogeneity in the sample, the test specimens should be as thin as possible while still meeting the required minimum number of Leca pellets through the thickness. This minimum number is set to be 3 in order to reduce the heterogeneity of the shear zone while at the same time not forcing the thickness far beyond 12 mm.

Section 7.2 shows how the thickness of the unconstrained shear zone affect the concentration of shear stress. A thick shear zone distributes the shear stress over a large area as opposed to a thin shear zone that concentrates the shear stress and thereby reducing the effect of stress components disruptive for the purpose of the test. For this reason the gap between the punch tool and the specimen constraining rigid plates should be as small as possible. The final gap size is defined through a trade-off between aspiring to reconstruct the mechanical testing where the gap is 3 mm, and keeping the number of elements in the Abaqus model at an acceptable level. Simulations were performed with both 0.5 mm, 1 mm and 2 mm. The results from the three alternatives did not deviate noticeably, with an average shear stress deviation of 0.3 MPa between 0.5 mm and 2 mm, as shown in Figure 7.10. For this reason, the clearance between the punch tool and the hole in the die surface was set to be 1 mm.

In the failure analysis four scenarios were created. Scenario 3 and 4 is considered

unrealistic. When the average shear stress is just below the critical value, 49% of the elements can be above the critical value and 51% below. In this case, 49% of the elements have failed, and the load is distributed to the remaining 51%. This will increase the stress in the remaining elements and the sample will break. This reflection suggest that the sample will fail before the average stress reaches the critical value and supports the one-fail-all-fail theory given in scenario 1. However, due to the complex geometry, local stresses might cause small areas around a hole to fail before the load is high enough to break the remainder of the sample, shown by the large deviation between the "absolute maximum" and "center maximum" stress curves in Figure 7.15. All considered, scenario 2 is believed to be the most realistic case when estimating the point of failure in the sample. Scenario 2 gives an estimated load of 5.7 kN required to break the pressure tested sample in the lab, this estimate is evaluated when discussing the results.

With Leca

The simulations for punch tool penetration above 2 mm aborted because the required time increment was too low, and the solution did not converge. This is due to large plastic deformations. When the elements are deformed they become long and slim, to counter this, remeshing can be done. This means stopping the simulation, mesh the part again so that the deformed elements can be "repaired", before continuing the simulation. However, the evaluation of the shear stress at 90 s, or 1.8 mm penetration of the punch tool shows that failure has already occurred. No serious attempt to finish simulations of penetration beyond 2 mm was initiated for this reason.

In the model without Leca, the spheres were compressed creating an increased curvature on the side of the center of the spheres, this created stress concentrations in these areas. In the Leca model similar behavior is observed, shown in Figure 7.12. The compression of the PP around the pellets are, however, reduced by the Leca's structural integrity contribution, even though this contribution is limited by the low crush resistance.

Looking at Figure 7.13 it is clear that 7.13d has broken as almost all areas have shear stress above 18 MPa. In contrast, 7.13a shows the entire model except from a small section at the top, with stress below 14 MPa, thus the sample has might not suffered failure at this stage. In 7.13b the areas around the pellets have exceeded the critical value for shear while the areas distanced from the pellets have shear stress below 14.5 MPa. In 7.13c most areas have shear stress above 38 MPa, and consequently, failure has most likely occurred. Identifying the exact point of failure based on this shear stress plot is a matter of educated guessing, if the shear zone have a high volume percentage of Leca, the sample will fail shortly after 0.3 mm punch penetration. If the shear zone has a low volume percentage of Leca, the sample might not fail until around 0.9 mm punch penetration as the areas beyond critical value are located around the pellets.

When using plots to identify the point of failure, Scenario 2 is considered to be the most realistic and the estimated load required to break the unpressurized sample in shear is found to be 6.5 kN. This is 0.8 kN higher than for the model without Leca and indicates that pressure testing to the point of Leca pellets crushing, reduces the shear strength of the sample by 12.3%. The shear strength is still lower than the expected shear strength of PP calculated to be 14.5 MPa. This will be further elaborated later in the report.

Chapter 8

Mechanical Shear Testing

8.1 Test Procedure

Several test have to be performed to fully evaluate the material properties of the Compbuoy material. First, a test rig needs to be designed and built, tested and improved. Secondly, test samples must be produced and optimized.

Previously, pressure testing up to 500 bar has been conducted. To understand the effect of the hydrostatic pressure, test specimens from the pressure test will be reused in the shear strength test and compared to specimens that have not gone through the pressure test. During the production of the Compbouy elements, different types of PP have been used. The testing will therefore include test Compbuoy samples made from two types of PP in order to evaluate the difference in properties. For reference purposes, samples made from pure PP, with no Leca pellets in the mix, will also be tested to see what influence the pellets have on the shear strength. This will also help evaluate the test procedure by comparing the test results with the information given in data sheets supplied by the manufacturer of the PP.

8.2 Test equipment

For the testing, the test rig was clamped into a Instron model 1342 test machine shown in Figure 8.1. This machine is part of the 1340-series of servohydraulic fatigue testing machines, manufactured by Instron between 1980 and 1986. The machine has a 2-column frame and dynamic capacities up to 100kN[17]. 100kN is way more than the force necessary to break the Compbuoy samples, and other test machines in the fatigue laboratory with lower capacities may provide a more accurate result. However, the other machines are frequently used by other students and the Instron 1342 was selected for availability reasons.

Figure 8.1: Instron model 1342

The equipment shown in Figure 8.2 was used to connect the Instron model 1342 to a computer and obtain data from the testing.

<table>
<tr><td>(a)</td><td>(b)</td></tr>
</table>

Figure 8.2: **(a)**Instron control module **(b)** Nation Instruments box

8.3 Testrig

A standard test method to to determine the shear strength of plastics is the ASTM D732-10[7]. This kind of shear punch tests have been widely used to evaluate the properties of metals, ceramics, semi-crystalline polymers and other plastics[22]. The test is, however, created to measure strength of homogeneous isotropic materials. For Compbuoy samples, special concerns must be taken, and the ASTM test method is developed to suit the Compbuoy material. To start the testing, a simplified version of the ASTM D732 (Figure 8.3) test rig was constructed, as shown in Figure 8.4.

Figure 8.3: Cross-sectional view of the original ASTM test rig. Adapted from[7]

Modifications to ASTM D732

Some modifications was done to the original setup in order to make the production of the test rig possible. The guide should be 1" according to ASTM, the purpose of the guide is to hold the sample in place and guide the punch tool. A 3 mm thick steel plate can do the same job as almost none of the forces from the punch tool will be absorbed in the guide plate. During testing, the guide plate was observed with no displacements and the test specimen was held in place perfectly.

The guide pin on the punch tool was dropped as it complicated the setup below the test sample. Because the punch tool is secured in the Instron test machine, which provides a guided, rectilinear movement, the guide pin is considered redundant. In the ASTM test rig, the diameter of the punch is 1" and the hole drilled in the test specimen is 11 mm. The recommended diameter of the test specimens is 50 mm. However, after experimenting with different diameters it was clear that 50 mm was a good diameter for the samples, but more clearance between the outer diameter(50mm) and the nominal shearing zone (area around $\frac{1}{2}$" from the center) were desirable to avoid crack propagation. Therefor, the punch diameter was reduced to 20 mm. This modification was considered valid as different

shear punch tests use punch tools with diameter varying from $12\,\text{mm}$(steel)[10] to $250\,\text{mm}$(concrete)[12].

In the ASTM test rig the die is $1\frac{1}{2}$inches. In the simplified version however, it is a $4\,\text{mm}$ thick steel plate. This alone is not strong enough to absorb the forces from the test (up to $5\,\text{kN}$ loaded at the center of the plate). The $4\,\text{mm}$ steel plate was chosen for accessibility reasons. During testing the die plate was deformed and was not able to maintain a horizontal support surface for the test specimen. The die had to be reinforced.

When testing shear strength, the ideal case is to break the sample in a pure shear break. To achieve this, as discussed in chapter 3, the clearance between the punch tool and the diameter should be as small as possible. At the same time, too small clearance may result in contact between the punch and the die which will corrupt the test results. With a punch tool diameter of $20\,\text{mm}$, the inner diameter of the die was drilled $20.3\,\text{mm}$.

The fist version of the test rig was made from thin steel plates and a solid steel rod. The compbuoy specimens were cut to a thickness of $12\,\text{mm}$ as instructed in the ASTM D732. In order to secure the test rig in the Instron test machine, the rig was bolted to a steel plate, welded to a solid steel rod with a $25\,\text{mm}$ diameter, like shown in Figure 8.4.

Figure 8.4: Punch tool lowered down through the guide and die

Rig Testing

The first test was performed. The punch tool was placed at $15\,\mathrm{mm}$[1]. The test specimen was loaded at a cross-head speed of $1.24\,\mathrm{mm/min}$. The results from the first test is shown in Figure 8.5
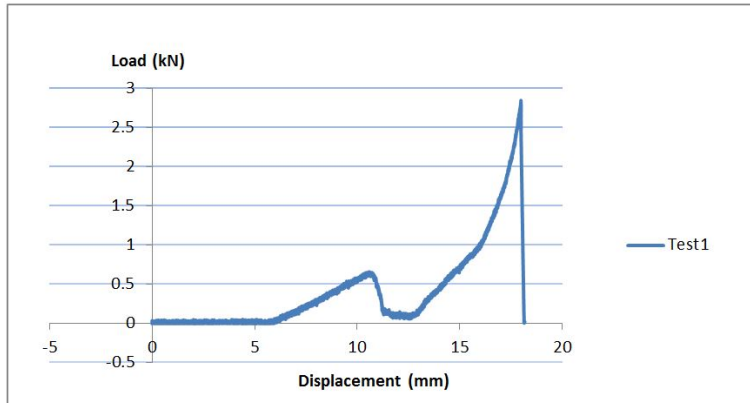
Figure 8.5: Test plot from the rig test

When looking at the result from the test, it looks like the force needed to break the test specimen is around $650\,\mathrm{N}$. What the graph shows is that the force needed to push the punch through the specimen increases from contact is established, to the point where the specimen breaks and the force decreases. After break, the force increases again. This is because the clearance between the specimen and the bottom plate is not big enough, and the broken-off piece is being compressed until the test is aborted at $18\,\mathrm{mm}$ displacement.

From the result, it is clear that the clearance below the specimen must be increased so that the separated piece can fall down and not interfere with the testing. During the test, the test rig was deformed due to the forces applied, and the die-surface was not horizontal during the entire test period. This results in bending moments in the test specimen and the break will not be from pure shear. To minimize the effects of bending moment, the rig must be reinforced. Before the rig was reinforced, the load from the punch tool was transferred through the test sample, onto the die which was supported in the corners with a bolt to the plate below. Because the loads are supported far away from the axis of the force, the bending moments were too big for the rig to handle.

---

[1]relative to the zeropoint of the test machine

Three 5 mm thick steel plates were cut to 50*50 mm and welded together. A 22 mm hole was drilled in the center of the plates. This 50*50*15 mm cube was placed under the die. This results in a situation where almost all forces from the test are transferred through the center of the rig, reducing the momentum and thereby also the deformations. The reinforced test rig is shown in Figure 8.6

Figure 8.6: Reinforced test rig with sample

Running the test after the reinforcement showed no sign of rig deformations. The die-surface remained horizontal throughout the test, which is most important. Also, the reinforcements added space under the test specimen, so that the broken off parts fell down and did not continue to interfere with the testing.

The test rig was modeled in Siemens NX to provide an informative visualization of the geometry and technical drawings. Figure 8.7 shows the test rig, and technical drawings can be found in Appendix D.2.

<div align="center">(a)   (b)</div>
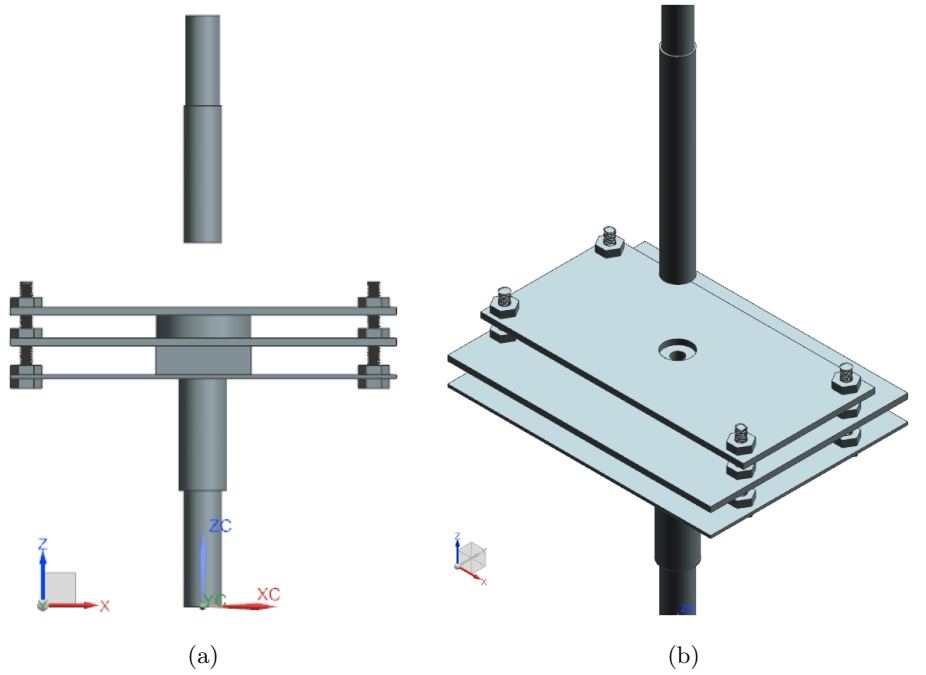
Figure 8.7: Test rig modeled **(a)**Front view **(b)** Isometric view

8.4   Test specimen

Geometry

The testing started with semicircular specimens. The reason for this was the initial shape of the buoyancy elements. After pressure testing the BEs are broken in two pieces to inspect the LECA spheres. The semicircular test specimens are showed in Figure 8.8.
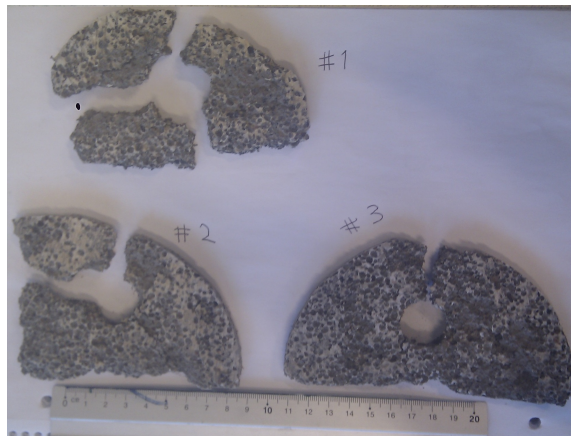
Figure 8.8: Semisircular test specimens

This test geometry was chosen because it was easy to produce. However, the asymmetrical geometry implies very different distances from the nominal shear zone to the nearest edge. Testing showed that all samples cracked from the punch hole to the nearest edge, implying a weak spot. This combined with the large differences in the results from the tests, made it obvious that the specimen should have a circular shape.

Figure 8.9: Large sircular test specimen before testing

Uncut (into two halves) buoyancy elements were acquired and cut to circles with 100 mm diameter and approximately 12 mm thickness as shown in Figure 8.9. The testing of the large circular specimen was considered partly successful as it was the first specimen that did not break into pieces during the test, which could imply a more pure shear break. However, a downside with this specimen size was that only one test specimen could be produced from each Compbuoy element. Because the internal structure in the elements can vary, more than one sample from the same element is beneficiary for the reliability of the tests.

To answer this requirement, smaller circular specimens were produced. By reducing the diameter to 50 mm, four samples could be produced from each element. Also, reducing the distance from the load to the bearing points reduce the bending moment in the sample, facilitating a more pure shear break. The machining of the samples are crucial as the top and bottom surface must be parallel and horizontal in order to obtain valid results. This is easier achieved with smaller samples. Figure 8.10 shows the produced specimens.

Figure 8.10: Small sircular test specimens

During testing the specimens were destroyed and ended up as shown in Figure 8.11.

Figure 8.11: Specimen after shear testing

Sample thickness

As discussed in Chapter 3, a concern regarding the testing is that the samples are not homogeneous. The ASTM D732 test states that the thickness of the sample shall not exceed 0.5 inches, or 12.7 mm[7]. With Leca pellets in the size range of 2-4 mm, the Compbuoy shear samples will have 6 or less pellets through the thickness of 12 mm. To control how many pellets are located in the shear zone is impossible, instead, the effect of this variable needs to be managed. This is done by varying the thickness around 12 mm, testing multiple samples, and creating average values. The samples are inspected after testing. If the failure surface of the sample has decisively too few pellets in the shear zone compared to the rest of the samples, the results are discarded. This however proved unnecessary, as non of the samples showed obvious deviations from the norm. Figure 8.12 shows a typical sample with between 4 and 6 pellets through the thickness.
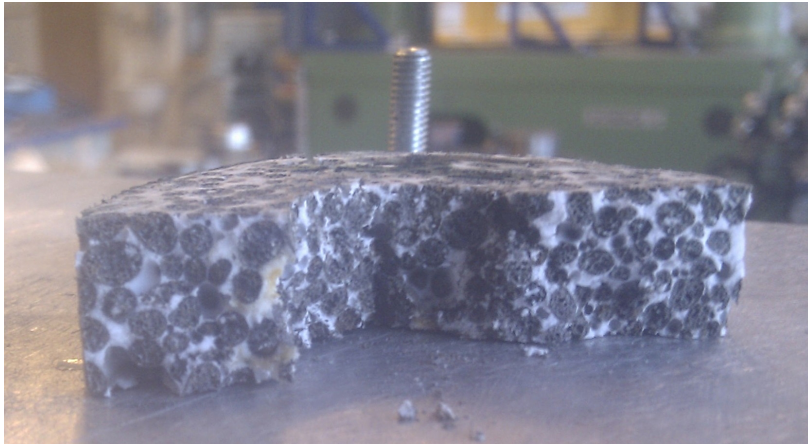
Figure 8.12: Typical number of pellets through the thickness of sample

Sample condition

The main difference between the different samples produced is the condition of the Leca pellets. For the samples that did not undergo pressure testing, the Leca pellets are completely intact even after the shear test has been performed. The pellets are broken, but not crushed and seems to continue to provide a contribution to the strength of the sample. For the pressure tested samples, most of the pellets are crushed leaving nothing but concrete dust. Before the shear test is performed, the spheres in the PP where the pellets used to be are relatively structurally intact. After the shear test, the spheres in the PP are collapsed and the fracture surface is transformed to a disorganized chaos of PP cavities smeared in concrete dust. The difference is shown in figure 8.13.

(a) (b)
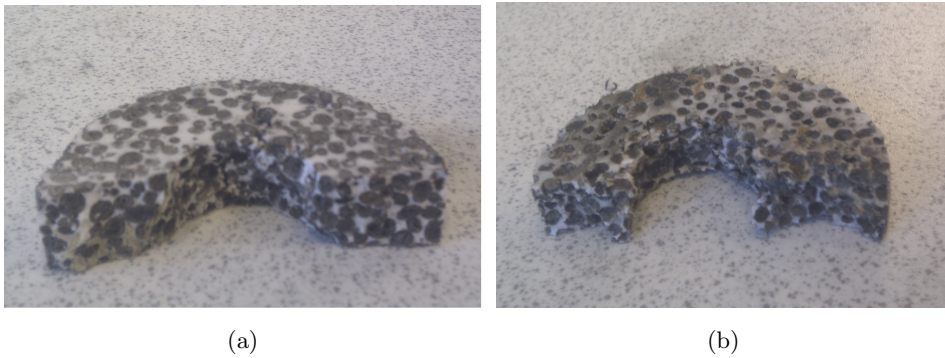
Figure 8.13: Tested samples **(a)** With intact Leca pellets **(b)** Without intact Leca pellets

Pure PP-sample

To completely understand the impact on material properties adding Leca pellets to the PP has, a reference is needed. The shear strength of the Compbuoy samples should be somewhere in the range between the crushing strength of Leca, and the shear strength of the PP. The material data sheet for the two types of PP gives us the value of tensile yield stress according to the ISO 527-2 test. Equation 3.1 gives us the shear stress from the yield stress. This value however, is not considering the heat treatment that the BEs undergo during production. To take this into account, a sample containing nothing but PP was produced, cut into similar test specimens as earlier and tested in the same test rig. As shown in Figure 8.14 the white PP sample has some brown areas. This is believed to be due to contact with air during production. The bottom of the sample was all white, while the top had a lot of brown areas. Both the top and bottom was cut away and the test specimen was produced from the core of the PP brick, as it was done with the test specimens from the Compbuoy material. Even so, the test specimen also shows brown areas. This might be because gas is produced when PP melts, the gas is trapped inside the material, and the PP is degraded through oxidation, leaving brown marks.

| (a) | (b) |
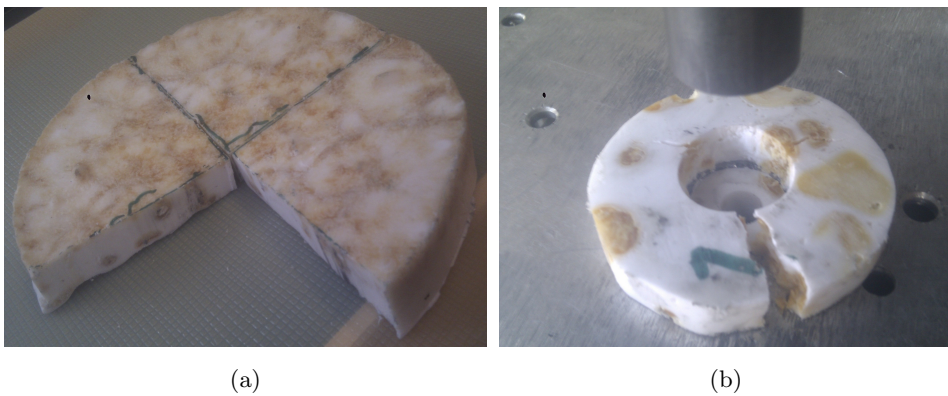
Figure 8.14: Test rig modeled **(a)**Top view **(b)** Tested sample

This test will not only reveal if the heat treatment reduces shear strength in the PP, but also reduce the impact on any flaws in the testing procedure causing the break to deviate from pure shear as it gives an equally flawed reference value. The data given by manufacturers are suspected to be somewhat manipulated to give as impressive results as possible. The yield stress in the data sheet is given at a cross-head speed of 50 mm/min, and as shown in figure 6.5, higher cross-head speed during the test will result in higher measured yield stress. Testing the PP at 1.24 mm/min will give a more conservative and accurate value for the shear strength of the PP.

Chapter 9

Test Results

The results from the shear tests are presented in this section. The test equipment measures displacement of the punch tool and the reaction force measured in a load cell. These values are plotted, and from the area of the fracture surface the shear strength is calculated using the formula: $\tau = \dfrac{F}{A}$ The area in this formula is the circumference of the punch tool times the thickness of the sample. This gives a nominal shear stress at the point of failure, the true shear stress in the sample will be a little lower as the fracture surface is uneven and this is not considered in the calculations.

9.1 Large samples

As discussed in Chapter 8.4, samples with different geometries were tested. Figure 9.1 shows results from testing of semicircular and circular specimens with 50 mm radius.

Test	PP used	Geometry /Radius /Thick	Pressure tested at	Shear Strength
2.1	BJ365MO	Semicircular / 50mm / 10.5	300 bar	0.75 MPa
2.2	BJ365MO	Semicircular / 50mm / 12	300 bar	0.92 MPa
3.1	BJ365MO	Semicircular / 50mm / 11	1 bar	2.12 MPa
3.2	BJ365MO	Semicircular / 50mm / 13	1 bar	3.44 MPa
4.1	BH340MO	Circular / 50mm / 12	50/100/.../300bar	3.99 MPa

Table 9.1: Test specimen information

Figure 9.1 shows that the pressure tested, semicircular samples, has a shear strength
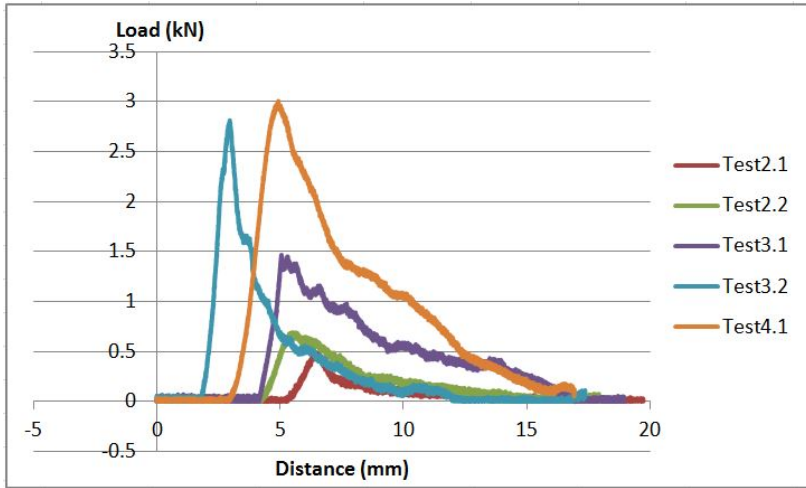
Figure 9.1: Results from testing of semicircular specimens

below 1 MPa. The geometrically similar samples who did not undergo pressure test-ing, shows shear strength of 2.1 and 3.3 MPa. This is a clear indication of the differ-ence in strength due to the pressure testing, but as the geometry of these samples is considered invalid, no further interpretation of the results is necessary.

9.2 Small samples

After experimenting with different geometries for test samples, the chosen one was a circular specimen with a diameter of 50mm and a thickness between 8 and 13 mm.

Pressure tested samples

Results from shear testing of pressure tested specimens shown in Figure 9.2, 9.3 and 9.4.
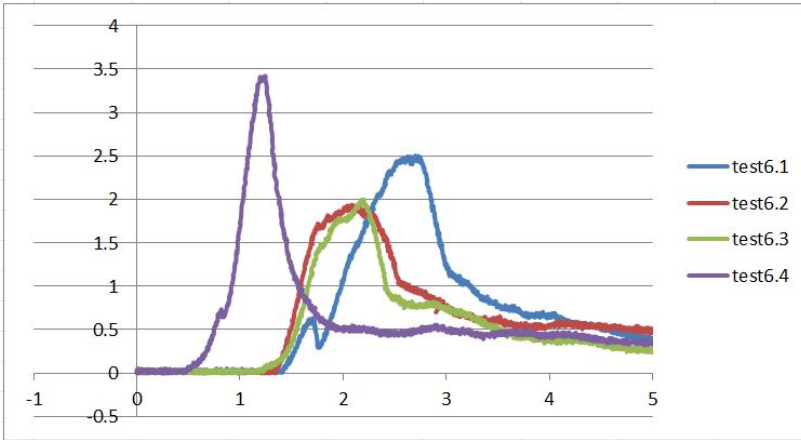
Figure 9.2: Results from test number 6
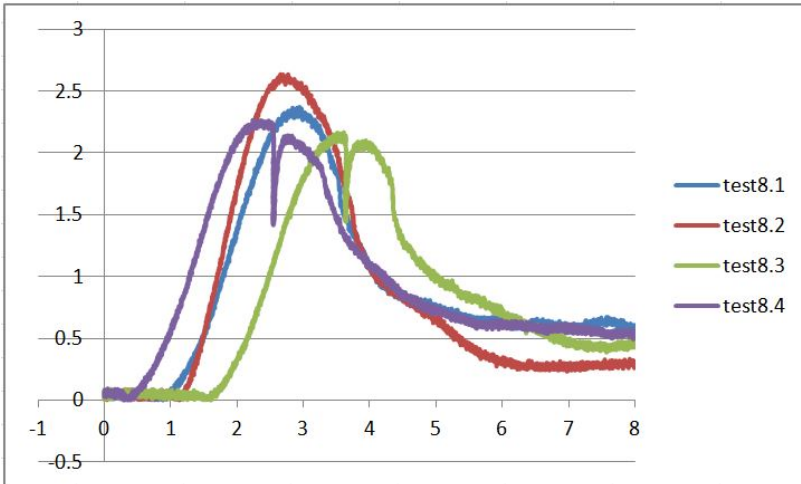
Figure 9.3: Results from test number 8

The load curves presented show a linear increase in loads absorbed until a penetration depth between 0.5 and 1.5 mm. At this critical point the sample suffers failure and the load bearing capacity is reduced dramatically. The sample breaks through the entire thickness. From this point the loads measured are due to the friction created from pushing the broken part through the sample. As the penetration distance increases, the contact area between the broken part and the rest of the sample decreases, as shown by a close to linear decreasing section at the end of the load curve. The tests 8.3 and 8.4 were paused right after the peak of the load curve to inspect the samples for cracks. After inspection, the tests were continued. This stop-and-go is shown as an irregularity in the load curve.

The samples in test 10 shown in Figure 9.4 are made from BJ356MO and pressure
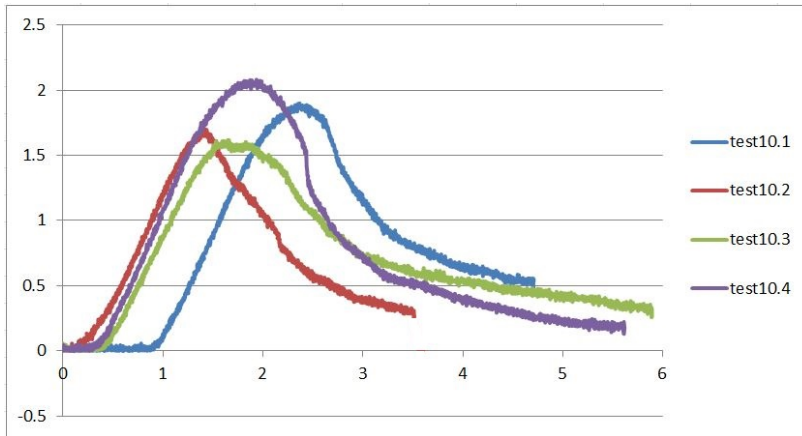
Figure 9.4: Results from test number 10

Test #	PP used	Pressure tested at	Thickness	Strain	Shear Strength
6.1	BJ356MO	300 bar	12.5 mm		3.19 MPa
6.2	BJ356MO	300 bar	12 mm		2.57 MPa
6.3	BJ356MO	300 bar	10 mm		3.18 MPa
6.4	BJ356MO	300 bar	11.5 mm		4.73 MPa
8.1	BH345MO	300 bar	11.5 mm		3.28 MPa
8.2	BH345MO	300 bar	11.4 mm		3.68 MPa
8.3	BH345MO	300 bar	11 mm		3.13 MPa
8.4	BH345MO	300 bar	11.8 mm		3.06 MPa
10.1	BJ356MO	50/100/.../350 bar	13 mm		2.33 MPa
10.2	BJ356MO	50/100/.../350 bar	12 mm		2.26 MPa
10.3	BJ356MO	50/100/.../350 bar	12 mm		2.14 MPa
10.4	BJ356MO	50/100/.../350 bar	13 mm		2.55 MPa

Table 9.2: Shear test sample information

tested several times, at 50, 100, ... , 350 bar. In test number 10 the test was aborted before the punch had penetrated all the way through, when the load dropped below 500 N. This was done to save time as the interesting point is the peak of the curve, and the test was aborted after this point had been reached.

Table 9.2 shows sample details from the testing, all the specimens from test 10 shows a lower strength than the rest of the samples. The samples in test 10 have undergone more pressure test than the other samples and also at higher pressure. The condition of test 10 samples is shown in Figure ??. Very few Leca pellets are intact and several places the PP matrix surrounding the pellets have collapsed.

Not pressure tested samples

Results from shear testing of specimens not having been pressure tested are shown in Figure 9.5, 9.6 and 9.7.
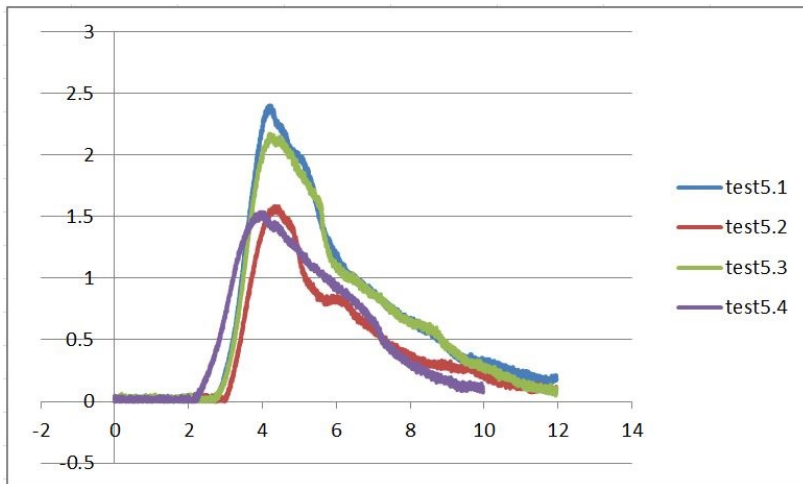
Figure 9.5: Results from test number 5
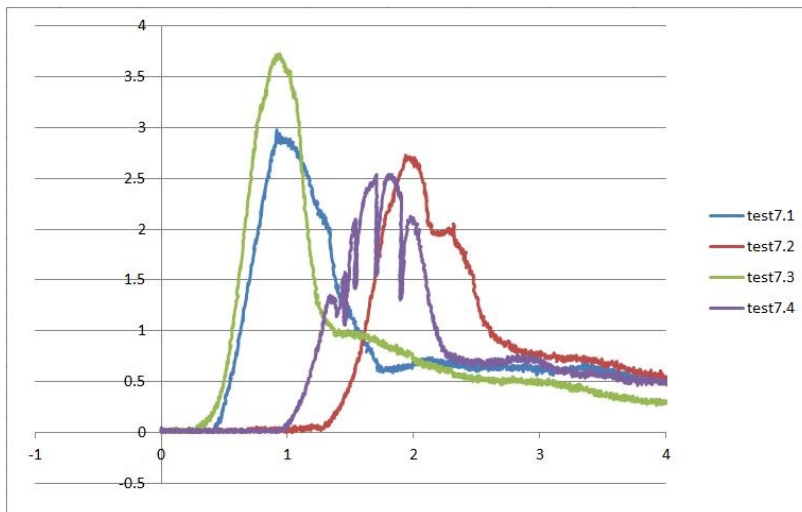
Figure 9.6: Results from test number 7
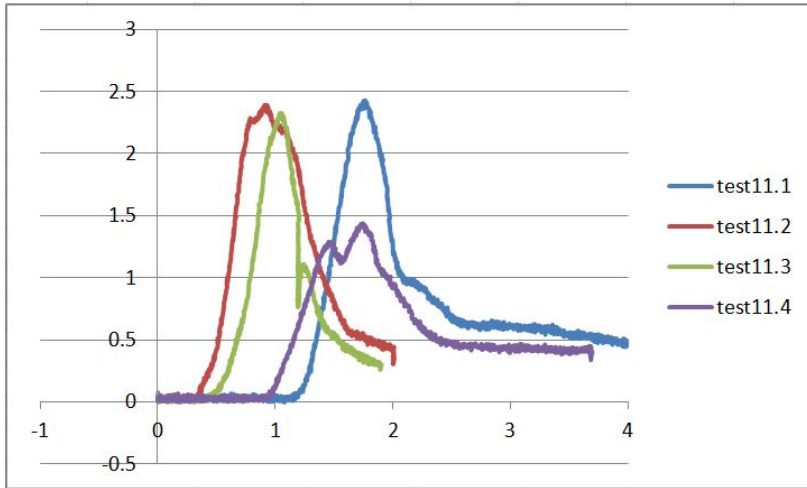
Figure 9.7: Results from test number 11

Test #	PP used	Thickness	Shear Strength
5.1	BJ356MO	8.5 mm	4.5 MPa
5.2	BJ356MO	8.1 mm	3.12 MPa
5.3	BJ356MO	8.5 mm	4.07 MPa
5.4	BJ356MO	7 mm	3.5 MPa
7.1	BJ356MO	13.5 mm	3.42 MPa
7.2	BJ356MO	13 mm	3.31 MPa
7.3	BJ356MO	13.5 mm	4.36 MPa
7.4	BJ356MO	12.5 mm	3.24 MPa
11.1	BJ356MO	9.5 mm	4.1 MPa
11.2	BJ356MO	12 mm	3.17 MPa
11.3	BJ356MO	8.5 mm	4.34 MPa
11.4	BJ356MO	7.5 mm	3.1 MPa

Table 9.3: Shear test sample information

The samples that did not undergo pressure testing produce load curves similar to the pressure tested once. The same linear behavior from start up to the point of failure and in the end of the tests is found for the samples in this section.

Just like test 10, test 11 was aborted when the load curves dropped below $500\,\mathrm{N}$ as the remaining part of the curve is not interesting.

As with test 8.3 and 8.4, test 7.4 was also paused to inspect the sample for cracks. Instead of just checking for cracks right after the peak of the load curve, several stop-and-starts were performed on this. The test was stopped 4 times, at $1.5\,\mathrm{kN}$, $2.0\,\mathrm{kN}$, $2.5\,\mathrm{kN}$ and right after the decline of the load curve was observed. No signs of cracking was observed during the three first stops, after reaching the critical

point of 2.54 kN, the load curve dropped quickly. The next stop was performed at 2.3 kN and now, a small crack development was detected. When the test was started again, the crack grew and before the load had dropped to 1 kN several cracks completely separated the sample.

In contrast to the pressure tested samples, the Leca pellets in the unpressurized samples had not been crushed. Post failure inspection revealed that the pellets had broken without beeing crushed, thereby maintaining some strength contribution to the material system even after the break. A sample from test 11 is shown in Figure 9.8.

Figure 9.8: Sample from test 11

Pure PP sample

GRAF av PP testingen
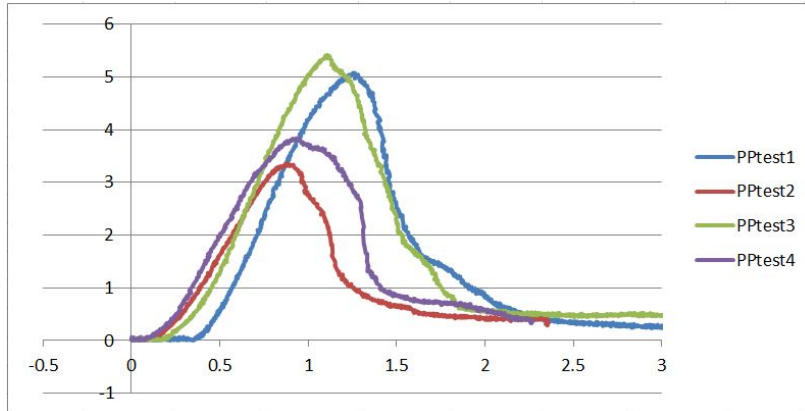
Figure 9.9: Results from testing of pure PP samples

Test #	PP used	Thickness	Shear Strength
PP1	BJ356MO	10 mm	8.1 MPa
PP2	BJ356MO	12 mm	4.45 MPa
PP3	BJ356MO	10.5 mm	8.21 MPa
PP4	BJ356MO	9.5 mm	6.44 MPa

Table 9.4: Shear test sample information

The test samples made from pure PP show similar behavior as the Compbuoy samples. The measured shear strength however, is significantly increased compared to the Compbuoy material. Test PP2 stands out in the bulk with much lower strenght than the other samples, this sample is the thickest one, shown in Figure 9.10 with the sample that tested the highest strength, PP3.

(a)	(b)
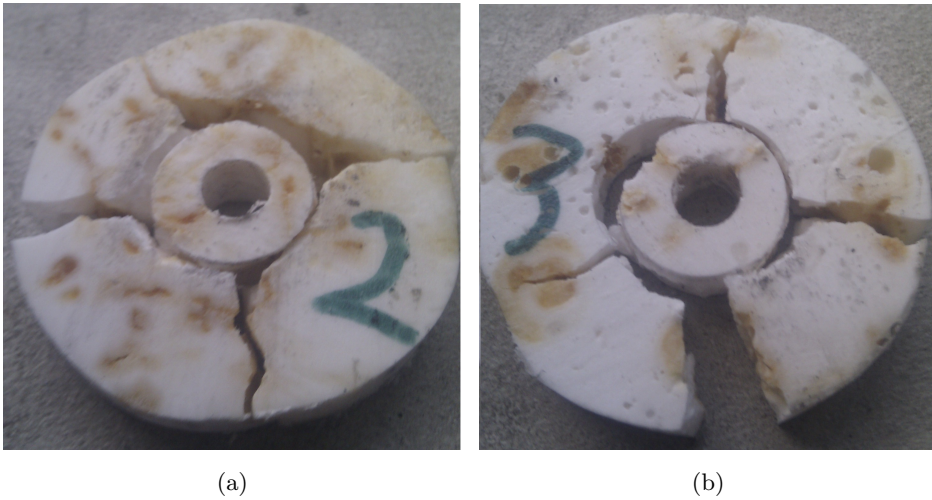
Figure 9.10: Tested PP samples **(a)**PP2 **(b)** PP3

As shown PP2 has large areas of degraded brown PP in the shear zone. PP3 also has some degraded areas, but not as much, and placed outside the critical areas. In PP3, three of four cracks have gone through large brown areas, which support the assumption that these areas are weaker than the white areas.

Because the PP samples are to a much bigger extent homogeneous through the thickness than the Compbuoy material, shear testing could be performed on very thin samples. This was not done, as the point of the testing is to create a reference value to the Compbuoy testing. For this reason, the PP samples for the shear test were produced in the same size range as the Compbuoy specimens.

9.3 Calculations

After 8 pressure tested samples have been shear tested, an average is calculated. Test6 and test8 give an average shear strength of 3.008 MPa as shown below.

$$\tau_{\text{yield,avg}} = \frac{3.19 + 2.57 + 3.18 + 4.73 + 3.28 + 3.68 + 3.13 + 3.06 + 2.33 + 2.26 + 2.14 + 2.55}{12}$$

$$\tau_{\text{yield,avg}} = 3.008\,\text{MPa}$$

After 8 similar samples have been tested, an average is calculated. Testing of unpressurized BJ365 (test6 and test7) give an average shear strength of 3.685 MPa as shown below.

$$\tau_{\text{yield,avg}} = \frac{4.5 + 3.12 + 4.07 + 3.5 + 3.42 + 3.31 + 4.36 + 3.24 + 4.1 + 3.17 + 4.34 + 3.1}{12}$$

$$\tau_{\text{yield,avg}} = 3.685\,\text{MPa}$$

The sample variance, σ^2 is given by equation 9.1.

$$\sigma^2 = \sum_{i=1}^{n} \frac{(x_i - x_{\text{avg}})^2}{n-1} \tag{9.1}$$

Where n is the number of samples.

The sample standard deviation, denoted by σ, is the positive square root of σ^2, that is, $\sigma = \sqrt{\sigma^2}$.

Chebyshev's Theorem states that the probability of any random variable X will assume a value within k standard deviations of the mean is at least $\frac{1}{k^2}$. This is shown mathematically in equation 9.2.

$$P(\mu - k\sigma < X < \mu + k\sigma) \geq 1 - \frac{1}{k^2} \tag{9.2}$$

Where μ is the mean value of X.[34]

The normal distribution curve is shown in Figure 9.11 and the probabilities are given by the empirical rule, a continuation of Chebyshev's equation.
To create a conservative estimate for the shear strength of the Compbuoy specimens tested, the confidence level is set to be 95.4%. As shown in figure 9.11, this requires an confidence interval of $\pm 2 * \sigma$. The calculations to a shear strength estimate with a 95.4% confidence level are shown in equations 9.3 and 9.4.

$$x_{avg} = 3.008\,MPa$$

$$\sigma^2 = \sum_{i=1}^{12} \frac{(x_i - 3.008)^2}{12 - 1}$$
$$\sigma^2 = 0.52231$$

$$\sigma = \sqrt{0.52231} = 0.72271$$

$$\tau_{estimate} = 3.262 - (2 * 0.62272) = 2.01656\,MPa$$

(9.3)
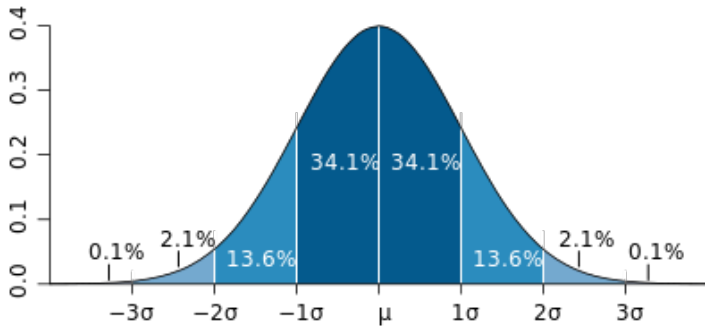
Figure 9.11: Normal distribution curve

$$x_{avg} = 3.685 \, MPa$$

$$\sigma^2 = \sum_{i=1}^{12} \frac{(x_i - 3.685)^2}{12 - 1}$$
$$\sigma^2 = \underline{0.29446}$$

$$\sigma = \sqrt{0.29446} = \underline{0.54264}$$

$$\tau_{estimate} = 3.681 - (2 * 0.60551) = \underline{\underline{2.6005 \, MPa}}$$

(9.4)

9.4 Hardness Testing

Some tests were performed to verify the data supplied by the PP manufacturers. Because the Compbuoy elements are heat treated over a long time, some of the given values may not be valid. Therefore, the Vickers hardness test was performed on a PP sample produced with the same procedures as the Compbuoy element. After production, the samples showed degraded areas, as discussed in Section 8.4.

A Vickers hardness testing machine from Mitutoyo was used as shown in Figure 9.12.

Figure 9.12: Test equipment for the vickers hardness test

A PP sample was tested in both the degraded and the flawless areas. The resulting dents in the material are shown in Figure 9.13

As shown in Table 9.5 the hardness is substancially reduced in the degraded areas. The hardness values in the degraded areas are not as accurate as in the flawless area, as the dent is clear and the edges easy to define in the flawless area, as opposed to the blur dent in the degraded area.

The yield strength of the material can be determined from the hardness by us-
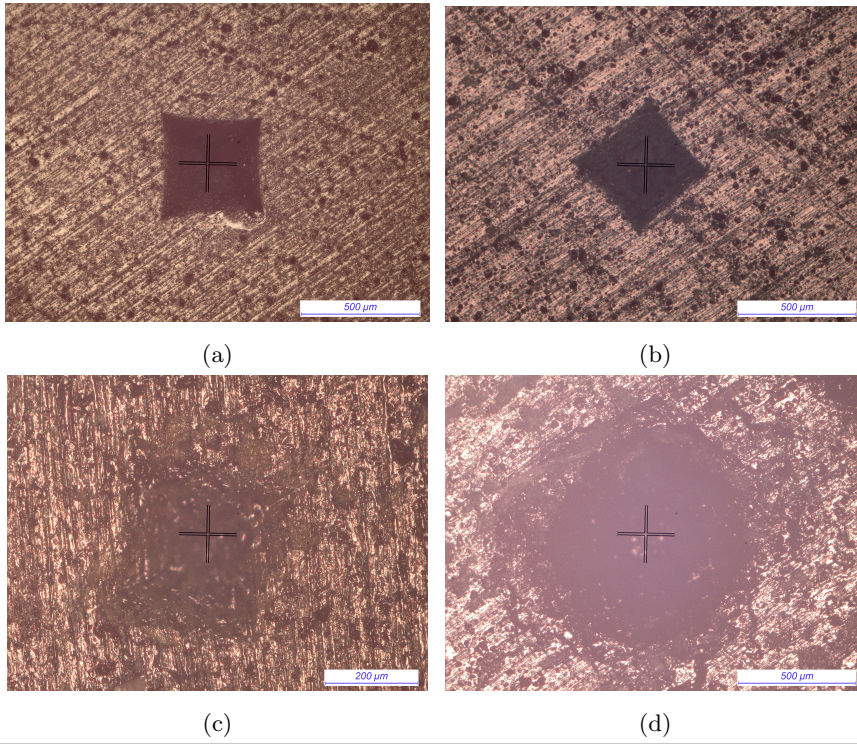
Figure 9.13: Microscope images **(a)**Flawless area 1 **(b)**Flawless area 2 **(c)**Degraded area 1 **(d)**Degraded area 2

Test #	Area	Test load	Vickers hardness
1	Flawless	1	5.2 HV
2	Flawless	1	5.3 HV
3	Degraded	0.1	0.7 HV
4	Degraded	0.1	1.5 HV

Table 9.5: Test specimen information

ing Equation 3.4. Applying the standard empirical constant value of 3, gives the flawless PP an average yield strength of 2 MPa, and the degraded area an yield strength close to zero. These results indicate that the c=3 is probably not as applicable for PP, as for metals and ceramics, but the hardness value suggest a serious reduction of strength in the degraded areas, as the hardness value is reduced by approximately 80%.

9.5   Discussion

A concern in the testing was the cracks developing in the samples during testing. The cracks indicate forces in the horizontal plane, and might be a phenomenon caused by bending moments in the sample which can cause the breakage to deviate from pure shear. To investigate this, it was necessary to identify when the cracking occurred. Test 7.4 was stopped and started several times. The test was stopped at 1.5 kN, 2 kN, 2.5 kN and right after the peak around 2.6 kN, all without any sign of cracking. When the force measured in the load cell had dropped to 2.3 kN, a small crack initiation was found, this grew bigger as the test continued, completely cracking the sample at 0.75 kN measured load. Test 8.3 and 8.4 were also paused for the same reason, but only one time, right after the peak. In both cases, no sign of cracking was discovered.

The fact that the cracking occur after the peak, support the validity of this value. The reason for the cracking is believed to be an expansion of the piece separated from the sample. When this part expands, and is pushed through the sample, it creates a pressure in the radial direction on the fracture surface of the sample. This causes a crack, starting at the fracture surface, moving all the way through the radius of the sample.

An important an unexpected discovery was that the Leca pellets did not crush during shear testing. As shown clearly in Figure 9.8 the pellets fail in a clean break and sustaining a strength contribution. Although the Leca pellets remain intact, it is clear that the crushing resistance is too low. The Compbuoy material is designed for an environment at 2500 m water depth with hydrostatic pressure up to 250 bar. Testing at 300 bar resulted in mostly crushed pellets which to some extent negates the results from the unpressurized samples, as the material system needs modifications.

It seems pretty clear that the sample thickness affect the results. The trade-off between a homogeneous material and a focused shear field is discussed in Chapter 3. Through the testing it is shown that 5/6 pressure tested samples above 12 mm have shear strength below 3 MPa, while no samples below 12 mm tested strength below 3 MPa. Also, 4/5 from the not pressure tested samples above 12 mm show a shear strength below 4 MPa, while only 3/7 samples below 12 mm show shear strength below 4 MPa.

The samples who had previously been pressure tested showed bigger spread in the results than the fresh samples. The standard deviation of the results is more than 30% higher for the pressure tested samples. The reason for this may be the different types of PP used for these samples and the variation in the extent of the pressure test, some tested on time at 300 bar, and some tested several times up to 350 bar. The value of the standard deviation implies that the results from non pressurized samples are more reliable than from the pressure tested samples.

The non-pressure tested samples have an average shear strength of 3.7 MPa and

the pressure tested samples have an average shear strength of 3 MPa. Comparing this to the theoretical shear strength of PP followed by Equation 3.1 of 14.5 MPa and the crush resistance of Leca given as 1.4 MPa its clear that the Compbuoy strength is between the strength of PP and Leca, as expected. It is however in the weaker end of the interval.

In Chapter 7, four scenarios were defined, and Scenario 2 was considered the most realistic. Based on data sheet values and the conditions given by Scenario 2, the critical load was estimated to be 5.7 kN for the pressure tested sample, and 6.53 kN for the non-pressure tested sample. In the shear tests, the critical load is divided by the fracture area to create an average value for the shear strength. The two estimated loads from the numerical analyses divided by $A = 2 * \pi * r * t = 2 * \pi * 10 * 15$ gives an average shear strengths of 6 MPa and 6.93 MPa. Comparing the numerically estimated values with the test results show a deviation of 3 MPa for the pressure tested sample and 3.24 MPa for the non-pressure tested sample. Combined, the experimental test results in shear strength approximately 50% lower than the strength estimated based on data sheet values.

Further comparison of the experimental and numerical results show that both pressure tested and non-pressure tested samples have a measured failure strain higher than estimated numerically. In Section 7.3 the estimated failure strain was 0.011 for the pressure tested sample and 0.0136 for the non-pressure tested sample. From the test result plots, the strain value is extracted, and shown together in Appendix C. The average strain for the pressure tested samples are 0.111, and 0.103 for the non-pressure tested samples.

The large deviations can be explained by several factors. In Abaqus, the sample is constrained by fixed rigid plates, in the test rig, the sample is constrained by steel plates. The test rig will have some degree of flexibility, and will not be able to instantaneously resist all forces applied when the test is started. In addition, several of the tests were stopped and started to check for cracks, this elongates the displacement-force curve and increases the nominal strain value calculated by Equation 7.1. Also, the hardness testing showed another important source of error. The PP in the Compbuoy is weaker than modeled in Abaqus, which implies larger strain and lower stress in the test than in the numerical model due to a more flat stress-strain curve.

The hardness testing of PP gave another result for strength of PP post heat treatment. This test indicated 80% hardness reduction in the degraded area. The Leca pellets are filled with air which might cause large degraded areas in the Compbuoy sample, which could be the explanation for the large deviations between numerical and experimental results.

Comparing the strength results with the requirements from earlier work, where the Compbuoy elements are required to handle shear stress of 5 MPa, is concerning. Even without a safety factor and not considering standard deviations, only a few samples showed strength above 4 MPa (6/24 samples).

Chapter 10

Conclusion

The shear strength of Compbuoy is identified as a critical factor when the buoyancy elements are operating under harsh conditions with a combination of extreme hydrostatic pressure and buoyancy loads. Compbuoy buoyancy elements have been produced and shear tested. No test method existed for measuring shear strength of the multiphase Compbuoy material. A new method was developed, tested for its validity and used to obtain the shear strength. The shear test method is based on pressing a ring through the material. This new punch test method was evaluated with numerical testing.

From the numerical analyses performed the following is concluded.
Interference from stress components other than shear in z-direction is found to be correlated with increased sample thickness. Recommended sample thickness is found to be as thin as possible, while meeting a requirement of minimum 3 Leca pellets through the thickness in the shear zone.
The radial width of the shear zone is related to the concentration of shear stress through the thickness, a thin shear zone has large concentration of the shear stress, thereby reducing the effect of interference from other stress components. A shear zone with a 1 mm is found to be beneficiary for both the concentration of shear stress, and the number of elements in the Abaqus model.
Based on data sheet values for Leca and polypropylene, pressure tested Compbuoy samples have an estimated failure strain of 0.011 and an estimated average shear strength of 6 MPa. Non-pressure tested Compbuoy samples are found to have an estimated failure strain of 0.0136 and shear strength of 6.93 MPa.

From the shear test in the lab the following is concluded.
Shear testing has been performed on 24 comparable Compbuoy samples, both pressure tested samples and samples without any previous load exposure. In the pressure tested samples, the Leca pellets had been crushed by pressure leaving only concrete dust filled spheres in the PP. The 12 pressure tested samples tested an

average shear strength value of 3 MPa, while the unpressurized samples were found to have an average shear strength of 3.7 MPa. Because of the randomness in the placement of Leca pellets and degraded PP areas in the test sample, the test results show a spread with a standard deviation of 0.5 MPa for the unpressurized samples. Shear strength estimate with 95.4% confidence level for the pressure tested sample is 2 MPa and 2.6 MPa for the non-pressure tested samples.

The difference in shear strength between the numerical and the experimental results is explained by the inaccuracy of supplied material properties. For Leca, material properties were obtained from testing large bulks, while in the Compbuoy sample, Leca pellets are placed in PP, separated from a bulk. For PP, the material properties are supplied by the manufacturer, with an intention to present as impressive as possible results. The yield stress given is obtained through a tensile test with 50 mm/min cross-head speed. This results in a unreal high value compared to a test with 1.24 mm/min and consequently the numerical analyses estimate a higher shear strength than measured in the experimental shear tests. Also, the numerical analyses does not account for the production method used to produce the Compbuoy samples, which is found to degrade the PP.

Polypropylene has a measured Vickers hardness of 5.3 HV in the flawless areas. The Vickers hardness test indicated 80% hardness reduction in areas degraded during production of the Compbuoy elements.
The production of the Compbuoy elements including a comprehensive heat treatment, the polypropylene shows seriously degraded areas, discolored and brittle. The degradation found in the PP after heat treatment is considered to be the result of contact with air/gas during the process. This occur both on the surface of the Compbuoy element which is in open contact with air, and internally as gas bubbles are trapped inside the material during the heat treatment. This dramatically reduce the strength of the PP, and if this can be reduced it will increase the strength of the Compbuoy material.

Earlier work performed to provide design criteria for the buoyancy elements suggest the Compbuoy needs to handle shear stress up to 4 MPa. Evaluating the test results versus these requirements it is crystal clear that the material needs to be reinforced. It is clear from numerical analyses and mechanical testing that the Leca pellets and heat treatment degraded PP are the weakest links.

10.1 Further work

Avoiding or reducing the PP degradation problem may be done by covering the mold with a plastic bag and applying vacuum, this will reduce the area of degraded PP on the surface. Using a PP with higher melting flow rate will make the material less viscous during the melting and may reduce the amount of gas trapped inside the material. Another possibility is to melt the Compbuoy elements in several steps. Today, all layers of PP and Leca are placed in the mold and then placed

in the oven. This will melt the outer parts of the BE first, trapping air in the center of the sample. By placing a few layers at the time, melting the mix before adding more layers and repeating the process, less air will be trapped inside the sample.

The other weak link in the material system is the Leca pellets, the current situation with crushed pellets after pressure testing is not acceptable. Two possible solutions are presented. The Leca pellets could be reinforced by coating the pellets before mixing them with PP. This requires a strong, light and inexpensive coating material suited for Leca pellets. Otherwise, stronger Leca pellets could be developed. This is a job for the producer of Leca, and increased crushing resistance must not compromise the main benefit of Leca, light weight.

Alternatively, buoyancy elements with different shapes can be produced and tested. Spherical buoyancy elements will perhaps be able to handle the hydrostatic pressure better than the cylindrical elements produced today, as they will not have the large flat top and bottom surfaces that accumulates large compressive forces.

Bibliography

[1] Abaqus. *Abaqus Analysis Manual*. Abaqus, 6.12 edition.

[2] Abaqus. Abaqus/cae user's manual.

[3] API. Specification for marine drilling riser equipment api specification 16f, Nov 2009.

[4] CompBuoy AS. http://compbuoy.com/.

[5] ASTM. D5379 standard test method for shear properties of composite materials by the v-notched beam method., 1993.

[6] ASTM. D7078 standard test method for shear properties of composite materials by v-notched rail shear method, 2005.

[7] ASTM. D732-10 standard test method for shear strength of plastics by punch tool, 2010.

[8] Robert M. Caddell and Alan R. Woodliff. Yield behavior of unoriented and oriented polycarbonate and polypropylene as influenced by temperature. Technical report, Department of Mechanical Engineering, University of Michigan, Ann Arbor, Mich. 48109 (U.S.A.), 1979.

[9] Yih Chang and Yyh-Chau Yang. Mechanical properties of the polypropylene copolymer measured by the impression method. *Journal of Polymer Science, Part B: Polymer Physics*, Volume 34, Issue 13:8, 1998.

[10] Adil Javed Chaudhary. Direct shear and punching test. Scribd, 10 2008.

[11] J. L. Clark. *Structural Lightweight Aggregate Concrete Performance*. Blackie Academic & Professional, 1993.

[12] Mikael Hallgren, Sven Kinnunen, and Birgitta Nylander. Punching shear tests on column footings. *Tekna*, 1:23, 1998.

[13] R. C. Hibbeler. *Mechanics of Materials*. Prentice Hall, 2011.

[14] HMCPolymers. Pp properties.

[15] Endre Magnus Hva and Ander Samstad Gylland. Documentation of material properties for leca aggregates. Technical report, Sintef, 2009.

[16] Ineos. Typical engineering properties of polypropylene.

[17] Instron. Product information.

[18] Granta Material Intelligence. Yield strength, elastic limit, and ultimate strength. http://inventor.grantadesign.com/.

[19] ASTM International. Standard terminology relating to methods of mechanical testing.

[20] Fridtjov Irgens. Formelsamling mekanikk. Tapir akademisk forlag, 1999.

[21] E. Kontou and P. Farasoglou. Determination of the true stressstrain behaviour of polypropylene. Technical report, Department of Engineering Science, Section of Mechanics, National Technical University of Athens, 1998.

[22] S.M. Kurtz. Miniature specimen shear punch test for uhmwpe used in total joint replacements. *sciencedirect.com*, 23:12, 2002.

[23] Kristin Lippe. *Offshore Insulation and Buoyancy materials - Development of a Novel Material System.* PhD thesis, NTNU, 2008.

[24] P. K. Mallick and Yuanxin Zhou. Yield and fatigue behavior of polypropylene and polyamide-6 nanocomposites. *Journal of materials science*, 38:3183–3190, 2003.

[25] MatWeb. Datasheet - arkema group appryl 3120 mu 5 polypropylene-polyethylene copolymer.

[26] J.P.G. Mijnsbergen, S. Helland, M. Maage, T. Hammer, I. Holland, E.L. Sveinsdttir, and K. van Breugel. Economic design and construction with stuctural lightweight aggregate concrete. Technical report, EUROMAT99, 1999.

[27] M.P. Nielsen and L.C. Hoang. *Limit Analysis and Concrete Plasticity, Third Edition.* Taylor & Francis, 2010.

[28] Emil Okstad. material oversikt. XLdoc recieved by mail.

[29] Ram Raghava, Robert M. Caddell, and Gregory S. Y. Yeh. The macroscopic yield behaviour of polymers. Technical report, Department of Mechanical Engineering, The University of Michigan, Ann Arbor, Michigan, USA, 1973.

[30] John Scheirs. *Compositional and Failure Analysis of Polymers - A Practical Approach.* John Wiley & Sons, 2000.

[31] Y.L. Shen, N. Chawla, E. S. Ege, and X. Deng. Deformation analysis of lap-shear testing of solder joints. *Acta Materialia*, 53:2633–2642, 2005.

[32] Toolingu. Class vocabulary.

[33] Nils Petter Vedvik. Analysis guidelines: Composite failure. It's Learning, 2012.

[34] Ronald E. Walpole, Raymond H. Myers, Sharon L. Myers, and Keying Ye. *Probability & Statistics for Engineers & Scientists -Ninth Edition*. Pearson Education, Inc., 2012.

[35] P. Zhang, S. X. Li, and Z. F. Zhang. General relationship between strength and hardness. *Materials Science and Engineering A*, 529:62–73, 2011.

[36] Zhongping Zhang, Qiang Sun, Chunwang Li, and Wenzhen Zhao. Theoretical claculation of the strain-hardening exponent and the strength coefficient of metallic materials. *Journal of Materials Engineering and Performance*, 15:4, 2006.

Appendix A

Technical Drawings
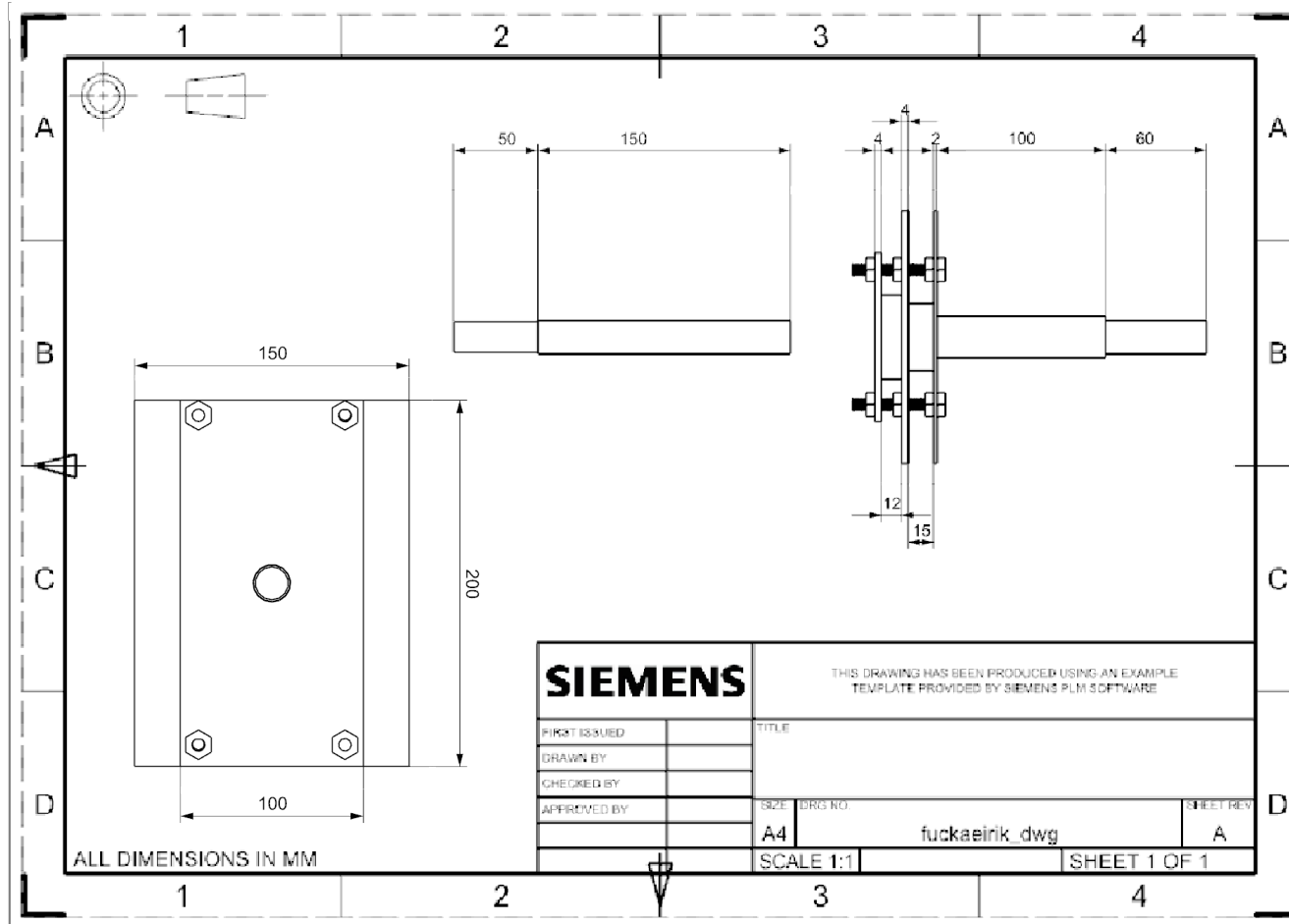
Figure A.1: technical drawing test rig, cross-section
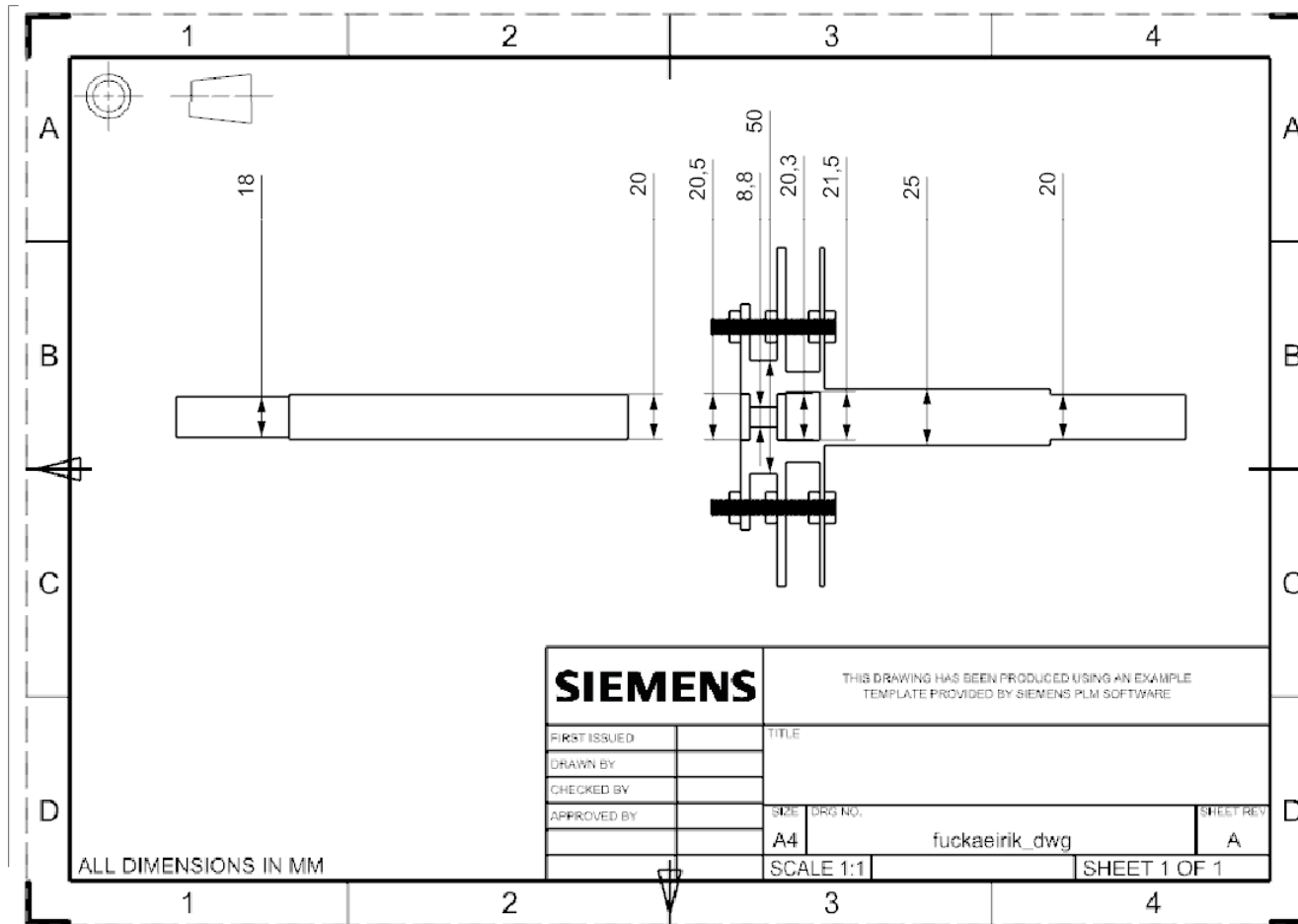
Figure A.2: Technical drawing test rig, diameters

Appendix B

Data Sheet and Safety Evaluation

Polypropylene
BJ356MO

Description

BJ356MO is a heterophasic copolymer. This grade provides very high melt flow rate, very high stiffness and medium impact strength. and is designed for high-speed injection moulding and contains nucleating and antistatic/demoulding additives.

Components moulded from this grade show good ejectability and combine excellent stiffness with very good gloss, good antistatic and excellent organoleptic properties.

Applications

Thin wall containers   Technical parts
Household applications

Special features

High stiffness   Shows excellent antistatic performance
Medium impact strength   Good gloss

Physical Properties

Property		Typical Value Data should not be used for specification work	Test Method
Density		906 kg/m3	ISO 1183
Melt Flow Rate (230 °C/2,16 kg)		100 g/10min	ISO 1133
Tensile Modulus (1 mm/min)		1.650 MPa	ISO 527-2
Tensile Strain at Yield (50 mm/min)		4 %	ISO 527-2
Tensile Stress at Yield (50 mm/min)		29 MPa	ISO 527-2
Heat Deflection Temperature (0,45 N/mm²) [1]		105 °C	ISO 75-2
Instrumented Falling Weight (0 °C)	Max Force		ISO 6603-2
	Total Penetration Energy	10 J	
Instrumented Falling Weight (-20 °C)	Max Force		ISO 6603-2
	Total Penetration Energy	10 J	
Charpy Impact Strength, notched (23 °C)		4,5 kJ/m²	ISO 179/1eA
Charpy Impact Strength, notched (-20 °C)		2,5 kJ/m²	ISO 179/1eA
Hardness, Rockwell (R-scale)		93	ISO 2039-2

[1] Measured on injection moulded specimens acc. to ISO 1873-2

Processing Techniques

This product is easy to process with standard injection moulding machines.

Following moulding parameters should be used as guidelines:
Melt temperature   210 - 260 °C
Holding pressure   200 - 500 bar   Minimum to avoid sink marks.

BOREALIS

Polypropylene
BH345MO

Description

BH345MO is a heterophasic copolymer. This grade is characterized by optimum combination of very high stiffness, good flow properties and good impact strength. and is designed for high-speed injection moulding and contains nucleating and antistatic/demoulding additives.

Components moulded from this grade show good ejectability and combine excellent stiffness with very good gloss, good antistatic and excellent organoleptic properties.

Applications

Thin wall containers
Frozen food packaging
Closures

Household applications
Technical parts
Pails

Special features

Shows excellent antistatic performance
High impact strength

High stiffness
Good gloss

Physical Properties

Property		Typical Value Data should not be used for specification work	Test Method
Density		904 kg/m3	ISO 1183
Melt Flow Rate (230 °C/2,16 kg)		45 g/10min	ISO 1133
Tensile Modulus (1 mm/min)		1.400 MPa	ISO 527-2
Tensile Strain at Yield (50 mm/min)		5 %	ISO 527-2
Tensile Stress at Yield (50 mm/min)		26 MPa	ISO 527-2
Heat Deflection Temperature (0,45 N/mm²) [1]		95 °C	ISO 75-2
Instrumented Falling Weight (0 °C)	Max Force		
	Total Penetration Energy	30 J	
Instrumented Falling Weight (-20 °C)	Max Force		
	Total Penetration Energy	22 J	
Charpy Impact Strength, notched (23 °C)		6,5 kJ/m²	ISO 179/1eA
Charpy Impact Strength, notched (-20 °C)		4,0 kJ/m²	ISO 179/1eA
Hardness, Rockwell (R-scale)		89	ISO 2039-2

[1] Measured on injection moulded specimens acc. to ISO 1873-2

Processing Techniques

This product is easy to process with standard injection moulding machines.

Following moulding parameters should be used as guidelines:
Melt temperature   210 - 260 °C

BOREALIS

Sikkerhets- og kvalitetsgjennomgang av laboratorietester og verkstedsarbeid
Safety and Quality Evaluation of Activities in the Laboratory and Workshop

NTNU

Perleporten

1 Identifikasjon - *Identification*	Dokumentnr. – *Document no.*:	
Kundenavn – *Customer name*	Prosjektnavn – *Project name*	Projektnr. – *Project no.*
COMPBUOY	FAILURE PREDICTION IN COMPBUOY	46071100
Beskrivelse av arbeid – *Description of job*		Dato – *Date*
SKJÆRPRØVE AV COMPBUOY		18/3 - 13

2 Projekt - *Team*

Prosjektleder og organisasjon – *Project manager and organisation*	ANDREAS ECHTERMEYER	Ansvarlig for instrumentering – *Responsible for instrumentation.*	EIRIK HOEL
Leiestedsansvarlig – *Laboratory responsible*	— '' —	Operatør – *Operator*	— '' —
Auditør for sikkerhets og kvalitetsgjennomgang – *Auditer for safety check*	— '' —	Ansvarlig for styring av forsøk – *Responsible for running the experiment.*	— '' —
Ansvarlig for eksperimentelt faglig innhold – *Responsible for experimental and scientific content*	— '' —	Ansvarlig for logging av forsøksdata – *Responsible for logging and storing experimental data*	— '' —
Ansvarlig for dimensjonering av last og trykkpåkjente komponenter – *Reponsible for dimensioning load bearing and pressurized components*	EIRIK HOEL	Ansvarlig for montering av testrigg – *Responsible for building the rig*	— '' —

3 Viktig!! – *Important!!*   J: Ja – *Yes* / N: Nei - *No*

Er arbeidsordren signert? – *Is the work order signed?*	
Har operatøren nødvendig kurs/trening i bruk av utstyret? - *Has the operator the required courses/training on the equipment?*	
Har operatøren sikkerhetskurs? (påbudt) – *Has the operator followed the safety courses? (mandatory)*	

4.1 Sikkerhet – *Safety* (Testen medfører – *The test contains*)   J: Ja – *Yes* / N: Nei - *No*

Stor last – *Bib loads*	N	Brannfare – *Danger of fire*	N
Tunge løft – *Heavy lifting*	N	Arbeid i høyden – *Working at heights*	N
Hengende last – *Hanging load*	N	Hydraulisk trykk – *Hydraulic pressure*	J
Gasstrykk – *Gas pressure*	N	Vanntrykk – *Water pressure*	N
Høy temperatur – *High temperature*	N	Lav temperatur – *Low temperature*	N
Deler i høy hastighet – *Parts at high velocity*	N	Farlige kjemikalier – *Dangerous chemicals*	N
Sprutaslerasjon ved brudd – *Sudden acceleration at fracture/failure*	J	Forspente komponenter – *Pre-tensioned components*	N
Farlig støv – *Dangerous dust*	N	Kraftig støy – *Severe noise*	N
Klemfare – *Danger of pinching*	J	Roterende deler – *Rotating parts*	N

4.2 Påkrevet verneustyr – *Required safety equipment*   J: Ja – *Yes* / N: Nei - *No*

Briller (påbudt) – *Glasses (mandatory)*	J	Vernesko – *Safet shoes*	N
Hjelm – *Helmet*	N	Hansker – *Gloves*	J
Skjerm – *Screen*	J	Visir – *Visir*	N
Hørselsvern – *earprotection*	J	Løfteredskap – *Lifting equipment*	N
Yrkessele, fallsele, etc. –*harness ropes, other measures to prevent falling down.*	N		

Sikkerhets- og kvalitetsgjennomgang av laboratorietester og verkstedsarbeid

◘ NTNU
Perleporten

5.1 Beskrivelse av aktivitet – *Description of the activity (see Appendix)*

Vurdering skal være basert på en skriftlig prosedyre for bruk av maskinen. I enkelte tilfeller kan prosedyre bli beskrevet direkte i tabellen nedenfor.

The evaluation shall be based on a written operating procedure for the machine. For simple cases the procedure can be directly described in the tables below.

Nr.	Beskrivelse av aktivitet – *Description of activity*	Fare - *Danger*	Prosedyre nr. – *Procedure no.*	Sannsynlighet – *Probability*	Konsekvens – *Consequence*	Risiko – *Risk*
1	SKJÆR TEST AV COMPBUOY	SPLINTER FRA TESTRØVER		3	1	3
2	SAGING AV PRØVER	SÅGE F.INGRE		2	3	6

5.2 Korrigerende Tiltak – *Corrective Actions*

Nr.	Korrigerende tiltak – *Corrective action*	Sannsynlighet – *Probability*	Konsekvens – *Consequence*	Risiko – *Risk*	Utført dato – *Date of action*
2	EKSTRA VARSOMHET UTØVD VED SAGING	1	3	3	20/3-13
1	SKJERMING AV SKJÆRLEST	1	1	1	21/3-13

Sikkerhets og kvalitetsgjennomgang av laboratorietester og verkstedsarbeid

NTNU
Perleporten

5.3 Feilkilder – *Reasons for mistakes/errors*

Sjekkliste: Er følgende feilkilder vurdert? – Check list: Is the following considered?   J: Ja – *Yes* / N: Nei - *No*

Tap av strøm – *Loss of electricity*		Overspenning – *Voltage surge*	
Elektromagnetisk støy – *Electromagnetic noise*		Manglende aggregatkapasitet av hydraulikk – *Insufficient power of the machine*	
Jordfeil – *Electrical earth failure*		Vannsprut – *Water jet*	
Ustabilt trykk av hydraulikk/kraft – *Unstable pressure or hydraulic force*		Tilfeldig avbrudd av hydraulikk/kraft – *Unintended interruption of power supply*	J
Last-/ forskyvnings grenser etablert ? – *Are load and displacement limits established?*	J	Lekkasjer (slanger/koblinger, etc.) – *Leakage of pipes, hoses, joints, etc.*	
Mulige påvirkninger fra andre aktiviteter – *Possible interference from other activities*		Mulige påvirkninger på andre aktiviteter – *Possible interference towards other activities*	N
Problemer med datalogging og lagring – *troubles in loading and storage*		Brann i laboratoriet – *Fire in the laboratory*	

6 Kalibreringsstatus for utstyr – *Calibration of equipment*

(ex: load cell, extensometer, pressure transducer, etc)

I.D.	Utstyr - *Equipment*	Gyldig til (dato) – *Valid until (date)*

7 Sporbarhet – *Tracebility*

Eksisterer – Is there   J: Ja – *Yes* / N: Nei - *No*

Er alle prøvematerialene kjente og identifiserbare? – *Are all experimental materials known and traceable?*	J
Eksisterer det en plan for markering av alle prøvene? – *Is there a plan for marking all specimens?*	J
Er dataloggingsutstyret identifisert? – *Is the data aquisition equipment identified?*	J
Er originaldata lagret uten modifikasjon? – *Are the original data stored safely without modification?*	J
Eksisterer det en backup-prosedyre? – *Is there a back-up procedure for the data (hard disk crash)?*	J
Eksisterer det en plan for lagring av prøvestykker etter testing? – *Is there a plan for storing samples after testing?*	J
Eksisterer en plan for avhending av gamle prøvestykker? – *Is there a plan for disposing of old samples?*	J

8 Kommentarer – *Comments*

9 Signaturer – *Signatures*

Godkjent (dato/sign) – *Approved (date/signature)*

Sikkerhets og kvalitetsgjennomgang av laboratorietester og verkstedsarbeid

◼ NTNU
Perleporten

APPENDIX Bakgrunn - Background

Sannsynlighetskategorier:	Probability Categories:
1: Lite sannsynlig, 1x pr. 50 år el.sjeldnere	1: Very unlikely, 1 time per 50 years or less
2: Mindre sannsynlig, 1x pr. 10 år el.sjeldnere	2: Unlikely, 1 time per ten years or less
3: Sannsynlig, 1x pr. år el.sjeldnere	3: Probable, 1 time per year or leaa
4: Meget sannsynlig, 1x pr. måned el. oftere	4: Very Probable, 1 time per week or more
5: Svært sannsynlig, 1x pr. år el.sjeldnere	5: Nearly certain, 1 time per week

Konsekvenskategorier: Consequence Categories:

	Gruppe / Group	Konsekvens / Consequence
1 Lite alvorlig *Not serious*	Sikkerhet, mennesket Safety	Ingen fysisk ubehag. Ingen helsemessig konsekvens. Enkelttilfeller med misnøye. No physical discomfort. No health consequences. In some cases feeling a bit badly.
	Omdømme Reputation	Liten påvirkning på troverdighet og respekt. Little influence on trustworthiness and respect.
	Ytre miljø Environment	Ubetydelig skade og kort restitusjonstid Negligible damage and short recovery time.
	Øk/matr. Economic/ material	Drifts eller aktivitetsstans <1 dag, økonomisk tap inntil NOK 50.000 Shutdown of operation or activities < 1 day. Economic loss less than NOK 50 000.
2 Mindre alvorlig *Slightly serious*	Sikkerhet, mennesket Safety	Skade som ikke trenger legehjelp. Belastende forhold for gruppe mennesker uten målbare konsekvenser Injury that does not need medical treatment. Unpleasant circumstances for a group of people are without measurable consequences.
	Omdømme Reputation	Negativ påvirkning på troverdighet og respekt. Negative influence on trustworthiness and respect.
	Ytre miljø Environment	Mindre skade og kort restitusjonstid. Little damage and short recovery time.
	Øk/matr. Economic/ material	Drifts eller aktivitetsstans <1 uke. Økonomisk tap inntil NOK 250.000 Shutdown of operation or activities < 1 week. Economic loss less than NOK 250 000.
3 Alvorlig *Serious*	Sikkerhet, mennesket Safety	Skade som trenger legehjelp. Misnøye som fører til fravær. Injury that needs medical treatment. Unpleasant circumstances may lead to sick leave.
	Omdømme	Troverdighet og respekt svekket.

	Reputation	Trustworthiness and respect are reduced.
	Ytre miljø Environment	Mindre skade og lang restitusjonstid. Little damage and long recovery time.
	Øk/matr. Economic/ material	Drifts eller aktivitetsstans <1 mnd. Økonomisk tap inntil NOK 5 mill Shutdown of operation or activities < 1 month. Economic loss less than NOK 5 million.
4 Meget Alvorlig *Very serious*	Sikkerhet, mennesket Safety	Skade som må behandles av lege og som medfører fravær. Stor grad av mistrivsel. Injury that needs medical treatment and will cause sick leave. Severe consequences for well being.
	Omdømme Reputation	Troverdighet og respekt betydelig svekket. Trustworthiness and respect are severely reduced.
	Ytre miljø Environment	Langvarig skade og lang restitusjonstid Long term damage and long recovery time.
	Øk/matr. Economic/ material	Driftsstans < 0,5 år. Aktivitetsstans i inntil 1 år. Økonomisk tap inntil NOK 5 mill. Shutdown of operation or activities < 0.5 years. Economic loss less than NOK 5 million.
5 Svært Alvorlig *Ex-tremely serious*	Sikkerhet, mennesket Safety	Død eller alvorlig skade på en eller flere personer. Gjennomgående fravær med stor grad av mistrivsel. Death or serious injury to one or more people. Will cause long term sick leave and leads to severe consequences for well being.
	Omdømme Reputation	Troverdighet og respekt betydelig og varig svekket. Trustworthiness and respect are severely reduced for a long time.
	Ytre miljø Environment	Svært langvarig og ikke reversibel skade. Very long term damage and non reversible damage.
	Øk/matr. Economic/ material	Drifts- eller aktivitetsstans> 1år. Økonomisk tap > NOK 5 mill. Shutdown of operation or activities > 1 year. Economic loss more than NOK 5 million.

Risikomatrise – Risk matrix:		
Risiko = Sannsynlighet * Konsekvens		Risk = Probability * Consequence
(Grønt – green)	Eventuelle risikoreduserende tiltak planlegges Eventually risk reducing actions have to be planed.	
(Gult - yellow)	Risikoreduserende tiltak skal planlegges. Risk reducing actions have to be planed.	
(Rødt - red)	Stopp. Risikoreduserende tiltak skal gjennomføres. Stop. Risk reducing actions have to be planed.	

Risikoverdi = Sannsynlighet x Konsekvenser
Beregn risikoverdi for menneske. Enheten vurderer selv om de i tillegg beregner risikoverdi for ytre miljø, Øk/ matr og omdømme. I så fall beregnes disse hver for seg.

Risk = Probability x Consequence
Calculate risk level for humans. The section shall evaluate itself if it shall calculate in addition risk for the environment, economic/material and reputation. If so, they shall be calculated separately.

Til Kolonnen "Korrigerende Tiltak":
Tiltak kan påvirke både sannsynlighet og konsekvens. Prioriter tiltak som kan forhindre at hendelsen inntreffer, dvs sannsynlighetsreduserende tiltak foran skjerpende beredskap, dvs konsekvensreduserende tiltak.

For Column "Corrective Actions"
Corrections can influence both probability and consequence. Prioritize actions that can prevent an event from happening.

Oppfølging:
Tiltak fra risikovurderingen skal følges opp gjennom en handlingsplan med ansvarlige personer og tidsfrister.

Follow Up
Actions from the risk evaluation shall be followed through by an action plan with responsible persons and time limits.

Verdisetting, prioritering og oppfølging

K O N S E K V E N S		Lite sannsynlig 1	Mindre sannsynlig 2	Sannsynlig 3	Meget sannsynlig 4	Svært sannsynlig 5
	Svært alvorlig 5					
	Meget alvorlig 4					
	Alvorlig 3					
	Mindre alvorlig 2					
	Lite alvorlig 1					
		SANNSYNLIGHET				

Appendix C

Complementary pictures and data

Path in edge of shear zone							
tykk10_mises		tykk10_s23		tykk15_mises		tykk15_s23	
dist.	stress	dist.	stress	dist.	stress	dist.	stress
0	16.1177	0	-1.5779	0	10.8212	0	-1.68647
1.49777	7.45372	1.49777	2.74749	1.50028	10.0139	1.50028	3.59669
2.99615	18.0995	2.99615	9.94477	3.00017	20.3103	3.00017	11.3931
4.4876	15.2162	4.4876	4.88076	4.49437	14.1051	4.49437	6.14354
5.97597	14.0996	5.97597	3.12668	5.98526	16.4147	5.98526	6.64285
7.46324	20.3183	7.46324	7.72391	7.47448	27.7897	7.47448	13.9906
7.46324	21.5353	7.46324	8.743	7.47448	28.4903	7.47448	14.6583
8.69977	22.4301	8.69977	7.11881	8.9586	25.9017	8.9586	7.51876
8.69977	22.638	8.69977	6.07876	8.9586	25.5291	8.9586	7.16313
9.93498	25.8513	9.93498	8.28508	10.439	22.6715	10.439	3.29265
9.93498	25.0001	9.93498	9.58193	10.439	22.572	10.439	3.22453
				11.9194	25.4728	11.9194	7.79574
				11.9194	27.3065	11.9194	8.74641
				13.3993	29.9265	13.3993	9.10444
				13.3993	29.1684	13.3993	8.99858
				14.8774	32.1124	14.8774	9.63258
				14.8774	29.9842	14.8774	10.9267

Figure C.1: Values for graphs 7.5

Without Leca

τ absolute max.			τ center max.			τ average			τ min.		
Stress (MPa)	Time (s)	Strain	Stress(MPa)	Time (s)	Strain	Stress(MPa)	Time (s)	Strain	Stress(MPa)	Time (s)	Strain
0	0	0	0	0	0	0	0	0	0	0	0
4.71405	1	0.001377778	1.90693	1	0.001377778	1.06311	1	0.001377778	0.312648	1	0.001377778
9.95027	2	0.002755556	3.96809	2	0.002755556	2.22598	2	0.002755556	0.640301	2	0.002755556
16.5183	3.5	0.004822222	7.06074	3.5	0.004822222	3.96493	3.5	0.004822222	1.12858	3.5	0.004822222
17.0446	5.75	0.007922222	11.7713	5.75	0.007922222	6.44819	5.75	0.007922222	1.87238	5.75	0.007922222
18.2086	9.125	0.012572222	15.3598	9.125	0.012572222	9.42461	9.125	0.012572222	3.08025	9.125	0.012572222
19.9573	14.1875	0.019547222	16.5501	14.1875	0.019547222	12.0212	14.1875	0.019547222	4.91484	14.1875	0.019547222
22.4657	20.1875	0.027813889	16.9128	20.1875	0.027813889	13.4246	20.1875	0.027813889	5.1412	20.1875	0.027813889
26.6819	26.1875	0.036080556	17.5131	26.1875	0.036080556	14.1762	26.1875	0.036080556	3.79869	26.1875	0.036080556
33.7176	32.1875	0.044347222	18.0355	32.1875	0.044347222	14.7033	32.1875	0.044347222	3.07067	32.1875	0.044347222
41.023	38.1875	0.052613889	18.4321	38.1875	0.052613889	15.1433	38.1875	0.052613889	2.85588	38.1875	0.052613889
46.4311	44.1875	0.060880556	18.9028	44.1875	0.060880556	15.5412	44.1875	0.060880556	3.48595	44.1875	0.060880556
46.7726	48.38	0.066656889	19.2052	48.38	0.066656889	15.8048	48.38	0.066656889	4.26947	48.38	0.066656889

Figure C.2: Values for graphs 7.15

Without Leca

Contact Force 3			Reaction Force 3		
CF(N)	Time (s)	Strain	RF(N)	Time (s)	Strain
0	0	0	0	0	0
819.515	1	0.001378	866	1	0.001378
1715.57	2	0.002756	1811.14	2	0.002756
3055.27	3.5	0.004822	3223.99	3.5	0.004822
5005.92	5.75	0.007922	5256.7	5.75	0.007922
7513.78	9.125	0.012572	7816.9	9.125	0.012572
9897.33	14.1875	0.019547	10240.8	14.1875	0.019547
11199.7	20.1875	0.027814	11598.3	20.1875	0.027814
11896.4	26.1875	0.036081	12353.2	26.1875	0.036081
12376.9	32.1875	0.044347	12900.9	32.1875	0.044347
12770.8	38.1875	0.052614	13366.7	38.1875	0.052614
13123.8	44.1875	0.060881	13792.7	44.1875	0.060881
13356.6	48.38	0.066657	14075.8	48.38	0.066657

Figure C.3: Values for graphs 7.19

Test	Disp (mm)	Thick (mm)	Strain
5.1	1.42	8.5	0.1671
5.2	1.354	8.1	0.1672
5.3	1.493	8.5	0.1756
5.4	1.65	7	0.2357
6.1	1.14	12.5	0.0912
6.2	0.633	12	0.0527
6.3	0.804	10	0.0804
6.4	0.753	11.5	0.0655
7.1	0.521	13.5	0.0386
7.2	0.693	13	0.0533
7.3	0.651	13.5	0.0482
7.4	0.75	12.5	0.0600
8.1	1.83	11.5	0.1591
8.2	1.53	11.4	0.1342
8.3	1.86	11	0.1691
8.4	1.81	11.8	0.1534
10.1	1.461	13	0.1124
10.2	1.265	12	0.1054
10.3	1.206	12	0.1005
10.4	1.529	13	0.1176
11.1	0.6	9.5	0.0632
11.2	0.58	12	0.0483
11.3	0.657	8.5	0.0773
11.4	0.8	7.5	0.1067
PP1	1.14	10	0.1140
PP2	0.72	12	0.0600
PP3	0.903	10.5	0.0860
PP4	0.818	9.5	0.0861

Figure C.4: Failure strain table

Appendix D

Alternative approach to numerical analyses

D.1 PP - Deformation plasticity

In order to perform a simulation of deformation plasticity, Abaqus requires data from the following mechanical properties: Young's Modulus, Poisson's Ratio, yield stress, strain hardening exponent and the yield offset[2, 23.2.13].

Young's Modulus and the tensile yield stress are given in the BJ356MO material data sheets as 1650 MPa and 29 MPa.

The Poisson's Ratio for polypropylene is found to be 0.45[16].

As discussed in chapter 3, the yield offset is given the standard value of 0.2%.

The strain hardening exponent, noted as n, is expressed mathematically in equation 3.8.

Figure D.1 show the same test as shown in figure 6.5 plotted with logarithmic scales.
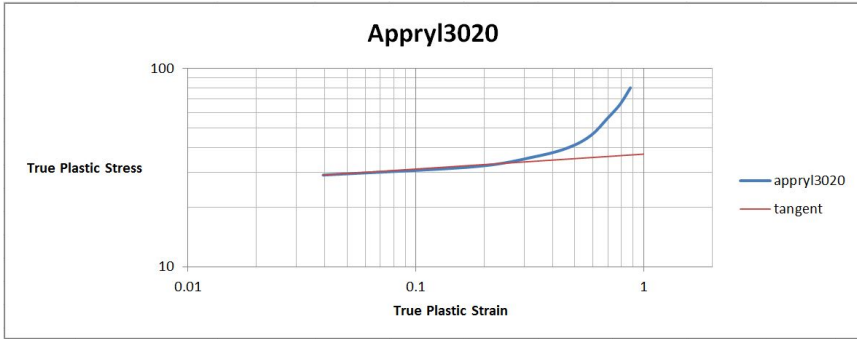
Figure D.1: Stress-strain curve at cross-head speed of 1mm/min

Because the test is not performed to reach a plastic strain of 1, and the end of the test is in a region of non-uniform plastic deformation, a tangent is constructed in the linear region to provide the necessary data. The value of K is from figure D.1 found to be 37 MPa. The strain hardening exponent is the slope of the true stress-strain curve in a log-log plot, in this case, the slope of the tangent in figureD.1[36]. The strain hardening exponent for the Polypropylene used is found through the following calculations: $\frac{\log 37 - \log 29}{\log 1 - \log 0.03922} = \underline{0.07522}$

The loads, boundary conditions and meshing were performed as described in Chapter 6.

Results

The deformations in z-direction in shown in Figure D.2. Maximal displacement is in the red area and have between 1.4 and 1.6 mm displacement.
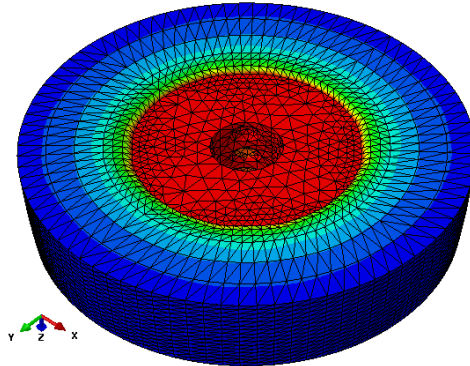
Figure D.2: Displacements

The mises stress is shown in Figure D.3. Maximal stress is found in the green area, at 1.5mm displacement the stress in the green area is between 140 and 170 MPa. The shear stress is shown in Figure D.4 and Figure D.5. In both figures, the
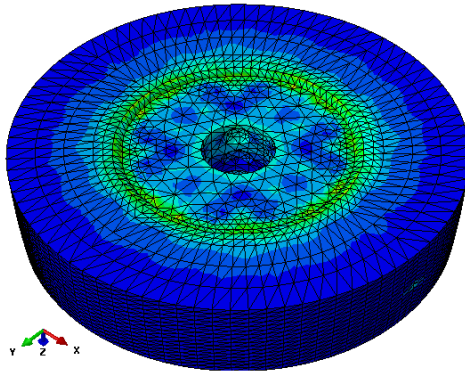
Figure D.3: Mises stress at $1.5\,$mm punch tool penetration

maximal shear stress at $1.5\,$mm displacement is found in the red areas, with a value between 85 and 110 MPa.
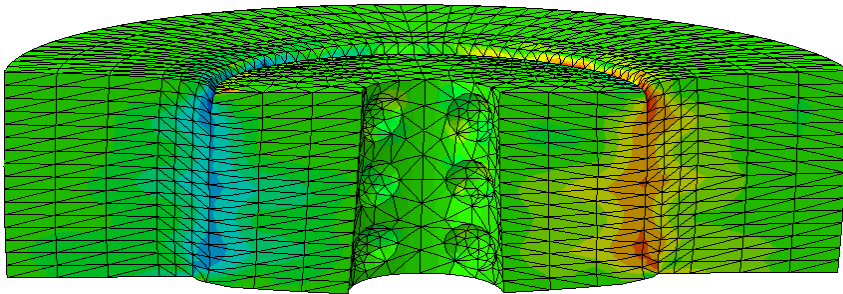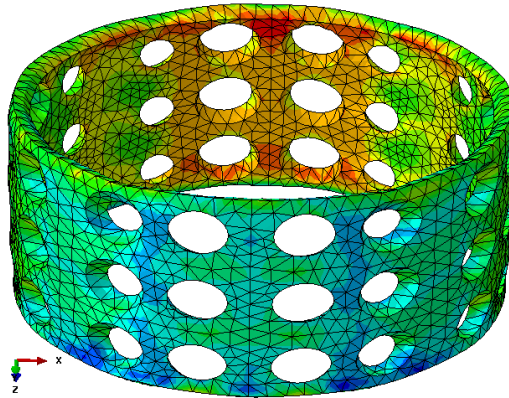

Figure D.4: Shear stress, s23, at $1.5\,$mm punch tool penetration, cut view

Figure D.5: Shear stress, s23, at 1.5 mm punch tool penetration, shear zone

To identify when the sample breaks, a cylindrical coordinate system is created and the shear stress in z-direction, on the plane perpendicular to the radial direction is shown in figure D.6. The break is estimated to occur after 0.75 mm punch tool penetration. In Figure D.6a, most areas are colored green, with a shear stress between 3 and 30 MPa. In Figure D.6b, most areas have by far exceeded the critical value calculated by Equation 3.1 to be 15MPa. Yellow color indicates here stress between 50 and 70 MPa.

(a)   (b)
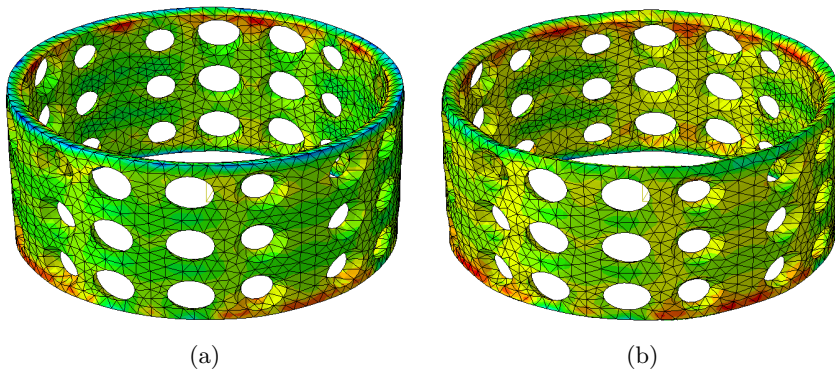
Figure D.6: Shear stress in shear zone **(a)**0.75mm penetration **(b)**1.5mm penetration

The shear strength is calculated from the force needed to break the sample. As the breakage of the sample is estimated to occure at around 0.75 mm punch tool penetration, this is at time 0.5 in this simulation. The reaction forces from the center surface, where the displacement is applied, are extracted at this point of the simulation. The nodes selected are shown in Figure D.7.
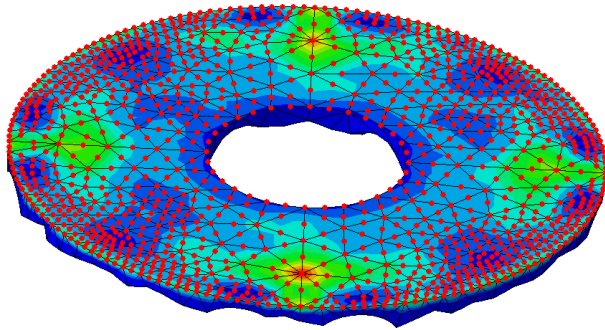

Figure D.7: Nodes where reaction forces are extracted

The reaction forces were plotted versus time in Figure D.8, one curve pr node. The curves were summed and plotted, as shown in Figure D.9.
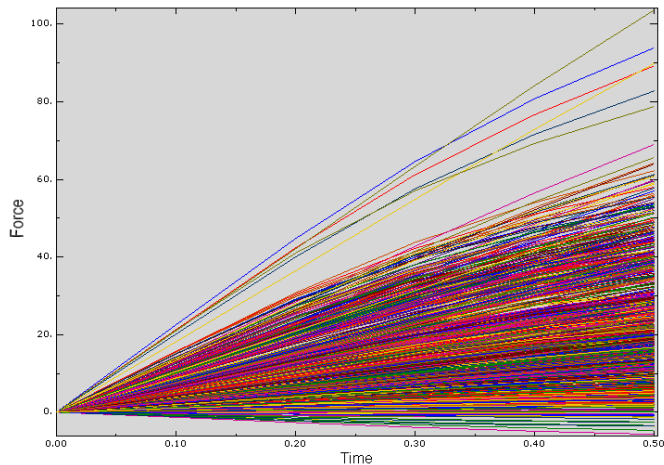

Figure D.8: Nodal reaction forces plotted vs time, for each singular nod
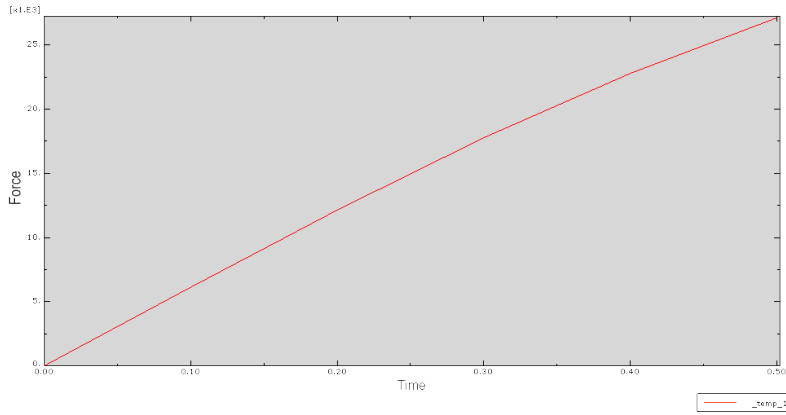
Figure D.9: Nodal reaction forces plotted vs time, all nodes summed

The total force required to break the sample is found to be 25 kN. The failure surface is somewhere in the shear zone which is between 13 and 14 mm radius, through the thickness of 15 mm. The shear strength of the material is then calculated from Equation D.1.

$$\tau = \mathrm{frac}FA = \frac{25000}{2 * \pi * 13.5 * 15} = 20\,\mathrm{MPa} \tag{D.1}$$

D.2 Leca - Concrete damaged plasticity model

The concrete damaged plasticity model requires input of the following data: Dilation Angle, ψ, in degrees. Eccentricity, ϵ, defines the rate at which the hyperbolic flow potential approaches its asymptote. $\frac{\sigma_{b0}}{\sigma_{c0}}$, the ratio of initial equibiaxial compressive yield stress to initial uniaxial compressive yield stress. K_c, the ratio of the second stress invariant on the tensile meridian, to that on the compressive meridian. And finally μ, a viscosity parameter. The Abaqus user's manual provides the default values for concrete as $\epsilon = 0.1$, $\frac{\sigma_{b0}}{\sigma_{c0}} = 1.16$, $K_c = 0.666$ and $\mu = 0$[2, 12.9.2]. The angle of friction for concrete is $\phi = 37\,°$[27], the dilation angle is calculated from the relationship $sin(\phi) = tan(\psi)$[1, 11.5.3] which gives, $\psi = 31\,°$.

In this simulation, the shear tool radius was set to be $10\,mm$ as in the test in the laboratory. The displacement was applied as a controlled velocity and the meshing and boundary conditions were the same as in the simulations presented in Chapter 6. The PP was modeled with elastic and plastic properties, without the deformation plasticity model.

The deformations and mises stress are not shown because they are very similar to the once shown in the previous section, the shear stress in the shear zone however, differs from the model without Leca as shown in Figure D.10. This image is taken at $0.6\,mm$ punch tool penetration and is considered the point of failure as most of the surface has exceeded the critical value of $15\,MPa$. The light blue areas have shear stress between 10 and $20\,MPa$ and the green areas have shear stress between 20 and $60\,MPa$.
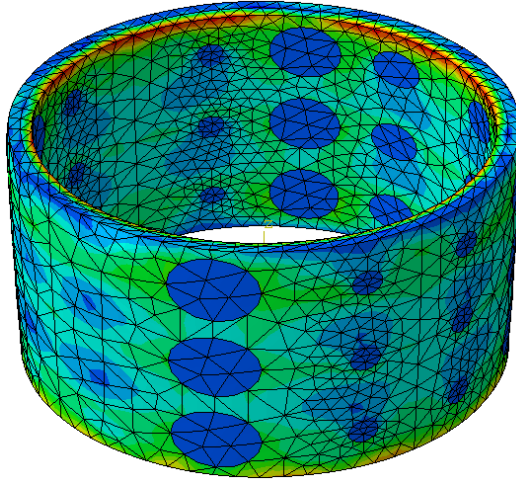

Figure D.10: Shear stress in shear zone $0.6\,mm$ penetration

The node selection and summation procedure followed as in Figure D.7, D.8 and D.9. For this model, the node selection and summation are shown in Figure D.11 and D.12.
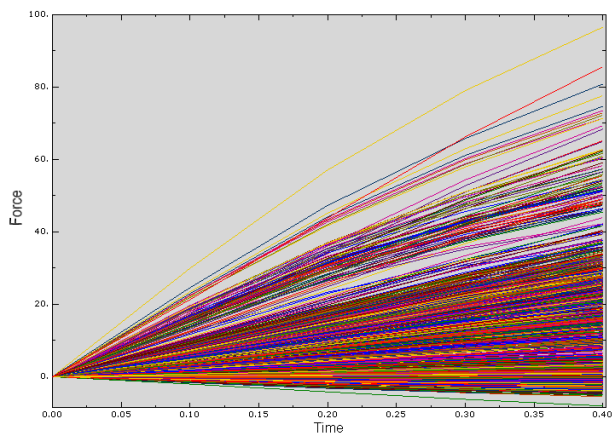

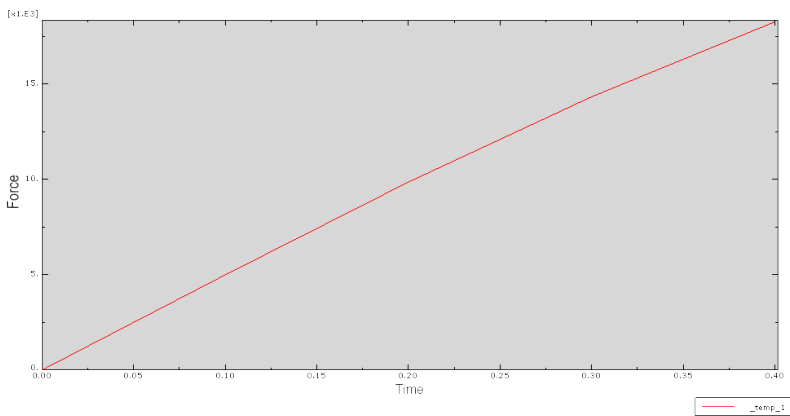Figure D.11: Nodal reaction forces plotted vs time, for each singular nod

Figure D.12: Nodal reaction forces plotted vs time, all nodes summed

The total force required to break the sample is found to be 17 kN. The failure surface is somewhere in the shear zone which is between 10 and 11 mm radius, through the thickness of 15 mm. The shear strength of the material is then calculated from Equation D.2.

$$\tau = \frac{F}{A} = \frac{17000}{2 * \pi * 10.5 * 15} = 17\text{MPa} \tag{D.2}$$